Battelle
The Business of Innovation

# REPORT ON MODEL MODULES TO ASSIST ASSESSING AND CONTROLLING SCC

By
**H. Castaneda, B. N. Leis, and S. E. Rose**

Battelle's Energy Systems
505 King Avenue
Columbus, OH 43201

Prepared for
**US Department of Transportation PHMSA**

April 4, 2008

Client Contract No. DTRS56-05-T-0003
Battelle Contract No. G005189

# Report

on

# Model Modules to Assist Assessing and Controlling SCC

**Prepared for**

## US Department of Transportation PHMSA

Client Contract No. DTRS56-05-T-0003
Battelle Project No. G005189

**by**

**H. Castaneda, B. N. Leis, and S. E. Rose**

April 4, 2008

**BATTELLE'S ENERGY SYSTEMS**
**505 King Avenue**
**Columbus, Ohio 43201-2693**

# Acknowledgments

This report presents work that leverages co-funding from research done under IR&D funding by Battelle, in assisting companies understand and control SCC, and in the conduct of field data gathering to assist in developing that understanding in work done by and/or in conjunction with J. E. Marr and Associates. Useful discussions with Dr. Ray Fessler, consultant, and with Mr. Steve Rapp of Duke Energy Gas Transmission, Mr. Jerry Rau of Panhandle Energy, and Mr. Ron Scrivner then of Transco, and others to numerous to name in the transmission pipeline community also are gratefully acknowledged. Finally, the efforts of Dr. R. E. Kurth played a major role in the initial computer algorithm of the model for high-pH SCC, which is gratefully acknowledged.

# REPORT DOCUMENTATION PAGE

*Form Approved*
*OMB No. 0704-0188*



| **1. REPORT DATE** *(DD-MM-YYYY)* | **2. REPORT TYPE** | **3. DATES COVERED** *(From - To)* |
|---|---|---|
| 05/02/2007 | Final | 08/12/2004 – 07/12/2006 |

**4. TITLE AND SUBTITLE:**
Model Modules to Assist in Assessing and Controlling SCC

**5a. CONTRACT NUMBER**
DTRS56-05-T-0003

**5b. GRANT NUMBER**

**5c. PROGRAM ELEMENT NUMBER**

**6. AUTHOR(S)**
H. Castaneda, B. N. Leis, and S. E. Rose

**5d. PROJECT NUMBER**
164

**5e. TASK NUMBER**

**5f. WORK UNIT NUMBER**
132

**7. PERFORMING ORGANIZATION NAME(S) AND ADDRESS(ES) AND ADDRESS(ES)**
Battelle
505 King Avenue
Columbus, OH 43201

**8. PERFORMING ORGANIZATION REPORT NUMBER:**
G005189

**9. SPONSORING / MONITORING AGENCY NAME(S) AND ADDRESS(ES)**
US Department of Transportation
Mr Jim Merritt and Mr Robert Smith
400 7th Street, SW
Washington, DC 20590

**10. SPONSOR/MONITOR'S ACRONYM(S)**

**11. SPONSOR/MONITOR'S REPORT NUMBER(S)**

**12. DISTRIBUTION / AVAILABILITY STATEMENT**

**13. SUPPLEMENTARY NOTES**

**14. ABSTRACT**

This project developed and validated tools to assist in integrity assessment and management both forms of SCC. Because the understanding that underlies integrity management tools was most comprehensive for high-pH SCC, development targeted NN-pH SCC, with work on high pH SCC being more application oriented. To broaden the utility of the deliverables, this project targeted technology in the context of generic modules applicable to both forms of cracking, recognizing their key difference lies in the mechanisms of cracking and how that impacts their kinetics and pipeline susceptibility. For the high-pH scenario the work was focused on tools to facilitate evaluation of factors that drive day to day integrity-management decisions. In contrast, work for NN-pH situations targeted was at the level of understanding the mechanisms that underlie the evolution of hydrogen involved with this form of SCC.

Some key conclusions include: a mechanism for NN-pH SCC was developed and modeled in a fundamental framework, and found to produce hydrogen in sufficient quantity to support crack nucleation and growth under typical pipeline service conditions; a spectrum of reversible environments exist that sandwich NN-pH SCC between corrosion at lower pH levels and high-pH SCC that bounds the high end, each of corrosion, high-pH SCC, and NN-pH SCC is possible either individually or in association with the same crack; conditions driving NN-pH SCC were found to be consistent with temperature conditions throughout the United States. A host of other conclusions and recommendations also were developed.

**15. SUBJECT TERMS**
stress-corrosion cracking (SCC), near-neutral pH, high pH, cracking, threat assessment, threat severity and prioritization, re-inspection interval, hydrogen, dissolution, anodic dissolution, electrochemical impedance spectroscopy (EIS), transmission-line model, real and imaginary numbers, modeling, pipelines, service history, hydrotesting

| **16. SECURITY CLASSIFICATION OF:** Standard | | | **17. LIMITATION OF ABSTRACT** | **18. NUMBER OF PAGES** | **19a. NAME OF RESPONSIBLE PERSON** |
|---|---|---|---|---|---|
| **a. REPORT** | **b. ABSTRACT** | **c. THIS PAGE** | | | **19b. TELEPHONE NUMBER** *(include area code)* |
| Final | | iv | | 103 | Brian Leis<br>614.424.4421 |

**Standard Form 298 (Rev. 8-98)**

# Executive Summary

The challenge of efficiently and safely operating the natural gas and hazardous liquid transmission system in the US has existed since pipelines were recognized as the best long distance mode of hydrocarbon transport. As time passed, exposure to the environment and the effects of service expanded this challenge to include consideration of maintenance, which has evolved into systemic integrity management as we know it today – which includes concerns such as stress-corrosion cracking (SCC). Technologies and the tools to implement them to manage SCC have developed as the concern for SCC has expanded. Hydrotesting and aftercoolers have been used for decades to manage SCC on gas pipelines, with in-line inspection (ILI) becoming increasingly viable for liquid / product pipelines. SCC direct assessment (SCCDA) also is developing to meet the need to characterize pipeline condition, along with ILI specific to gas transmission pipeline applications. Where the presence of SCC is confirmed, fitness-for-service assessment tools are needed to determine its severity and to help identify and prioritize integrity management options and re-inspection intervals. Thereafter, an integrity management plan is needed to manage risk to provide safe serviceable operation until the next re-inspection for high pH as well as near-neural (NN) pH cracking.

This project developed and validated tools to assist in integrity assessment and management both forms of SCC. Because the understanding that underlies integrity management tools was most comprehensive for high-pH SCC, development targeted NN-pH SCC, with work on high pH SCC being more application oriented. To broaden the utility of the deliverables, this project targeted technology in the context of generic modules applicable to both forms of cracking, recognizing their key difference lies in the mechanisms of cracking and how that impacts their kinetics and pipeline susceptibility. For the high-pH scenario the work was focused on tools to facilitate evaluation of factors that drive day to day integrity-management decisions. In contrast, work for NN-pH situations targeted was at the level of understanding the mechanisms that underlie the evolution of hydrogen involved with this form of SCC. Thus, the work targeted the spectrum of environments plausible on pipelines such that once might infer from above ground the nature of the cracking processes affecting the serviceability of a pipeline. Ultimately, this must be transformed into practical algorithms before this understanding can have a direct impact on integrity management.

Key conclusions developing from this project included:

- Optimum conditions for NN-pH SCC kinetics were established via beaker studies, with bicarbonate ion identified as the essential constituent,
- A mechanism for NN-pH SCC that leads to significant hydrogen generation derived from the bicarbonate ion was developed and modeled in a fundamental framework,
- It was found that this mechanism produced hydrogen in sufficient quantity to support crack nucleation and continued cracking under typical pipeline service conditions,
- It was indicated that a spectrum of reversible environments exist that sandwich NN-pH SCC between corrosion that controls at lower pH levels and high-pH SCC bounding the high end, with each of corrosion, high-pH SCC, and NN-pH SCC possible either individually or mutually nearby or even in association with the same crack,
- Reversibility of the environments was found to be driven by seasonal factors that affect temperature (hydrogen solubility) and the availability of other constituents that modify

the kinetics of dissolution, anodic dissolution, and hydrogenation and its ingress and interaction with the microstructure,

- The viability of NN-pH SCC mechanism was demonstrated by nucleation in the laboratory, which confirmed NN-pH SCC is possible throughout the United States, as the bounding temperatures reflect that range of climatic conditions,
- The extent of hydrogen generated by this mechanism was quantified as was its effect on microplastic response,
- It was found that bicarbonate ion can be generated in copious quantities thus providing a more that adequate source of hydrogen to drive environmentally assisted cracking,
- While the role of hydrogen was demonstrated, the specific form of environmentally assisted cracking has not yet been quantified – each of the three recognized and competing forms of hydrogen interaction with the microstructure remain plausible – with some traits observed being consistent with hydrogen enhanced localized plasticity (HELP) and others being more typical of hydrogen embrittlement (HE),
- Electrochemical impedance spectroscopy (EIS) was found to be an effective tool in evaluating the interaction of hydrogen and cycle dependent changes in the steel's surface, and the behavior of the interface that forms between the steel and the cracking environment,
- Functional relationships characterizing NN-pH SCC kinetics were identified and controls for hydrogen effects discussed,
- The environment supporting the NN-pH SCC mechanism was found to be consistent with the constituents typically found with this cracking in the field, particularly in the vicinity of severe cracking that led to in-service ruptures,
- Field criteria to assess high pH SCC severity were assessed and their validation considered in the context of computer simulation of this process and parametric analysis done to simulate control of such SCC via operational changes,
- The effect of in-service factors on NN-pH SCC susceptibility was discussed, with factors that drive the hydrogen generation mechanism being of greatest concern,
- Until the effects of cycle dependent changes in the steel's surface are isolated from the inherent influence of microstructure and its impact on cyclic softening and this is quantified, there is no reasonable expectation that macroscopic empirical testing to probe and empirically trend this behavior will prove effective.

In closure, while rather limited in scope, this work points clearly to the utility of EIS as the means to uncouple the interacting roles of cycle-dependent mechanical effects (like cyclic softening), microstructure, environment, and loading. Until the effects of cycle dependent changes in the steel's surface are isolated from the inherent influence of microstructure and its impact on cyclic softening and the outcome is quantified, there is no reasonable expectation that trending the results of macroscopic empirical testing will prove effective. This assertion is proven by the lack of insight from such testing after more than 70 years of such work coupling the effort first for high-pH and then NN-pH SCC. It follows that the central recommendation from this project is to initiate a combined analytical and experimental assessment targeting isolation of the roles of cycle-dependent microplasticity, mechanical loading history, electrochemical environment, and microstructure, via focused experiments incorporating EIS coupled with related modeling of the phenomenology and analysis of trends and their implications. Only then can we anticipate incremental insight, and thereafter control of SCC.

# Table of Contents

## Table of Contents (continued)

Page

## List of Figures

# Table of Contents (continued)



# List of Tables

# Table of Contents (continued)

Page

# Background

The challenge of efficiently and safely operating the natural gas and hazardous liquid transmission system in the U.S. has existed since pipelines were recognized as the best way to transport hydrocarbons. This project was one of four concurrent activities completed under a consolidated program designed to improve the integrity of the pipeline infrastructure in the U.S. Developing the government's high-level structure and requirements for **Integrity Management Plans** (IMPs)[1,2]# in response to recent legislation was a significant effort. However, the real challenge lies in its successful implementation. Within each company, engineers must develop the IMP, and inspectors must concur that the expectations of regulatory requirements have been met by it. Such assessment or concurrence can be much easier for newer pipelines because modern construction practices and materials are typically coupled with quality controls – and the effects of service and time have not yet become a critical factor. However, for systems made with vintage steels and construction practices, or those whose operation and RoW (RoW) opens the door to possible in-service degradation over time, such is often not the case. Inspectors must be able to track the efforts of the pipeline engineer throughout the IMP, and agree the objectives of the plan have been met. Tools must exist or be developed to effectively implement the IMP and track the related assessment and management processes, and continuous improvement in safety records. This project develops technology and tools to facilitate assessment and management processes specifically for stress-corrosion cracking (SCC). These aspects are developed consistent with guidance in the industries responses[e.g., 3,4] to the governments recent regulatory actions.

IMPs currently target pipeline segments in **high-consequence areas** (HCAs) for lines 500 miles or longer. Such requirements can be anticipated to eventually apply to smaller segments so the risk to human life and the environment in remote communities will ultimately be the same as it is in HCAs. For this reason, tools must be developed for use by larger companies that could be as effective in use by smaller companies. Likewise, tools must be simple and practical, and be equally understood and useful to industry and regulator, whether federal or state.

As for other **time-dependent threats**, it is necessary to characterize the pipeline's **condition**, with hydrotesting broadly used for this purpose for SCC on gas pipelines with in-line inspection (ILI) is potentially useful for hazardous liquids / products pipelines. SCC direct assessment (SCCDA) is also developing to meet the need to characterize pipeline condition, with ILI developing for applications specific to gas transmission pipelines. Once the condition is known, tools are needed to support the **threat assessment** and where SCC is confirmed as a threat integrity assessment tools are needed to determine the **severity** of the threats identified along the RoW, and to identify and prioritize integrity management options. These tools must address complex time dependent factors controlling SCC, and determine the **re-inspection interval** when the condition must be re-evaluated to ensure safety.

Companies operating pipelines prone historically to SCC or lines whose operation and other risk factors indicate a predisposition for SCC based on the baseline threat assessment must develop an IMP whose scope ensures safe serviceable operation until the next re-inspection. The need for integrity assessment and management tools covers both **high pH** and **near-neural (NN) pH** cracking, although the understanding leading to such tools is more acute for NN SCC as

# Numbers in superscript parenthesis relate to the list of references at the end of the report

understanding of high-pH SCC is much more advanced. This project develops and validates tools to assist in integrity assessment and management for both forms of SCC in the context of modules to enhance the capabilities of just-developed technology for high-pH SCC, and to extend the utility of such technology to applications involving NN SCC.

# Introduction

The occurrence of external stress-corrosion cracking (SCC) on high-pressure pipelines was recognized as a unique failure process first in 1965[1] during analysis of a gas-transmission pipeline rupture that occurred in Louisiana. One distinguishing feature evident in metallographic analysis was branched intergranular (IG) cracking. Over the next four years, 11 more gas-transmission pipeline ruptures occurred in the United States, all branched showing apparently IG cracking as a common trait(1). Initial analyses of the liquids under coating disbonds and of the soils in the vicinity of SCC determined the cracking environment was ground water with pH the order of 10, with principle components noted to be carbonate and bicarbonate ions, but this work was not conclusive(1). Subsequent extensive analyses(2) found that the pH ~9, which value was found to be controlled primarily by the balance between carbonate and bicarbonate ions that formed under coating disbonds as a consequence of the cathodic protection (CP) used to control pipeline corrosion[2]. Prior to these SCC-induced ruptures, soil-ground-water environments were not known to promote SCC, whose occurrence requires the concurrent effects of tensile stress on a material susceptible to SCC, in an environment that promotes cracking, whereas their independent effects are otherwise benign. The likely reason for these failures whereas SCC had not occurred in other steel structures operating in similar environments under CP was found to be the cyclic loading typical of pipeline service(3). Subsequently, similar SCC has been identified as the cause of ruptures on gas-transmission pipelines in the Australia, Iran, Iraq, Italy, Pakistan, Saudi Arabia and elsewhere.

To deal with the threat to public and environment posed by SCC-induced pipeline failure, and to ensure system reliability, the early work focused on understanding SCC as it occurred on pipelines. Work by Parkins and others indicated the mechanism was anodic dissolution, being controlled largely by electrochemical potential, temperature, and stressing conditions(e.g., see 2-4). Of these factors, SCC in the field was most simply controlled by reducing the compressor discharge temperature[3], while near-critical cracks developed due to SCC could be exposed before they failed in service through use of hydrostatic retesting. Operational factors controlling dissolution also were characterized as a means to minimize the threat, while maximizing pipeline throughput through models relating service conditions to conditions favoring cracking(e.g., see 5,6). Related work showed that SCC in ground water with pH~9 was IG at lower stress intensities, but can appear transgranular (TG) in pipeline steels potentially due to the presence of higher carbon content(1), and due to the effects of higher stresses(7).

In the mid-80s SCC again became a prevalent failure mechanism this time targeting Canadian gas-transmission pipelines(8). This SCC was soon recognized to be unique in comparison to the typical IG cracking that had occurred previously, as it showed evidence of TG cracking, was often associated with general corrosion or pitting, and it occurred at a much lower pH, being the order of 7. Because the pH of this environment was low in comparison to that first observed to

---

[1] Battelle file data indicate a failure on the same pipeline occurred in 1957 at a site not too far from this incident that showed similar traits – however the traits of this 1957 occurrence were not identified as SCC.

[2] The CP promotes formation of hydroxyl ions that facilitate absorption of $CO_2$ derived from decaying organic matter in the soil.

[3] The significance of proximity to the compressor discharge was already recognized in 1970, as reported in Reference 1. The fact that this involved locally higher temperatures was likewise recognized therein, while the significance of pressure cycles followed much later.

cause SCC on pipelines, it was sometimes termed “low pH” while that first observed to cause SCC was referred to as “high pH” SCC. Because the pH for these low-pH cases was consistently found near ~7, SCC in this environment eventually was termed “near neutral” SCC. Solutions found under disbonds in the vicinity of near-neutral (NN) environments often contain Cl, $SO_4$, and $HCO_3$ ions. Also found was a white paste or powdery substance whose form depended on the moisture content, which was identified as iron-carbonate. In addition to the failures in Canada, SCC with traits associated with near-neutral environments has occurred extensively in Russia, and is likely active elsewhere in the world.

As for high pH SCC, Parkins and his colleagues have done much to characterize cracking in the near-neutral environment[e.g., see 9,10]. The “gaps” analysis of Fessler[11] reflects on the detailed work of Parkins and others for both high pH and near-neutral pH SCC, wherein it is apparent that the mechanism for near-neutral SCC has not yet been determined, although the role of hydrogen appears clear. Insight into this environment has developed recently based largely on the iron carbonate that is often found in large quantities near by field failures and in digs done to locate or characterize SCC[12,13]. This work indicates a clear role for hydrogen. It also considers that cracking occurs within a reversible spectrum of environments from pH levels the order of ~4, where corrosion is driven by carbonic acid, into a regime where buffered solutions exist at pH ~6.4 and pH ~9.4 that favors SCC, and then onto high pH levels depending on the CP level, seasonal swings in ground water chemistry, and other factors that determine balance between $H_2CO_3$, $HCO_3^-$, and $CO_3^{-2}$. On this basis both NN-pH and high-pH SCC can coexist as unique processes, or can contribute to the growth of individual cracks at different times in the life of the pipeline. This coexistence explains the coexistence of the IG cracking shown in Figure 1 along with adjacent TG cracking and extensive local corrosion. Results developed according to this view of the cracking environment and its ability to generate hydrogen[12-15] indicate the “active ingredients” in the groundwater are $CO_2$ to produce $H_2CO_3$ along with a threshold concentration of $HCO_3^-$.

SCC again become newsworthy in the US during 2003, with several pipeline incidents ascribed to it, including splits on liquid pipelines. These incidents led to a US DOT Bulletin[16], which now requires US operators to consider SCC as a possible threat when developing their integrity management plans (IMPs). Unfortunately, assessing the threat of SCC and mitigating it is much

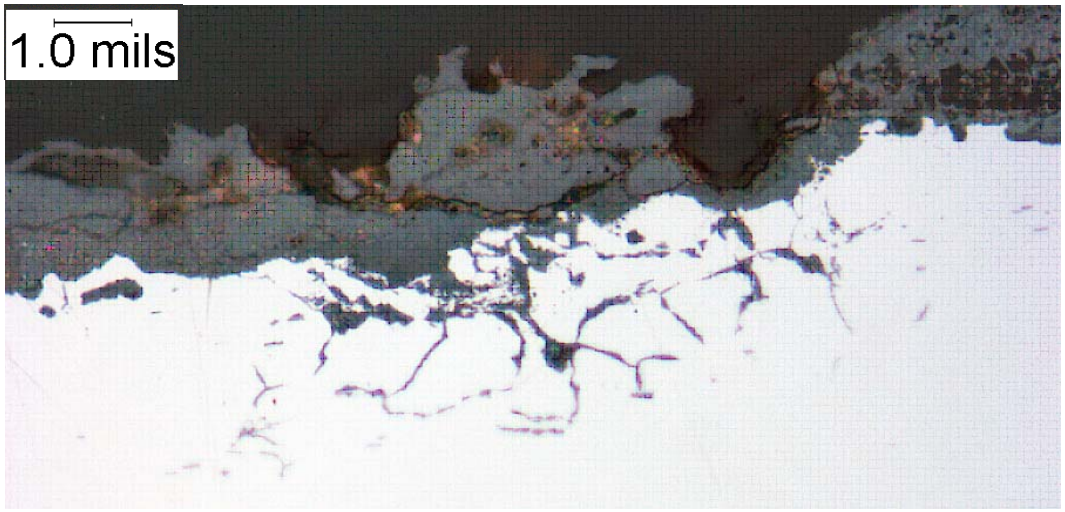


**Figure 1. IG features near the origin of a rupture due to NN-pH SCC**

more complicated now in light of two possible cracking environments as compared to the 1970s when only a single cracking environment was recognized. This complexity develops because factors controlling cracking kinetics in the two cracking environments can in some cases be in conflict. For example, reducing the temperature of the transported product decreases the cracking rate and susceptibility for high pH SCC. However, reduced temperature also increases the solubility of $CO_2$, so this change has the potential to enhance the chances for low pH SCC, all else being equal. It follows that models that can characterize the extent or likelihood of low and high pH SCC as a function of service conditions or circumstances along the RoW could play a significant role in developing IMPs for SCC.

This project developed models for high-pH as well as NN-pH SCC. Because the understanding of SCC differs to the extent the mechanism for one has been known for decades while that for the second is still evolving, the models considered in this project also differ. Models for high-pH SCC on pipelines began to develop in the late 1980s, building on the phenomenological work of Parkins[2-5] that showed the kinetics depending on strain and strain-rate, and Fessler's initial work to relate this dependency to the operation of pipelines[17]. Modeling in the late 1980s capitalized on the mechanics foundation that related strain and strain-rate at crack tips[5] or in favorably oriented grains on the pipeline's surface[6] to the remote loading. Transformation of the operating conditions for a pipeline into local strain and strain-rate led to a model for high-pH SCC on pipelines[18-20]. As initial discriminatory testing of the viability of this model through the 1990s demonstrated its utility[e.g., 21] and confirmed its blind predictability, work continued with it leading to its validation via correct predictions of field cracking in reference to metrics such as cracking frequency, and statistical distributions of cracking characteristics including crack length and aspect ratio[e.g., 22] and the historical role of spike-hydrotests in its control[e.g., 23]. Because SCC data developed under laboratory conditions show significant scatter[e.g., 2-4, 9-11], even though the samples were prepared and tested under nominally identical conditions, and because conditions in the field are uncertain, this validation was done using a probabilistic formulation of this model[20,22,23].

Central to the high pH model of SCC is the role of microplasticity in both the nucleation of cracking and its continued growth[e.g., see 18,19,21], which also appears central to these aspects for NN-pH SCC[24]. Given this commonality and the realization that aside from kinetics controlled by local environment the remaining elements of models for both forms of cracking were similar, this project has advanced the utility of such models for use by the industry in managing SCC. The ensuing sections herein consider the development of inputs to modules needed to relate operational factors to cracking response in reference to high-pH SCC, which is followed by discussion of its adaptation for NN-pH SCC applications.

# Objective and Scope

This project develops tools to assist in integrity assessment and management both forms of SCC in the context of modules to enhance the capabilities of just-developed technology for high-pH SCC, and to extend the utility of such technology to applications involving NN-pH SCC. For NN-pH SCC the objective is to develop and demonstrate a rational basis to formulate a kinetics module for NN-pH SCC, while for high-pH SCC the objective is to integrate predictions and field tendencies for high-pH SCC and demonstrate the utility of the high-pH model, and then deliver this model as software.

By contract, including reference to the cost-share companion work this project considered the scope presented in Table 1, with the results presented later providing coverage for each.

**Table 1. Work scope for this project, including coverage by the cost-share projects**

| Task | Deliverable / Milestone |
|---|---|
| CS1 | develop mechanism for NN-pH SCC |
| CS2 | establish optimum conditions for kinetics via beaker studies |
| CS3 | establish viability of mechanism by laboratory nucleation testing |
| CS4 | establish field criteria for high pH SCC severity assessment |
| CS5 | develop field validation for high pH SCC severity assessment |
| 1 | evaluate practices to quantify hydrogen effect on microplasticity |
| 2 | characterize effect of field-factors on NN-pH SCC susceptibility |
| 3 | develop parametric results quantifying evolution of hydrogen |
| 4 | establish pipeline flow and fracture properties and service histories |
| 5 | parametric analysis simulating field cracking |
| 6 | parametric analysis simulating controls via hydrotesting |
| 7 | parametric analysis simulating controls via operational changes |
| 8 | correlate hydrogen evolved and effects on microplastic response |
| 9 | develop functional relationships characterizing NN-pH SCC kinetics |
| 10 | trend controls for hydrogen effects into a field-useable format |
| 11 | develop I/O for user-friendly high pH SCC model |
| 12 | format high pH SCC model for delivery |
| 13 | report the results |

The ensuing sections of this report consider these topics in sequence, either in individual sections or as sections that cover a group of related topics.

# Approach and Deliverables

As in the laboratory, the occurrence of SCC on a pipeline requires three conditions be satisfied concurrently:

- an operating environment must exist that can develop into a cracking environment on the pipeline's surface;
- the pipeline steel must be susceptible in that environment; and
- a local tensile stress (applied or residual) must exist that exceeds the threshold for cracking in that environment.

While conceptually these mutually essential aspects of SCC are similar in the laboratory and the field, SCC on a pipeline involves many factors beyond the crack growth behavior (kinetics) evident in a simple laboratory specimen. For example, considering the first item in the list above, a laboratory test begins with a sample immersed in an environment that arguably contains the ingredients or circumstances considered comparable to those associated with cracking in the field. Field factors that can vary seasonally or depend on the functionality of the CP system, or the operating conditions are controlled. In contrast, the field cracking first requires the presence of carbonaceous and possibly other material present in the soil and ground water that over time gives rise to a cracking environment. Field reality also requires that the coating fail local to the presence of such conditions such that the cracking environment can form adjacent to the pipeline's surface, with other conditions related to CP coincidentally satisfied. This implicitly requires the existence of factors that promote coating failure, such as rocks in the backfill, or higher product temperature for some coatings. It further depends on selective CP levels that could enhance these processes. It follows that the field reality and uncertainty is idealized and typically controlled. Finally, where a pre-cracked geometry is used, this idealized response at this one crack deep, short crack tip is well removed from the complexity of the many longer, shallower cracks that develop, interact, and eventually coalesce leading to possible leaks or ruptures within a colony of SCC.

The second and third items above require the coincidental presence of steel susceptible to the cracking environment to exist at the site where the coating fails, coincident with operation causing local stressing conditions sufficient to initiate SCC. This aspect is critical – as without initiated cracking there can be no crack propagation. It is particularly significant for NN-pH SCC, as to date laboratory smooth specimens have been resistant to nucleation under conditions like those in operating pipelines, whereas pre-cracked specimens with deep pre-cracks are found to support cracking[(e.g., see 11,25-27)]. The second and third items require operation that causes local stress high enough to initiate SCC is equally important for high pH SCC. This is evident in results[(e.g., 28)] developed with the tapered-tension test[(29)] (TTT) under standard high-pH testing conditions[(30)] that clearly show the frequency and depth of cracking decreases sharply as the stress falls much below the yield stress to the nominally elastic levels typical of the maximum allowable operating pressure (MAOP) for pipelines[4]. Such data for steels clearly susceptible at

[4] TTT results indicate extensive and deeper cracking at higher stresses, with the frequency and depth of cracking diminishing at levels much below the yield stress. The many SCC sites active at high stresses diminish as micro-plasticity to drive such cracking decreases as the stress decreases emoving along the taper – with cracking become more sparse (which is the basis for defining a threshold for SCC with this geometry). Battelle file data indicate thresholds for SCC are usually well above the Class I maximum allowable operating stress when based on seven-day

stress levels typical of Class 1 gas-transmission service show that as the stress corresponding to Class 3 service is approached little to no cracking is evident[31]. On this basis any difference between the stressing conditions that exist in laboratory testing in contrast to the field situation also must be addressed in modeling, as must the possible interaction of cracking in SCC colonies as it moves toward possible failure.

It follows that modeling SCC on pipelines must consider first the formation of the cracking environment on the pipeline, and thereafter simulate the nucleation of the cracking, considering the extent and nature of the multiple cracking found in colonies through coalescence leading to a leak or eventual instability and rupture. Given the complexity of aspects following formation of the cracking environment, suffice it to begin modeling with the assumption the environment has formed. Consequently, the approach taken in modeling SCC is much like that for the laboratory testing – the cracking environment is assumed present such that the life calculated is a lower-bound to field conditions. Once aspects that follow this step are characterized, a module that addresses formation of the cracking environment should be developed – as this is the precursor for field cracking. To be useful as broadly as possible, a modular approach has been adopted that isolates and models each of crack nucleation, crack growth, and failure and their kinetics and its dependence on service conditions. To make the outcome useful to the industry, to the extent possible the technology is being formatted for use by pipeline engineers by integrating these modules into software specific that at present is specific to high-pH SCC.

This project demonstrates the basis for the software and its outcomes in regard to managing high-pH SCC, and delivers this software. Consistent with this modular approach, this project develops modules that characterize basic aspects of the kinetics for NN-pH SCC, in a format consistent with the literature that has developed since this project began. This approach parallels past developments whose results are consistent with current SCC management employed for natural-gas transmission pipeline systems based on hydrotesting. Trends will be developed to illustrate consistency of the high-pH model with the role of pressure and temperature, and the pressure ("R") ratio, which aspects of the kinetics for NN-pH SCC will be presented in a format that facilitates their eventual use in a similar software-based model. These deliverables should have near-term value in formulating IMPs to address SCC.

---

tests. For practical applications, thresholds should be based on cracking distributions and depths that have been projected forward in time to characterize values representative of many years of service-induced growth.

# Results

## Develop a Mechanism for NN-pH SCC

Field measurements in the vicinity of cracking (although not necessarily active cracking) indicate TG NN-pH SCC is associated with a dilute aqueous electrolyte with a pH in the range of ~6 to 7. This solution is trapped against the pipe surface by a disbonded coating that can shield the pipe from CP in this region. Solutions collected in the field in the vicinity of NN-pH SCC cracks contained appreciable quantities of chloride, sulfate, as well as bicarbonate and very small amount of carbonate ions[9-11]. Based on the analysis of solutions from the initial failures, solutions termed NS1, NS2, NS3, and NS4[5] were developed to simulate NN-pH SCC environments in the laboratory. The range of compositions for these is potassium chloride, 40 - 150 mg/l, sodium bicarbonate, 480 – 1000 mg/l, calcium chloride, 10 – 180 mg/l, and magnesium sulfate, 90 – 250 mg/l. Recently, NS4[e.g., 32,33] seems to have become the standard for *crack propagation* experiments in most laboratories when dealing with NN-pH SCC.

Near-neutral pH SCC tends to occur with extensive dissolution of the crack walls and evidence of related corrosion, including the formation of pitting. Because of crack wall dissolution, crack morphology is generally difficult to identify conclusively in many of these failures[e.g., 34]. The presence of secondary cracking on the fracture surface has pointed to hydrogen playing a role in this type of failure[9-11,34]. However, as noted in regard to Figure 1, shallow high-pH SCC is occasionally found in conjunction with quite deep NN-pH SCC, suggesting that the environment involves other than the effects of hydrogen – and implying environmental conditions that support more than one cracking mechanism. The presence of corrosion in conjunction with NN-pH SCC could reflect pitting focused at what previously was shallow high-pH SCC, which also is consistent with environmental conditions local to the pipe wall shifting over time, possibly seasonally.

The possibility of a changing environment opens the door to mechanisms contributing to failure in addition to that postulated herein which begins with consideration of the chemistry associated with $CO_2$ and water, and the presence of iron carbonate in the vicinity of NN-pH SCC failures. Given these observations, the next section postulates drivers for crack initiation in reference to the $CO_2$-$H_2O$ system in a framework that does not require other cations or anions. While other species undoubtedly will be confirmed to contribute to this process in the future, either positively or negatively, this paper seeks a framework for more systematic understanding.

## Chemistry of the $CO_2$-$H_2O$ System

Based on the composition of the NSx solutions noted above it is appropriate to consider aspects of the $CO_2$-$H_2O$ system as background to a postulated mechanism for hydrogen-related cracking. Figure 2 shows the result of calculations that provide the regions of predominance for the three equilibrium species that can coexist when carbon dioxide dissolves in water[35]. The nature of the species as a function of the pH of the solution develops in reference to Figure 2, as follows.

With reference to Figure 2, the lines shown on the diagram reflect the equilibrium constants for the reactions shown below as Reactions (1) and (2):

---

[5] Recently, NS4 seems to have become the standard for *crack propagation* experiments in most laboratories when dealing with NN-pH SCC.[e.g., 32,33]

$$H_2CO_3 \leftrightarrow HCO_3^- + H^+ \quad (1)$$

$$\log \frac{[HCO_3^-]}{[H_2CO_3]} = -6.37 + pH$$

$$HCO_3^- \leftrightarrow CO_3^{2-} + H^+ \quad (2)$$

$$\log \frac{[CO_3^{2-}]}{[HCO_3^-]} = -10.34 + \text{pH}$$

The concentration ratios from each of the two Reactions above were plotted versus pH, with the reciprocal of the first being used to facilitate visualizing zones of predominance. It is apparent from Figure 2 that the bicarbonate ion dominates the intermediate region defined by pH in the range between 6.4 and 10.3. At pH's more acid than 6.4, carbonic acid predominates, whereas at pH's more basic than 10.3, carbonate ion predominates. Where the above ratios have a value of unity, the species are in equal molar amounts and the solution is effectively buffered, which tends to stabilize the solution at that pH. The diagram also shows that a concentrated solution of bicarbonate tends to a pH of about 8.4 (the minimum on the diagram). A solution saturated with 1 atm of $CO_2$ at 25 C has a pH slightly less than 4, which means that it has more than 100 times carbonic acid compared to bicarbonate. An important point to note is that if $CO_2$ gas (at the appropriate partial pressure) is bubbled into distilled water to obtain a stable pH of 6.4, there will be approximately equal amounts of carbonic acid and bicarbonate ion because of the equilibrium. Finally, note that the formation of carbonic acid from $CO_2$ is thermodynamically favored over a relatively narrow temperature range between 10 and 35 C.

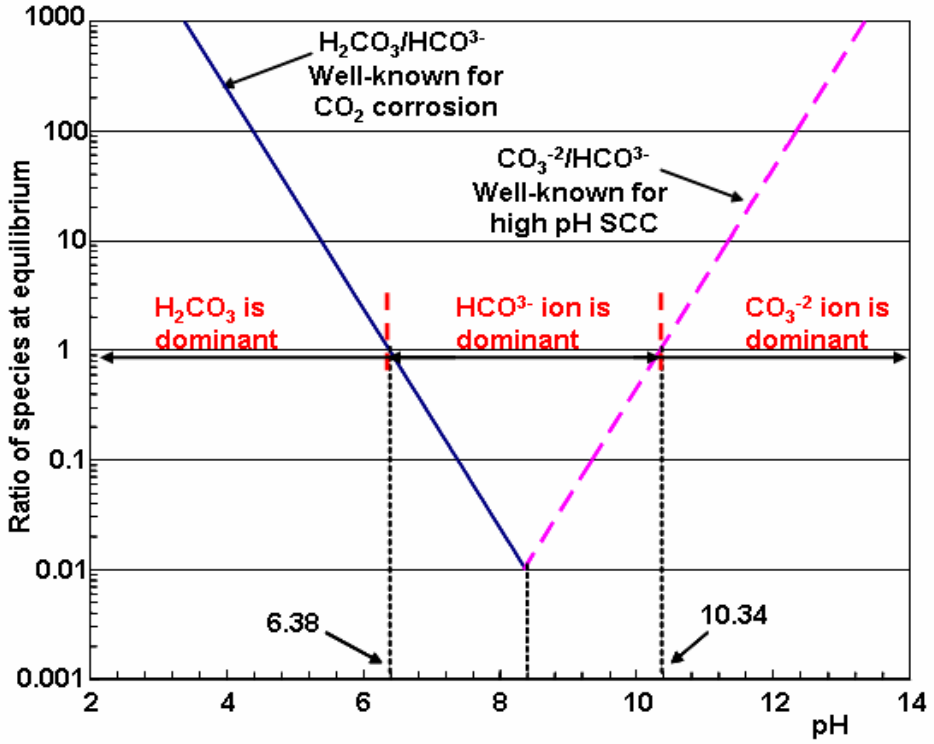


**Figure 2. Solubility curves for the predominant species in the $CO_2$-$H_2O$ system**

## Proposed Hydrogen Generation Mechanism

Previous efforts to define the mechanism(s) of near-neutral pH cracking have centered on the morphology of the cracking and the effect of the environmental species that have been detected under disbonded coatings in the field. One obvious postulate is that the hydrogen develops as result of the cathodic hydrogen reduction reaction that accompanies the corrosion of iron, and related discussion of the role of over-potential and other factors. However, it is not clear that this mechanism acting under typical field conditions can generate sufficient hydrogen to promote extensive cracking. Moreover, this mechanism implies NN-pH SCC would be expected where corrosion is experienced, which while observed in some cases is far from ubiquitous. Further, this mechanism also does not explain the formation of iron carbonate, which has been found in massive quantities under disbonded coatings where apparently cracking is found, nor does it account for the observation of a lack of cathodic protection on lines that typically crack. Finally, if this mechanism controlled, many types of steels would have been found to crack during many industrial corrosion processes because the hydrogen reduction reaction is the balancing cathodic process to the anodic iron oxidation reaction in many of these cases.

It follows that an alternative mechanism and explanation for NN-pH SCC is essential given the just-cited concerns with cathodic reduction as the source of hydrogen. An alternative mechanism is postulated next that is broadly consistent with the field scenario, which should help understand the initiation process en route to developing potential controls for NN-pH SCC and the eventual solution to this problem.

Consistent with the apparent role of hydrogen-related mechanisms for cracking in near-neutral environments noted above, a mechanism is postulated whereby significant hydrogen can be generated. This mechanism relies on the formation of $FeCO_3$ in $CO_2 - H_2O$ solutions, and thus is consistent with the evolution of copious amounts of $FeCO_3$. The first step in the mechanism is the evolution of carbonic acid, which forms through dissolution of $CO_2$. The $CO_2$ is made available from the decomposition of carbonaceous material in the soil, which then dissolves into the groundwater, with the solubility increasing as temperature decreases. As the $H_2CO_3$ migrates under disbonds and corrosion occurs, $FeCO_3$ forms from the bicarbonate as it releases its H, which can then diffuse into the steel causing embrittlement or activating any other hydrogen-related mechanism such as hydrogen-enhanced localized plasticity (HELP)[36].

That release of hydrogen from bicarbonate as just indicated is described by the following set of reactions:

$$\begin{array}{ccccc} H_2CO_3 & \leftrightarrow & HCO_3^- & + & H^+ \\ & & + & & + \\ Fe & \leftrightarrow & Fe^{2+} & + & 2e^- \\ & & \downarrow & & + \\ & & FeCO_3 & + & H^+ \\ & & & & \downarrow \\ & & & & 2H\ (adsorbed) \end{array} \qquad (3)$$

Once adsorbed, according to the literature the effect of hydrogen can range from enhanced plasticity 1 to the other extreme where it promotes embrittlement[36,37]. Of these two potential effects, embrittlement might be dismissed for pipeline applications because the hardness of line-pipe steels is typically not high enough to admit embrittlement. However, where plastic flow

occurs locally because the stress is locally increased due to wall thinning (corrosion) or the presence of a stress raiser (high-pH SCC or pitting), strain hardening occurring locally can facilitate embrittlement. Thereafter, the high localized triaxial stress facilitates hydrogen diffusion to the crack tip more readily, further enhancing subsequent crack propagation.

Significantly, Figure 2 indicates the solution is buffered as a result of nearly equal molar amounts of carbonic acid and bicarbonate ion at pH near 6.4. For this reason, the consumption of either component in the reactions defined as Reaction 3 will cause a shift in the equilibrium to the point where the pH will remain near 6.4, given adequate concentration of the species available for reaction. Hydrogen released from the bicarbonate consumed from formation of iron carbonate combines with the hydrogen from dissociated carbonic acid, along with the released electrons from iron oxidation, to generate hydrogen. As the process consumes equal amounts of the dissociated species of carbonic acid, the solution pH does not change – so long as carbonic acid is available to dissociate to replace the iron carbonate consumed in hydrogen generation.

The generation of hydrogen according to the postulated mechanism does not rely on hydrogen reduction from dissociated water, so the local pH on the steel surface does not become more alkaline as would occur during the normal corrosion of iron in acidic solutions. Another contributing factor may be the presence of bicarbonate on the steel surface. It may act as a hydrogen recombination poison as does hydrogen sulfide, but we have not investigated this yet to see if it plays this role as well. Consequently, given adequate concentration of the species this process is self-sustaining. In turn, this means that unless the environment promoting hydrogen generation according to the postulated mechanism is upset due to season or other changes, significant hydrogen will be available to drive any active hydrogen-related mechanism. The end result is the formation of hydrogen that if adsorbed can promote other hydrogen-related processes, such as embrittlement, that in turn can drive TG cracking provided the other microstructural and loading conditions necessary for SCC are also met.

## Compatibility with High pH SCC and the Corrosion Observed with NN-pH SCC

The reactions leading to hydrogen generation postulated in the form of Reaction 3 provide a simple mechanism to rationalize crack initiation in near-neutral pH environments, favoring a solution pH that is buffered in the region of 6.4. Field results do show a preference for NN-pH SCC at such levels. However, field results also indicate the presence of shallow high-pH SCC typical of high pH SCC, which means any mechanism postulated as the basis for NN-pH SCC should be compatible with the classical form of SCC on pipelines. Field results also indicate corrosion occurs in the vicinity of NN-pH SCC. Thus, it is appropriate to more broadly evaluate the $CO_2 – H_2O$ environment to assess the consistency of the hydrogen-generation reactions postulated above with scenarios that could promote high-pH SCC and corrosion.

Pipelines are buried in soils where depending on the RoW both carbonaceous material and groundwater may be present. Formation of the carbonate-bicarbonate solutions that are the cracking environment for high-pH SCC have been explained as a consequence of the CP, which promotes the formation of hydroxyl ions that, in turn, facilitate the absorption of carbon dioxide derived from decaying organic matter in the soil. The balance of the species present and the temperature and amount of water available control the pH of the environment. This makes possible the reactions noted above as Reactions 1 and 2, whose equilibria are shown in Figure 2.

It follows that the $CO_2 – H_2O$ environment that can form under coating disbonds could vary appreciably along a pipeline, as well as seasonally, and is reversible depending on these factors. Scenarios where the $CO_2$ concentration is high and bicarbonate low favor the left-side of Figure 2 and the reaction noted above as Reaction 1. In contrast, cases where the $CO_2$ concentration is low and bicarbonate high favor the right-side in Figure 2 and the reaction noted above as Reaction 2.

## Compatibility and Interplay between Corrosion and High-pH SCC

Conditions along the pipeline RoW where the $CO_2$ concentration is high and bicarbonate is low favor the left-side in Figure 2 and the reaction noted above as Reaction 1. In reference to Figure 1, this occurs for pH less than 8.4.

At pH less than 6.4, the environment can become very acid in highly concentrated $CO_2$ solutions. By reference to Figure 1 or Reaction 1 the bicarbonate concentration would be proportionately reduced as the concentration of $CO_2$ increases. According to the reactions that underlie the postulated mechanism (Reaction 3), the proportional reduction in bicarbonate as pH decreases indicates less hydrogen is generated, because bicarbonate is the source of the hydrogen generation according to the postulated mechanism. Thus, a more acidic environment means the rate of cracking due to hydrogen-related mechanisms slows, whereas the rate of corrosion is increased. Under such circumstances, weight-loss corrosion occurs, as is the case for $CO_2$ pipelines. Such corrosion will broaden and deepen already existing crack-like features, although eventually down-crack conditions will dictate the response at the tips of deeper cracks. In contrast, corrosion will occur on the flanks of shallow cracking, obliterating characteristic traces of their origins, and corrosion focused at other stress raisers will promote the presence of pit-like features. Such results are consistent with the presence of pitting often observed with NN-pH SCC, and underscore why high-pH SCC when observed is typically limited to relatively shallow cracks.

At pH between 6.4 and 8.4, the process characterized by the postulated mechanism and the reactions in Reaction 3 occurs, but not as readily. As bicarbonate would initially be consumed to make iron carbonate, $H^+$ from the water must also be used in the reaction because only one $H^+$ is released from the bicarbonate and the electrons from the anodic reaction must be balanced. But, because the buffering capacity of such environments is not great, the pH will eventually drift to higher levels, becoming more basic and causing some carbonate to form. As this process continues, bicarbonate continues to decrease whereas carbonate increases. This creates the possibility that initially near-neutral environment biased toward pH 8.4 will transition toward the high-pH environment, eventually moving up the right hand line in Figure 2. In such cases it is possible the pH will tend to 10.4, where another buffering reaction occurs, implying the cracking mechanism changes to the classical high-pH case.

Subsequent shifts in solution pH driven by seasonal or other changes give rise to the possibility of mixed environments that swing between the two buffered states, or become more acidic or basic. It follows that the postulated mechanism is consistent with a mixed cracking morphology that swings between high-pH SCC and NN-pH SCC depending on local pH. Of course, the extent to which cracking occurs in these environments depends on factors such as local electrochemical potential and temperature. Lower temperatures will favor acidic conditions, as temperature is inversely proportional to the solubility of $CO_2$. Conversely, where the

environment shifts to control by active/passive corrosion and high-pH SCC, the extent of cracking will be strongly dependent on the local potential and the influence of the loading on the formation of microplastic strains at strain rates that favor crack tip dissolution. Shifts between these cracking mechanisms are very likely the reason that both IG and TG cracking are occasionally found on a given pipeline (e.g., Figure 1), or down a given crack.

It follows that the above mechanism is compatible with corrosion and observations of mixed cracking including high-pH SCC. Whereas the above discussion focused on conditions where the balance of controlling factors lead to initially higher concentrations of $CO_2$, and proportionately lower concentrations of bicarbonate, it is possible that the initial conditions produce a pH above 8.4. For such circumstances the reaction noted above as Reaction 2 governs. As implied above the postulated mechanism for hydrogen generation and related cracking given by the reactions in Reaction 3 give way to the circumstances that control the classical form of pipeline SCC. Thus, the postulated mechanism is fully consistent with classical cracking, and compatible with high-pH SCC that shows occasional TG traits. Such features simply imply swings out of the predominantly high pH environment, driven by reductions in pH possible within the $CO_2 – H_2O$ environment noted in reference to Figure 2.

Near-neutral cracking is unique because it only occurs within a narrow band of pH and is controlled necessarily by the chemistry of the $CO_2$-$H_2O$ environment. While selective in reference to pH and the chemistry of the $CO_2$-$H_2O$ environment, this process is less selective than high pH cracking, which involves additional conditional requirements in terms of a narrow range of electrochemical potential on the pipeline's surface coupled with microstructure that supports the evolution of microplastic strain and strain rate within a narrow window that facilitate local active/passive dissolution. Thus, the postulated mechanism suggests cracking due to hydrogen-related processes will be more prevalent than has been classical pipeline SCC. Significantly, the formation of carbonic acid from $CO_2$ is thermodynamically favored over temperature in the range between 10 and 35 ºC, which indicates near-neutral cracking is not limited to colder climates.

## Effect of Oxygen

It is instructive to consider the effect of oxygen on the generation of hydrogen (described above in Reaction 3) in the liquid underneath disbonded pipeline coatings. Reactions that describe the role of oxygen are presented as Reaction 4. There it becomes evident that oxygen can accelerate corrosion by contributing to an additional cathodic reduction reaction that forms $OH^-$. While this might be expected to raise the local pH, it does not in this instance because it can react with free $CO_2$, which then allows for its consumption as indicated in the reactions shown in Reaction 4:

$$\begin{array}{ccccccc} 2CO_2 & + & 2OH^- & \leftrightarrow & 2HCO_3^- & & \\ & & & & + & & \\ & & Fe & \leftrightarrow & Fe_2^+ & + & 2e^- \\ & & & & \downarrow & & + \\ & & & & FeCO_3 & + & 2H^+ \\ & & & & & & \downarrow \\ & & & & & & 2H(adsorbed) \end{array} \qquad (4)$$

According to these reactions, excess $OH^-$ does not result as it is consumed by reaction with free $CO_2$ to form bicarbonate that could react with iron cations to form $FeCO_3$, as in Reaction 3. By these reactions the presence of oxygen leads to additional hydrogen generation, furthering possible adsorption and embrittlement of the line pipe steel.

Low or intermittent levels of CP also would lead to the formation of $OH^-$, and so favor hydrogen generation and so promote adsorbed hydrogen as conditions permit. Of course, normal levels of CP would be expected to have the effect of limiting the iron oxidation part of the process. This precludes subsequent reactions with bicarbonate, thereby limiting hydrogen generation and the possibility of related hydrogen adsorption. Thus, while one might expect that $Fe(OH)_2$ would form as a result of the presence of large amounts of $OH^-$, $FeCO_3$ is ultimately the stable phase, so any intermediate hydroxide would be converted to iron carbonate at equilibrium.

## Establish Optimum Conditions for Kinetics via Beaker Studies

Given the source of hydrogen in the postulated mechanism derives from iron carbonate (equally other carbonate species), discriminating tests were designed to evaluate the role of environmental parameters beginning with conditions that maximize production of iron carbonate. Such testing was done by exposing coupons to the test environment and thereafter noting the results. Because the literature notes that NN-pH SCC is associated with the pipeline sections where CP was ineffective, or not working, these experiments were done under open circuit potential conditions.

### Experimental Procedures for Coupon Exposure Tests

Experiments have been done to evaluate the sensitivity and chemical boundaries of environments that could develop conditions where hydrogen evolution according to Reaction 3 is optimized. These tests exposed coupons of line-pipe steel to various carbonic acid/bicarbonate environments while pH was monitored with or without bubbling different concentrations of carbon dioxide through the solution. Test parameters were systematically varied to investigate the stability of these environments, which included:

- Initial concentration of sodium bicarbonate in solution,
- Flow of carbon dioxide with and without nitrogen, and
- Test temperature.

Solutions containing different concentrations of sodium bicarbonate ($NaHCO_3$), ranging from 0.1 to 10.0 g/l, were prepared in a beaker with an air-tight lid, with openings for gas inlet and outlet. Samples with total surface area of ~27.50 $cm^2$ were machined from a section of X65[6] line-pipe steel and polished to 1000 grit finish. Thereafter, the samples were cleaned with acetone, after which the samples were weighed. Samples were placed in the test beaker holding 750 ml of solution using a glass holder that exposed all sides to the solution, which for these tests lasted for at least two days. During this interval, the pH of the solution was regularly monitored. In tests where $CO_2$ was bubbled through the solution, flow rate was maintained using a mass flow meter. Temperature in each test beaker was maintained within ±0.2 $^oC$ of the test temperature by

[6] Details of the mechanical and other properties including steel chemistry are reported later in reference to related testing that considered this aspect. Suffice it here to note that the steel was typical of X65 in all respects. While the joint of pipe evaluated came from a pipeline that had experienced NN-pH SCC, this line-pipe steel did not suffer particularly significant NN-pH cracking.

placing the beakers in a water-bath. Some tests included consideration of the constituents of the NS4 solution (i.e. potassium chloride, magnesium sulfate or calcium chloride), either individually or in combination, in the same concentrations as for the NS4 solution.

At the end of each test, the samples were removed from the solution and weighed after drying. The solution in the test beaker was filtered to remove any precipitates from it. The precipitates and the remaining solution were further analyzed to determine their chemical composition after the test. Precipitates were typically treated with perchloric acid, $HNO_3$ and HCl to dissolve them and the volume brought back by adding deionized water. The resulting solution was analyzed by Inductively Coupled Plasma Emission (ICP) Spectroscopy. Similarly the test solution from the beaker after filtration was tested for metal ions using ICP. The concentration of carbonate or bicarbonate in the solution or precipitates was determined through titration method. The metal samples were removed from the test solution dried, weighed, and placed in a sealed plastic bag for further characterization of the surface scale by x-ray diffraction method.

Because of the scope and complexity of this testing a legend was needed to track the results for each set of test parameters. A number preceding the letters in the legend represent the concentration of the bicarbonate solution in grams per liter; while letters were used to represent the chemical constituents of the solution. The last component of the legend was a number that represents the temperature of the solution in Celsius units. This legend was used throughout, unless the test conditions are otherwise explained. Symbols used in this legend were as follows:

- **P or N** : Plain Bicarbonate solution
- **K**: Bicarbonate solution with Potassium Chloride (KCl)
- **C**: Bicarbonate solution with Calcium Chloride ($CaCl_2$)
- **M**: Bicarbonate solution with Magnesium Sulfate ($MgSO_4$)
- **KMC**: Bicarbonate solution with all three ($KCl+CaCl_2+MgSO_4$)

For example, **1K35** demotes a 1g/l bicarbonate solution with potassium chloride tested at 35$^o$C.

## Coupon Test Matrix and Related Analyses

Discriminating experiments were done to evaluate several aspects, as follows:

- effect of bicarbonate composition on iron carbonate formation, with and without bubbled $CO_2$ including carbon dioxide concentration/flow rate,
- role of constituents in NS solutions, particularly KCl, $MgSO_4$, $CaCl_2$,
- role of oxygen in the process and apparent hydrogen-generation mechanism, and
- role of temperature from 10ºC to 45ºC in the process and hydrogen-generation mechanism.

Solutions with different initial concentrations of sodium bicarbonate were prepared using deionized water after which the steel was immersed in the solution. One test series was initiated without bubbling gas, where the solution was exposed to the air. In two other test series, carbon dioxide gas (either 100% $CO_2$ or 5% $CO_2$) was bubbled through the test solution during the test. In all cases, changes in solution pH were regularly monitored over the duration of the test, which were done at 15º, 25º, 35º and 45$^o$C to evaluate the effect of temperature on the carbonic acid / bicarbonate reaction equilibrium.

As indicated in the text above, for all testing the results were developed or analyzed, as follows:

- pH of the solution was monitored at regular intervals,
- solution samples and precipitates were collected and analyzed for Fe, $CO^{3-}$, $Ca^{2+}$ , $K^{+}$, and $Mg^{2+}$,
- conditions favoring $FeCO_3$ were identified as were the effects of $Ca^{2+}$ , $K^{+}$ and/or $Mg^{2+}$, and
- samples removed from solution were dried and sealed in plastic bags for analysis of surface film/scale via x-ray diffraction to identify composition.

## Results – Effect of Bicarbonate Concentration and $CO_2$ on Solution pH

Results from the coupon exposure tests are shown in Figures 3 through 8, with the composition of initial solution shown in each figure. The usual pH range for published NN-pH SCC experiments is between 6 and 7, which is shown by the shaded area in each figure.

Tests were conducted at different temperatures and different initial concentrations of bicarbonate solution as shown in Figure 3. Solutions were exposed to the air, so the dissolution of carbon dioxide from air was allowed to dissolve in these test solutions. The pH measurements show values between 8 and 9, which are closer to the values expected in solutions containing large ratios of bicarbonate ions/carbonic acid concentrations, as was shown in Figure 2. As the temperature increased, the pH for any solution with a given bicarbonate concentration increased, as is expected. However, the change in pH with temperature is very small keeping the pH in the near-neutral range even at very low temperatures above the freezing temperatures.

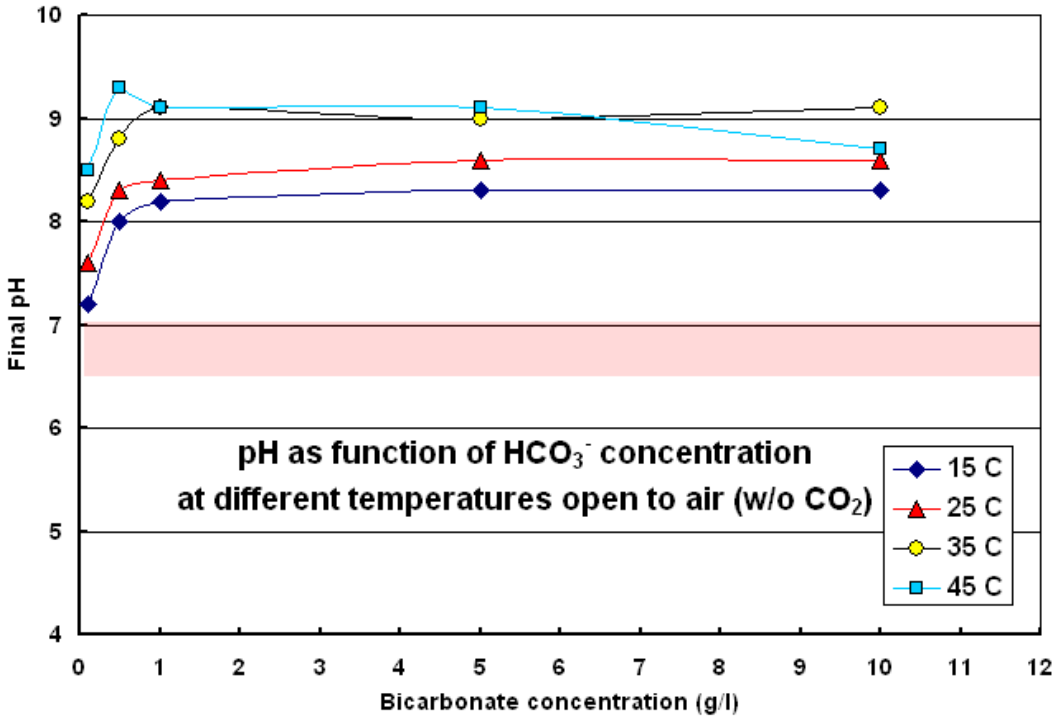


**Figure 3. Final solution pH as a function of bicarbonate concentration and temperature**

For next series of tests, pure carbon dioxide (100% $CO_2$) gas was bubbled through the solution throughout the test. Due to formation of carbonic acid in these solutions, the pH for solutions with very small concentrations of bicarbonate ions was between 4.5 and 5.5, as is shown in Figure 4. This is similar to the pH predicted by thermodynamic calculations for the situation where the $H_2CO_3/HCO_3^-$ ratios are high. Equilibrium pH at 15°C for the solutions with about 5 g/l bicarbonates or higher was in the range of NN-pH values. Addition of constituents that comprise the NS4 solution, at the same concentrations as in NS4 solution, did not have any significant effect on the equilibrium or the resulting pH.

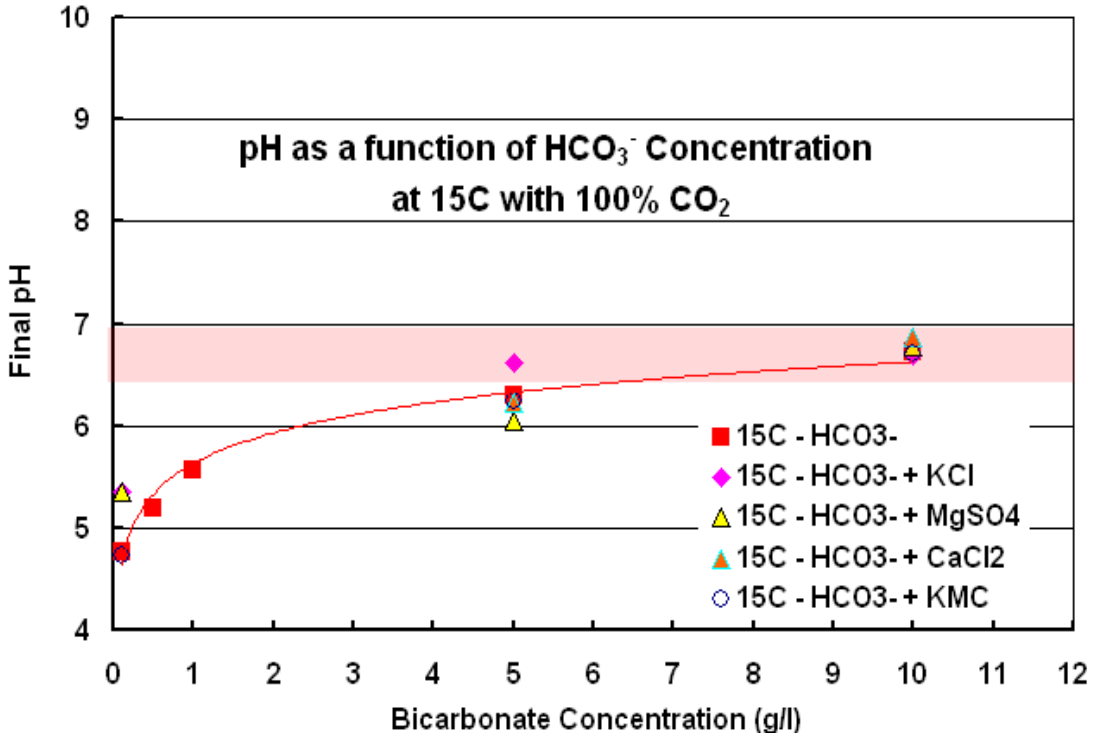


**Figure 4. Solution pH over time for coupon tests (15°C with 100% $CO_2$ bubbled gas)**

At higher temperatures, the value of pH is expected to be slightly higher for any given solution. Therefore, the NN-pH range may be attained for a dilute solution at higher temperatures. Tests at higher temperatures were not carried out with pure carbon dioxide bubbling as the results from other tests could be used to predict solution behavior at different temperatures.

Results in Figures 5 to 8 involve coupon exposure tests where a 5% $CO_2$ + $N_2$ gas mixture was bubbled through the solution with different initial concentration of bicarbonate at different temperatures. Comparing data in Figure 5 with data in Figure 6, as expected, the results show that the equilibrium pH for the solutions with 5% $CO_2$ is higher than that for solutions with 100% $CO_2$. A pH in the range of typical NN-pH SCC related field values can be attained for very dilute solutions when the $CO_2$ availability is lower, as may happen in the field, where $CO_2$ supply to the area of interest may be limited.

The equilibrium pH for bicarbonate solutions with 5% $CO_2$ at 25°, 35° and 45°C are shown in Figures 6, 7, and 8, respectively. Results from these curves support the previous observation that the pH in near-neutral range can be attained for more dilute bicarbonate solutions at higher

temperatures. Thus, as expected, the value of pH increases with temperature for any solution under otherwise similar conditions.

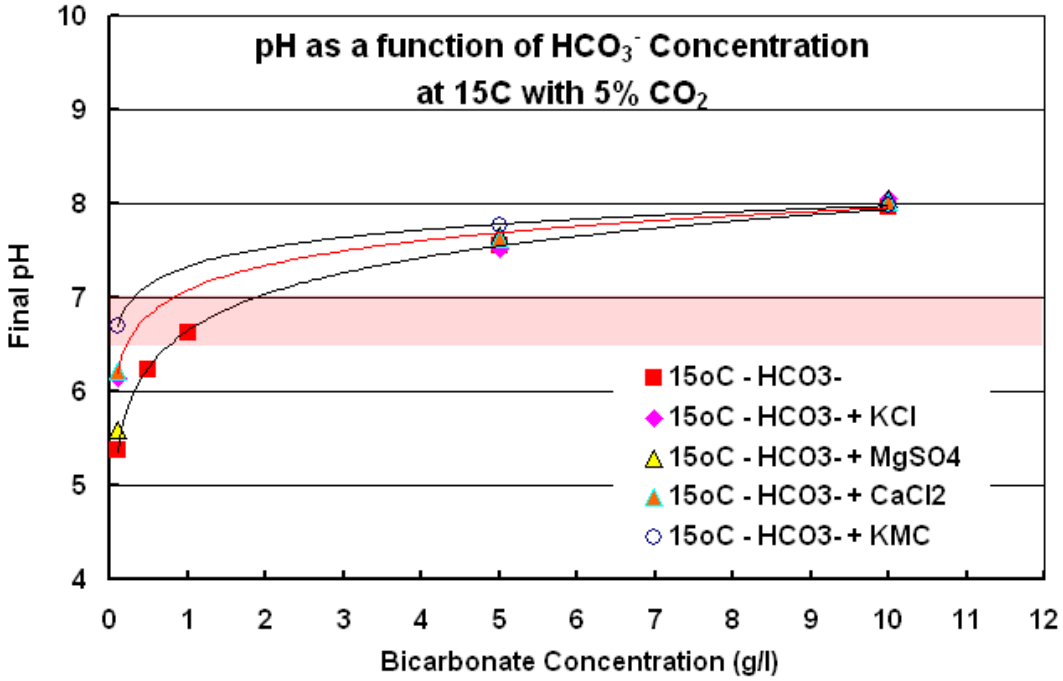


**Figure 5. Solution pH over time for coupon tests (15ºC with 5% CO2 gas - N2 Balance)**

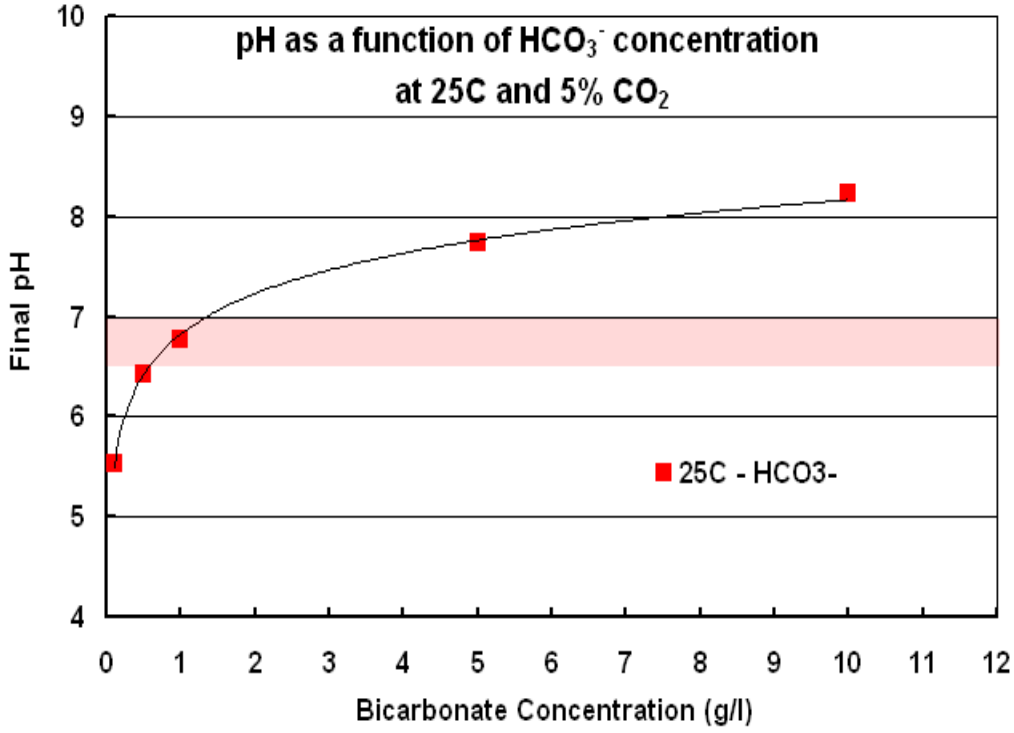


**Figure 6. Solution pH over time for coupon tests (25ºC with 5% $CO_2$ gas - $N_2$ Balance)**

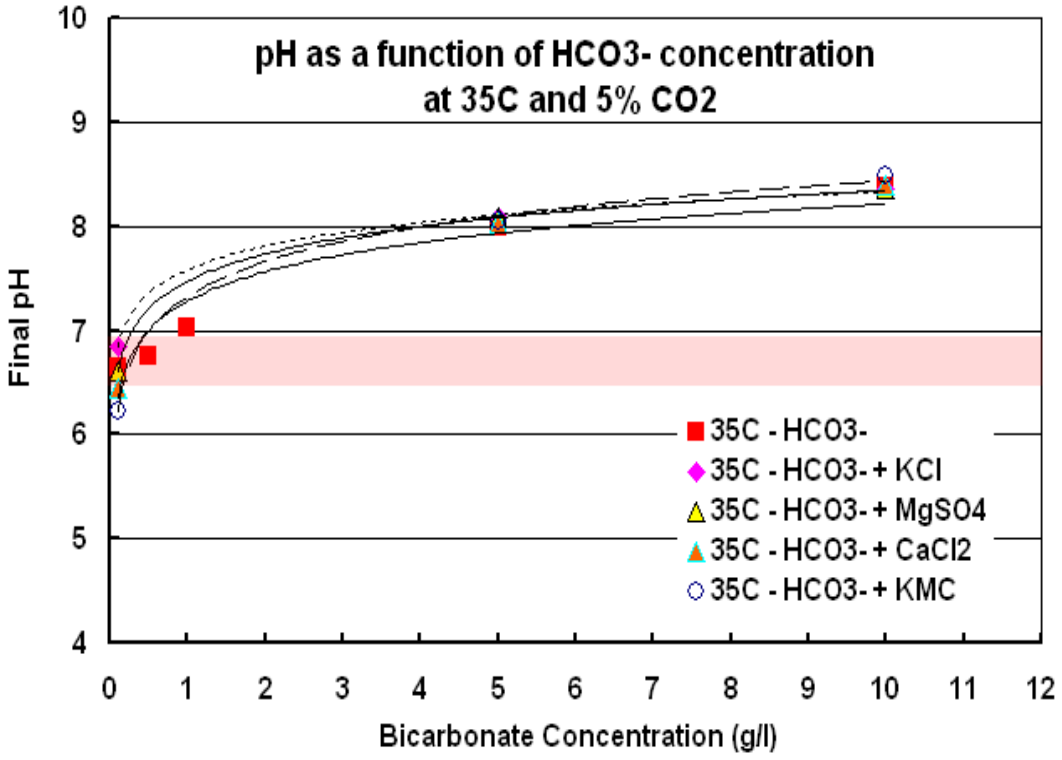


**Figure 7. Solution pH over time for coupon tests (35ºC with 5% $CO_2$ gas - $N_2$ Balance)**

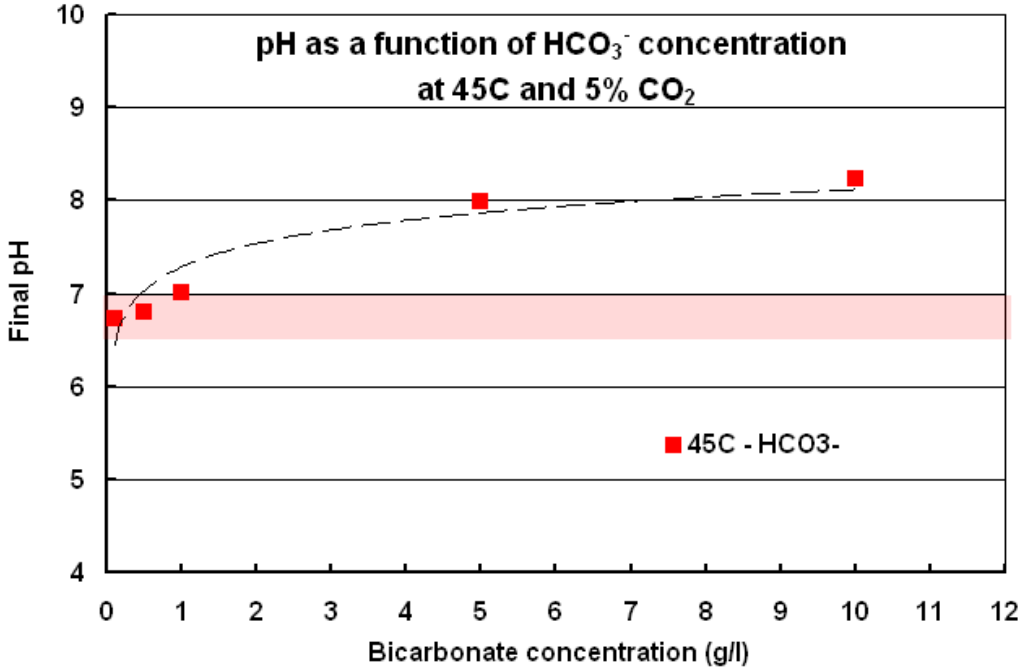


**Figure 8. Solution pH over time for coupon tests (45ºC with 5% $CO_2$ gas - $N_2$ Balance)**

## Results – Composition of Solution and Precipitates after Coupon Exposure

The postulated hydrogen generation mechanism develops hydrogen in relation to the formation of iron carbonate. The extent of this reaction evident in Reaction 3 can be quantified by measuring the total formation of iron carbonate. Iron carbonate can be either in the solution, or precipitate out in the solution, or it could be deposited on the coupon's surface.

Chemical analysis was done to identify iron carbonate in the solution, either as a precipitate in solution, or deposited on the coupon's surface. After each test the solution in the test beaker was filtered to remove precipitates, which were dissolved in acid and the volume of the resulting solution was adjusted by adding deionized water. As noted earlier, ICP Spectroscopy was used to analyze the resulting solution. Likewise, the solution was tested for metal ions using ICP, with the concentration of carbonate or bicarbonate in the solution or precipitates determined via titration. Finally, x-ray diffraction was used to detect iron carbonate on the coupon surface.

Results for testing with $CO_2$ bubbled into the solution are shown in Table 2. These results indicated that the corrosion products formed in bicarbonate containing solutions at 15$^{o}$C, with 100% $CO_2$, are largely insoluble. Insoluble precipitates formed under these conditions contain 40 to 50 weight-percent of iron. The addition of NS4 constituents for these test conditions did not change the concentration of iron ions in the solution or in the precipitates.

**Table 2. Iron ion concentration at the end of coupon exposure tests at 15$^{o}$C**

**a) different bicarbonate concentrations**

| Bicarbonate Conc. gm/l | Fe concentration mg/l in solid / mg/kg in precipitate |
|---|---|
| 0.1 | 6.04 / 490000 |
| 0.5 | 0.357 / 493000 |
| 1 | 0.054 / 496000 |
| 5 | 0.088 / 456000 |
| 10 | 0.666 / 478000 |

**b) different bicarbonate concentrations and NS4 constituents**

| Additional chemicals in Test Solution | Fe concentration, mg/l in solution / mg/kg in precipitates | | |
|---|---|---|---|
| | Bicarbonate concentration,gm/l | | |
| | 0.1 | 5 | 10 |
| KCl | 7.04 / 396000 | 0.21 / 492000 | 0.006 / 327000 |
| $MgSO_4$ | 23.5 / 510000 | 0 / 505000 | 0.009 / 488000 |
| $CaCl_2$ | 10.1 / 592000 | 0 / 478000 | 0.081 / 351000 |
| KCl +$MgSO_4$ +$CaCl_2$ | 37.5 / 511000 | 0.023 / 454000 | 0.235 / 419000 |

The results indicate there were no soluble carbonates in the solution; however, there were carbonates in the precipitates. The concentration of carbonate in the precipitates indicates the presence of some iron carbonate, with the bulk being predominately oxides of iron.

Extensive tables also were developed to evaluate trends for the broad matrix of test parameters considered, as the basis to screen environmental conditions most likely to promote NN-pH SCC in pipeline steels if the hydrogen-generation mechanism is viable. The trends indicate that the carbonates were only detected in loose precipitates which were filtered out of the solution. The addition of calcium ions in the solution favors the formation of carbonate precipitates (possibly calcium carbonate). This will facilitate the generation of hydrogen in the same way as iron ions may participate in the hydrogen-generation mechanism noted earlier. Some bicarbonate also was found in the precipitates. Again, the addition of calcium ions to the solution affects the bicarbonate concentration in the precipitates, in the same way as it affects the formation of carbonate precipitates. However, the concentration of solution bicarbonates was not affected by the addition of NS4 solution constituents. In the $CaCl_2$ containing solution, precipitates had lower levels of iron as compared to the others. The calcium composition in the precipitate suggests that carbonates and bicarbonates of calcium may be a significant part of the insoluble precipitates for such test conditions. For tests where carbon dioxide was bubbled through the solution, the precipitates contained iron, but mostly as an oxide, as the concentration of carbonate is very small in the solution or precipitates in general. There were however a few conditions where measurable quantities of iron carbonate were detected on the sample.

## X-Ray Diffraction of Coupon Surfaces

Surface films of the exposed coupons were characterized to determine if iron carbonate formed on the steel's surface under the test conditions evaluated. Tables 3a, 3b, and 3c summarize the x-ray diffraction results, which indicate whether or not iron carbonate was formed (ND in the table means none detected). Of significance is the observation that iron carbonate was not detected for any coupon tested when $CO_2$ was not bubbled through the test solution.

The tabulated data indicate that for different concentrations of bicarbonate solutions at 15$^{o}$C, with 100% $CO_2$, iron carbonate was not detected by x-ray diffraction on the coupon's surface, which also was the case with the addition of NS4 constituents did not lead to iron carbonate precipitation on the coupon's surface. In contrast, iron carbonate was detected on the coupon's surface for testing at temperatures above 25$^{o}$C for tests with 5% $CO_2$ + $N_2$ bubbled through the solution. Results in Table 3b indicate that iron carbonate precipitation on the steel surface was favored for solutions with concentrations of bicarbonate in the solution of 0.5 g/l or higher. Higher temperatures also favored precipitation on the coupon's surface. Conditions where $FeCO_3$ was not detected on the coupon's surface may also form iron carbonate in the solution or as precipitates in the solution. However, test conditions where iron carbonate was formed on the surface of the sample give clear indication of the possibility of hydrogen generation due to bicarbonate reactions, as follows from earlier discussion in reference to Figure 2.

**Table 3. Presence of iron carbonate on the coupon surface**

**a) bicarbonate only as well as bicarbonate and NS4 constituents at 15ºC for 100% $CO_2$**

| Bicarbonate concentration, g/l | Temperature 15ºC | Additional chemicals | film vs Bicarbonate concentration, g/l | | |
|---|---|---|---|---|---|
| | | | 0.1 | 5 | 10 |
| 0.1 | ND | | ND | ND | ND |
| 0.5 | ND | KCl | ND | ND | ND |
| 1 | ND | $MgSO_4$ | ND | ND | ND |
| 5 | ND | $CaCl_2$ | ND | ND | ND |
| 10 | ND | KCl +$MgSO_4$ +$CaCl_2$ | ND | ND | ND |

**b) temperature and bicarbonate concentration varied for 5% $CO_2$+ 95% $N_2$**

| Bicarbonate concentration, gm/l | Surface film after exposure | | | |
|---|---|---|---|---|
| | 15 ºC | 25 ºC | 35 ºC | 45 ºC |
| 0.1 | ND | ND | ND | ND |
| 0.5 | ND | ND | $FeCO_3$ | ND |
| 1 | ND | ND | ND | $FeCO_3$ |
| 5 | ND | ND | $FeCO_3$ | $FeCO_3$ |
| 10 | ND | ND | $FeCO_3$ | $FeCO_3$ |

**c) temperature and bicarbonate concentration varied with NS4 constituents for 5% $CO_2$+ 95% $N_2$**

| Additional chemicals | Carbonate concentration, mg/l in solid / mg/kg in precipitates | | | | | |
|---|---|---|---|---|---|---|
| | Bicarbonate concentration, g/l, at 15 ºC | | | Bicarbonate concentration, g/l, at 35 ºC | | |
| | 0.1 | 5 | 10 | 0.1 | 5 | 10 |
| KCl | ND | ND | ND | ND | $FeCO_3$ | $FeCO_3$ |
| $MgSO_4$ | ND | ND | $FeCO_3$ | ND | $FeCO_3$ | $FeCO_3$ |
| $CaCl_2$ | ND | ND | ND | ND | $FeCO_3$ | $FeCO_3$ |
| KCl +$MgSO_4$ +$CaCl_2$ | ND | ND | $FeCO_3$ | ND | $FeCO_3$ | $FeCO_3$ |

## Hydrogen Sources Evaluation

The postulated hydrogen generation mechanism produces hydrogen release from the bicarbonate as compared to hydrogen produced from cathodic reduction, which to this point has been the previously postulated source of hydrogen. A series of preliminary experiments and calculations has been done to compare the hydrogen generated from these sources, specifically considering hydrogen generation at 15°C in reference to reactions leading to iron carbonate. The

experiments were designed to compare the metal weight loss along with the corresponding hydrogen expected based on analysis of iron carbonate precipitation measurements. The results indicated an order of magnitude increase in total hydrogen produced via the mechanism postulated here as compared to that expected from the hydrogen reduction reaction alone. While in general the amount of hydrogen generated depends upon the temperature and other species that can contribute to the process, these calculations indicate the hydrogen generation mechanism can significantly increase adsorbed hydrogen available for diffusion into the steel.

### Summary for Coupon Testing

Throughout, the amount of iron carbonate formed was found to be negligible in tests where no carbon dioxide was bubbled through the test solutions. Hydrogen generation as postulated above is not expected to dominate in such environments. However, hydrogen generation due to cathodic reaction to counter the anodic dissolution of iron still occurs for these conditions.

The tabulated data in conjunction with Figure 2 and Figures 3 through 8 indicate that iron carbonate is formed across a broad range of idealized laboratory conditions, in otherwise quite dilute solutions. If the hydrogen-generation mechanism is validated as practically significant in subsequent crack nucleation experiments, these trends indicate NN-pH SCC can be anticipated in the field under a broad range of RoW parameters, although there will be selectivity in reference to the formation of carbonates.

Significantly, for US operators the results indicate that hydrogen-generation by the postulated hydrogen-generation mechanism supporting NN-pH SCC occurs from quite low temperatures, up through temperatures the order of 35ºC and higher. If cracking associated with this hydrogen-generation mechanism is found with the traits observed for NN-pH SCC in the testing reported in the next section, then these results indicate NN-pH SCC can occur across a wide range of geographical conditions – from the north of the US through the southern most states. Thus, the range of conditions found promoting such hydrogen generation indicate NN-pH SCC could occur throughout the US and Canada where the groundwater involves $CO_2$, carbonate, and bicarbonate. Other areas in the world with similar geology and temperatures, with suitable groundwater conditions, would be equally susceptible to this form of SCC. In contrast to high-pH SCC, such environments are simpler to develop – such that NN-pH SCC is anticipated to be more pervasive – all else being equal.

## Establish Viability of Mechanism via Crack Nucleation

Several discriminating experiments were devised to evaluate the mechanism postulated in reference to the reactions in Reactions 3 and 4 in terms of the cracking it generates. These experiments focused first on conditions that maximized the formation of $FeCO_3$, and thereafter determined whether cracking could be initiated under conditions that favored formation of $FeCO_3$ consistent with the postulate, and if so whether the morphology of that cracking was consistent with that observed in the field. These experiments included cases designed to determine if cracking can be turned on or off as the mechanism suggests, by selected changes to the environment in very specific ways. These experiments utilized the slow strain rate test (SSRT) practice[38] to screen cracking response, to determine whether cracking could indeed be initiated in reference to the reactions in Reactions 3 and 4 and if so, whether the crack morphology was consistent with that observed in the field. Environmental conditions throughout reflect nothing more severe than typical of the NS solutions.

The steel used in the SSRT was the same as that for the coupon testing, the results for which are shown in part in Table 4. As is evident from Table 4, SSRT were completed using an extension rate of 1 x $10^{-6}$ in/sec or 2 x $10^{-7}$, which for the 1-inch gauge length provided the same nominal strain rate in seconds$^{-1}$. In all cases the test temperature was 27 C (80 F). The environment was selected to evaluate possible cracking using only the species relevant to the postulated hydrogen generation mechanism, with the expectation that cracking would correlate with hydrogen generation if NN-pH SCC is driven by a hydrogen-related cracking process. Thus, cracking

**Table 4. Slow strain rate test results for a variety of environmental conditions**

| ID | Strain Rate (sec$^{-1}$) | Environment | Time to Failure hrs | % RA | Secondary Cracking (Y/N) |
|---|---|---|---|---|---|
| 1 | 1 x $10^{-6}$ | Inert (Reference Condition) | 60 | 48.9 | No |
| 2 | 1 x $10^{-6}$ | 1 g/l $NaHCO_3$ + $CO_2$ + air; pH 6.4 | 52 | 24.7 | Yes |
| 3 | 1 x $10^{-6}$ | 1 g/l $NaHCO_3$ + $CO_2$ + air; pH 6.4 | 46 | 27.7 | Yes |
| 4 | 1 x $10^{-6}$ | 1 g/l $NaHCO_3$ only; pH 8.3 | 51 | 44.0 | No |
| 6 | 1 x $10^{-6}$ | $CO_2$ only; pH 4 | 48 | 19.0 | No |
| 7 | 1 x $10^{-6}$ | $CO_2$ only; pH 4 to 5.6 | 47 | 29.0 | No |
| 9 | 1 x $10^{-6}$ | Ultrapure $H_2O$ – One time adjust of pH via $CO_2$ to 6.5 | 68 | 35.6 | No |
| 10 | 2 x $10^{-7}$ | 1 g/l $NaHCO_3$ + $CO_2$; pH 6.4 | 342 | 24.4 | Yes |
| 11 | 2 x $10^{-7}$ | 1 g/l $NaHCO_3$ + $CO_2$ + air; pH 6.4 | 297 | 18.4 | Yes |
| 12 | 2 x $10^{-7}$ | Inert | 493 | 43.5 | No |
| 13 | 2 x $10^{-7}$ | 1 g/l $NaHCO_3$ only; pH 8.4 | >510 | Test abandoned; No corrosion or cracking evident | |

environments involving only sodium bicarbonate and carbon dioxide were used in lieu of the more complex chemistry of the NS series of environments reported in the literature. Air was also bubbled into the aqueous environment in some cases to test the acceleration of the production of hydrogen, in accordance with the reactions discussed above in Reaction 4. The solution was made up with distilled water and initially contained 1 g/l $NaHCO_3$. Thereafter, $CO_2$ was then bubbled through the solution at a specific rate to fix the pH.

As can be seen from Table 4, the ductility of all the specimens tested in the environment at pH 6.4 was less than that found from an inert environment test. In addition, some secondary cracking was observed in addition to the primary fracture, indicating embrittlement. Inspection of Table 4 indicates more than a factor of two area reduction (% RA), with secondary cracking occurring where hydrogen generation was maximized according to the mechanism postulated in

Reactions 3 and 4. Increased acidity failed to produce cracking, although significant area reduction was evident. Air bubbled into the environment produced further area reduction in the case where the strain rate was lowest, which apparently facilitates greater discrimination through increased adsorbed hydrogen because of the longer test duration. While the results were limited, the trends all were consistent with expectations based on the postulated mechanism. As the cracking tracked the increased hydrogen available for absorption, the results imply NN-pH SCC evident in these results reflects a hydrogen-related mechanism.

## Laboratory Crack Morphology versus the Field

The specimen surface and cross-sectional metallography of one specimen is shown in Figure 9. The view to the left in this figure shows clear evidence of long rather straight cracking consistent with what would occur for NN-pH SCC. Extensive, deep multiple cracking is also evident, as are white precipitates (iron carbonate). This typical cracking for these experiments initiated and continued to grow on a smooth test specimen, in a simple cracking environment involving a solution of carbon dioxide and bicarbonate at pH 6.4. The view to the right in this figure shows a cross-section through another sample tested under comparable conditions through an area of shallower cracking. Very shallow cracks whose flanks are corroded can be seen, along with evidence of a tight crack continuing from that corroded feature, which is encircled by an ellipse. Also evident is a crack whose depth is the order of 100 microns, whose morphology is clearly TG. This crack also shows evidence of growth from its tip, as well as the presence of a crack like region ahead of its tip, as would be expected with hydrogen embrittlement. Again these features are encircled by an ellipse.

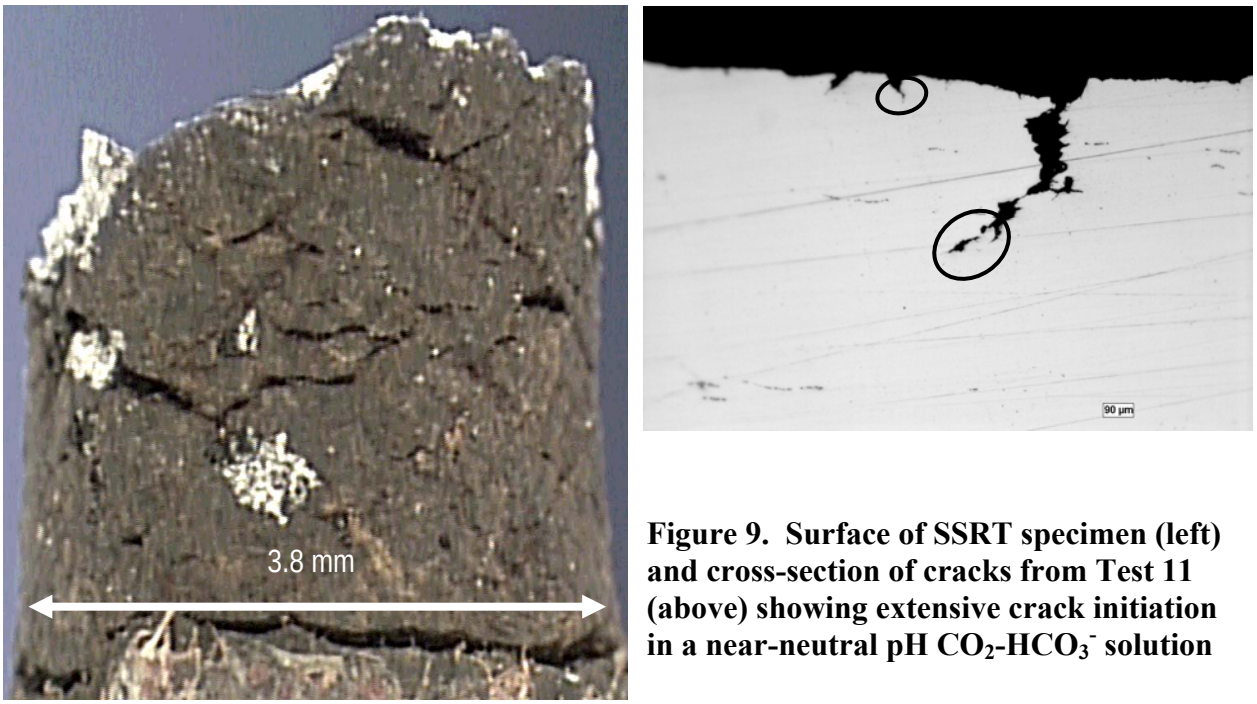


**Figure 9. Surface of SSRT specimen (left) and cross-section of cracks from Test 11 (above) showing extensive crack initiation in a near-neutral pH $CO_2$-$HCO_3^-$ solution**

For comparison, Figure 10 presents the morphology of shallow cracking observed in a sample removed from the field. The scale of magnification here is comparable to that of the cross-section shown in Figure 9. Comparison of the features evident here to those shown for the laboratory cracking show comparable features. Although there is less evidence here of flank

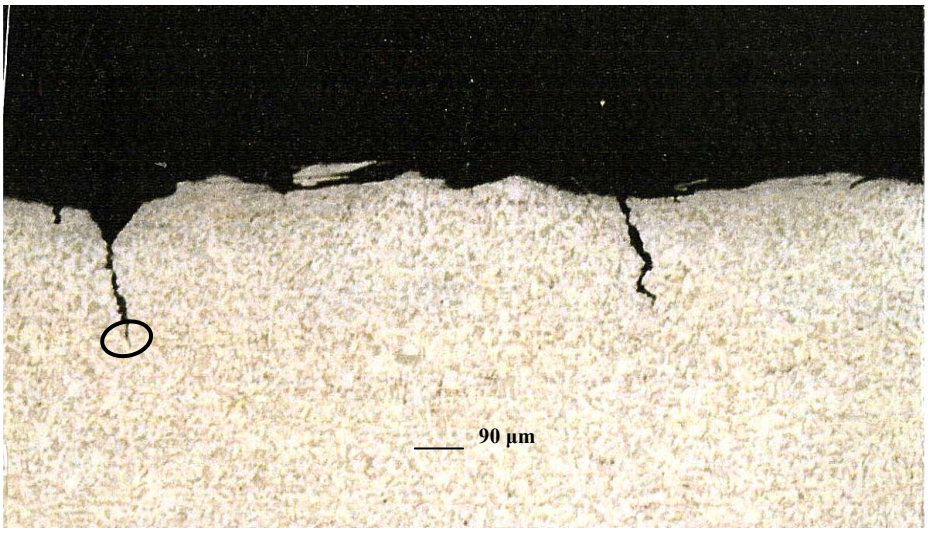


**Figure 10. Cross-section from the field – this morphology is comparable to Figure 9**

corrosion, both of the deeper cracks show the same sharpened crack tip evident in Figure 9. As in Figure 9, this sharpened tip is encircled for the left-most crack. It follows that the morphology of the laboratory cracking is consistent with cracking found in the field.

## Hydrogen Sources Evaluation

The postulated hydrogen generation mechanism produces hydrogen release from the bicarbonate as compared to hydrogen produced from cathodic reduction, which to this point has been the previously postulated source of hydrogen. A series of preliminary experiments and calculations has been done to compare the hydrogen generated from these sources, specifically considering hydrogen generation at 15 °C. The experiments were designed to compare the metal weight loss along with the corresponding hydrogen expected based on analysis of iron carbonate precipitation measurements. The results indicated an order of magnitude increase in total hydrogen produced via the mechanism postulated here as compared to that expected from the hydrogen reduction reaction alone.

While in general the amount of hydrogen generated will depend upon the temperature and other species that can contribute to the process, these calculations indicate the postulate hydrogen generation mechanism can significantly increase adsorbed hydrogen available for diffusion into the steel. This aspect is dealt with in detail in a subsequent section.

## Summary for Viability

The simple hydrogen-generation mechanism postulated in the first section leading to NN-pH SCC has been evaluated via discriminating tests using environments predicted to drive hydrogen-related cracking in contrast to those predicted not to. In all cases the results matched the predictions, indicating that that cracking can be turned on and off in the laboratory according to the proposed mechanism. Consistency of the trends predicted by the postulated mechanism and field observations lend credence to it, which is further supported by consistency in the cracking morphology. Although the data are limited, this consistency lends support to its underlying near-neutral pH cracking. As cracking correlated with hydrogen generated and available for absorption, the results indicate NN-pH SCC is driven by a hydrogen-related mechanism, which

the present results indicate involves embrittlement. Thus, the hydrogen generation mechanism was validated.

Significantly, while NN-pH SCC has been viewed by some to be associated with low-temperature climates, the mechanism postulated and demonstrated herein indicates near-neutral pH cracking is possible at temperatures at or slightly beyond 35°C. Near-neutral pH cracking motivated by hydrogen generation as described here is consistent with a lack of, or inconsistent CP on the pipeline. The presence of adequate CP would limit the near-neutral mechanism for two reasons. First, the lack of iron cations caused by CP would therefore limit the hydrogen released from bicarbonate, and second, effective CP would provide local alkalization and would therefore promote a shift in pH toward the other buffered region of pH of Figure 2, possibly setting the stage for high pH cracking instead. In this context it is not hard to visualize that the pH might cycle from one buffered region to the other, i.e., 6.4 to 10.3, depending upon intermittent CP, the ability to drive the pH more acid with $CO_2$ or other cations, and how dilute the solution is during these processes. Higher concentrations would be expected to take longer for any shifts to occur.

## Establish Field Criteria for Severity Assessment

While analytical work has been done to characterize the response of cracking in colonies of SCC referenced to high-pH cracking, little has been done to explore the response of NN-pH SCC. If it can be shown that NN-pH and high-pH SCC show similar cracking traits – aside from inherent differences in the role of grade and toughness of the steels involved – then the analytical work demonstrated viable for high-pH scenarios can be applied with little further work without regard to the cracking environment. This section assembles data developed from serial grinds of field colonies to characterize crack length and depths in these colonies. The practices used to generate data are the same as were developed and used previously[39]. Circumferential and axial crack spacings have been developed using such practices for a range of colonies for operational cases ranging from benign to critical. Results representing benign scenarios have been gathered for colonies remote to failures, whereas that for critical conditions reflect data gathered from crack origins for ruptures that occurred during hydrotesting or in-service. Logically, data for benign cases represent shallower or shorter cracking than for failures – all else being equal. The data represent SCC occurring in Canada, the US, and Australia. Results for high-pH cracking are shown as black symbols, while those for NN-pH are shown as red symbols.

Figure 11 presents results for field SCC ranges that from depths shallower than 0.0025 up to depths of ~0.0225 inch (0.06 to 0.13 mm). It is evident from this figure that when very shallow this cracking has an aspect ratio (length/depth) the order of unity, which is consistent with point-source response as might be expected to isolated SCC. However, as these cracks grow and become deeper, this aspect ratio increases significantly, to the order of ten. As is evident from this figure, the aspect ratio remains low for very shallow depths, but begins to transition to much higher values with some scatter at depths beyond about 0.005 inch (0.12 mm). In contrast, the adjacent surface tips for cracks deeper than 0.015 inch (0.38 mm) begin to show the effects of coalescence leading to increasingly longer cracks. Such cracks also show the effects of dormancy and shielding from the effects of the hoop stress in the wall, as the trend to increased crack depth diminishes as the cracks lengthen. These trends are consistent with the predictions of fracture mechanics[28]. There is a strong central tendency evident in Figure 11 for high-pH SCC whereas the red symbols for NN-pH cracking for colonies in several different pipeline

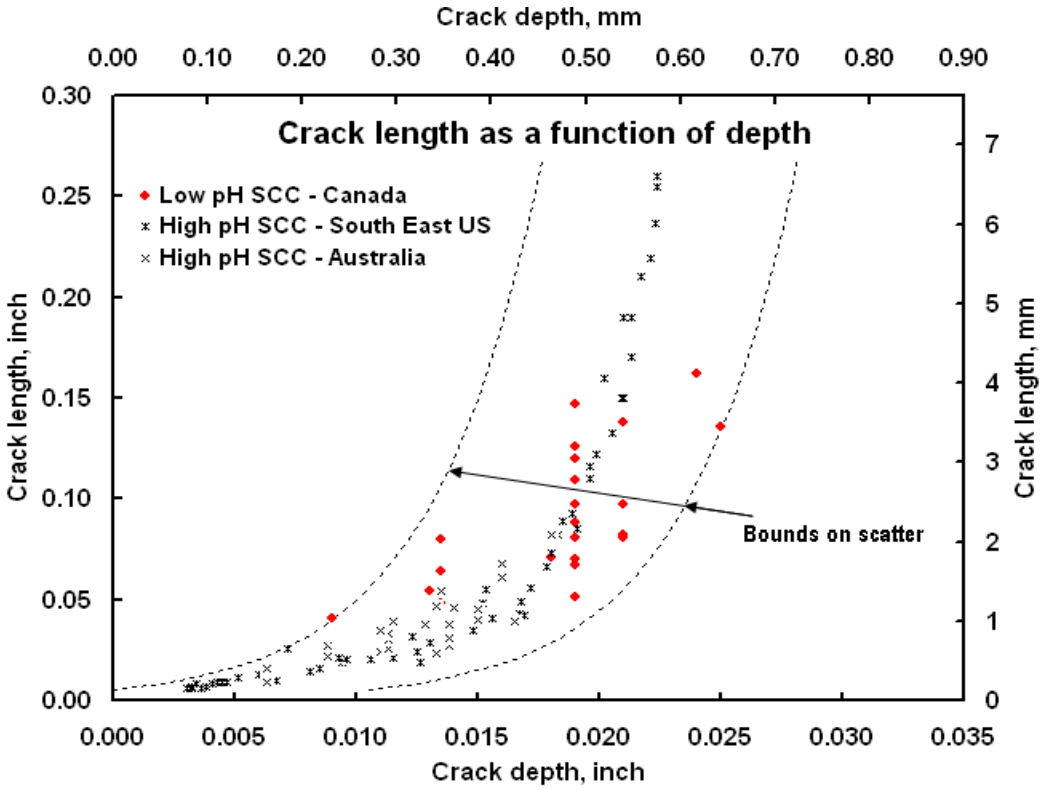


**Figure 11. Crack aspect ratio versus length for both types of SCC remote to failures**

valve sections in different pipelines scatter about this central tendency. There is no clear difference between the data in these two data sets.

Figure 12a presents crack length as a function of depth again for a range of colonies within a range of pipelines experiencing high-pH SCC as well as NN-pH SCC. Depths run up to 0.20 inches (~5.1 mm) in lengths up to 2 inches (~51 mm), with this cracking representing a mix of dense and sparse colonies for both forms of cracking. It can be seen that the NN-pH results lie within the bounds for the high-pH SCC, with comparable scatter. As such these data in this format do not imply any difference in the cracking for either environment. Figure 12b considers the same data although the crack length has been truncated to open up the plot and more clearly separate the data. The y-axis in this case is the crack aspect ratio, D/t plotted as a function on crack length. In this format it is clear that the results do not show any clear differences between the two cracking environments.

As the results in Figure 12 represent a range of wall thickness for pipelines operating at MAOP in Class 1 service, it is possible that some bias exists as a function of differences in relative crack depth. Figure 13 addresses this possibility plotting the aspect ratio from Figure 12b as a function of crack depth normalized by the wall thickness, D/t. As a mix of dense and sparse colonies is represented in Figure 12, these data reflect values of D/t up through ~0.55. The longer, deeper cracking regardless of the cracking environment reflects the response of the tougher steels in each of the databases, as larger cracking would not remain stable otherwise. As for Figure 12, in this format the NN-pH results lie within the bounds for the high-pH SCC, with comparable scatter. As such these data in this format do not imply any difference in the cracking as a

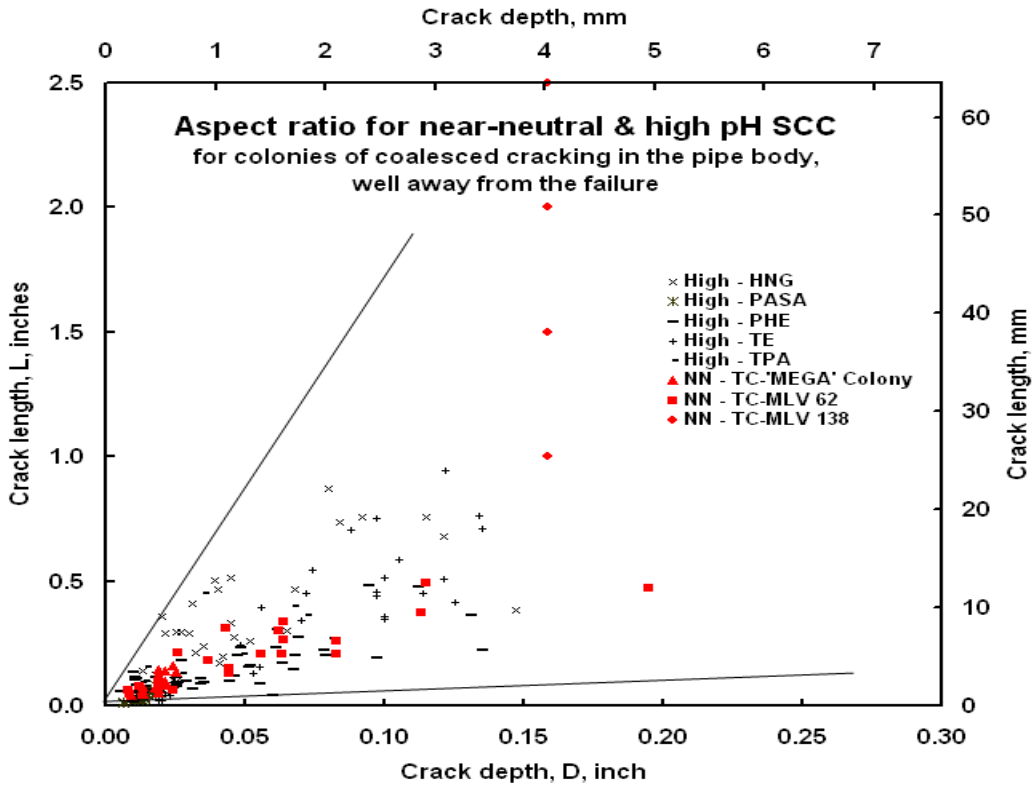


**a) L versus D**

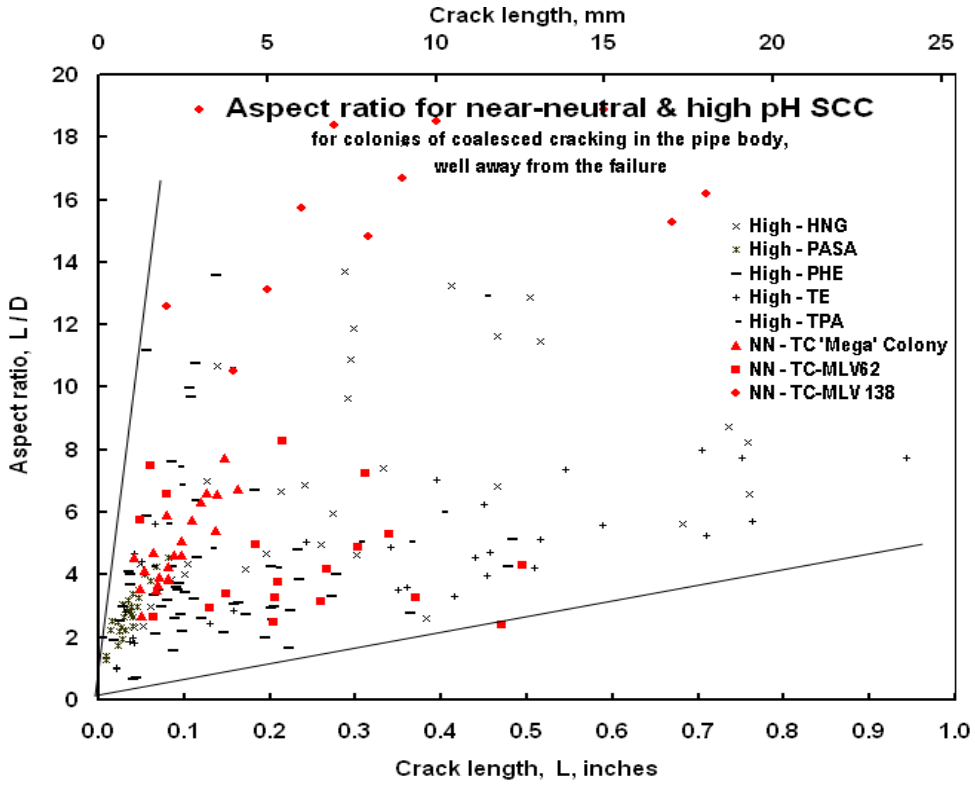


**b) L/D versus L**

**Figure 12. Cracking characteristics versus coalesced crack length remote to failures**

function of environment. While a role of hydrogen is evident in Table 4 as reduced elongation and apparent embrittlement at a local scale for SCC in the NN-pH environment, macroscopic embrittlement and reduced apparent toughness is not evident in Figure 13, as the data show similar scatter and results for the NN-pH environment develop long, deep, stable cracking.

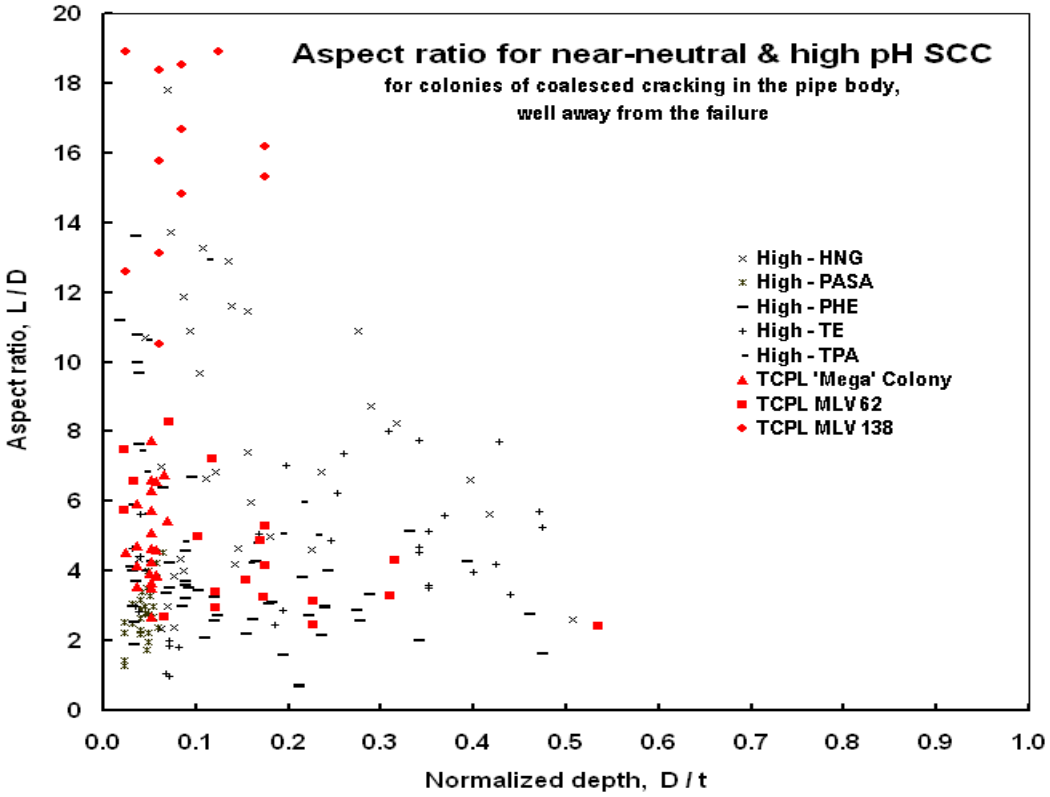


**Figure 13. Cracking characteristics versus D/t remote to failures**

Figures 14a and 14b involve SCC along failure planes for hydrotest and in-service failures. The data in these figures support the just noted view that macroscopic embrittlement and reduced apparent toughness does not develop. Again, the data exhibits similar scatter and results for the NN-pH environment develop long, deep, stable cracking. Figure 14a indicates this in reference to crack length as a function of crack depth normalized by the wall thickness. Figure 14b shows there is no bias in the results of Figure 14a in regard to crack depth, as the y-axis in this figure is crack aspect ratio.

## Summary for Cracking Characteristics

This task evaluated the potential utility of technologies developed and demonstrated for high-pH SCC in applications to NN-ph scenarios. This was done contrasting similarities and differences for field cracking developed by SCC in NN-ph and high-pH environments. Data determined for hundreds of cracks did not indicate clear differences. Regardless of the circumstances compared, field cracking from dense to sparse colonies, and at failures do not imply any difference in the cracking as a function of environment. As such, the fracture mechanics based technologies and modeling results developed for high-pH scenarios could be adapted for NN-pH applications with only limited case-specific validation for that cracking environment.

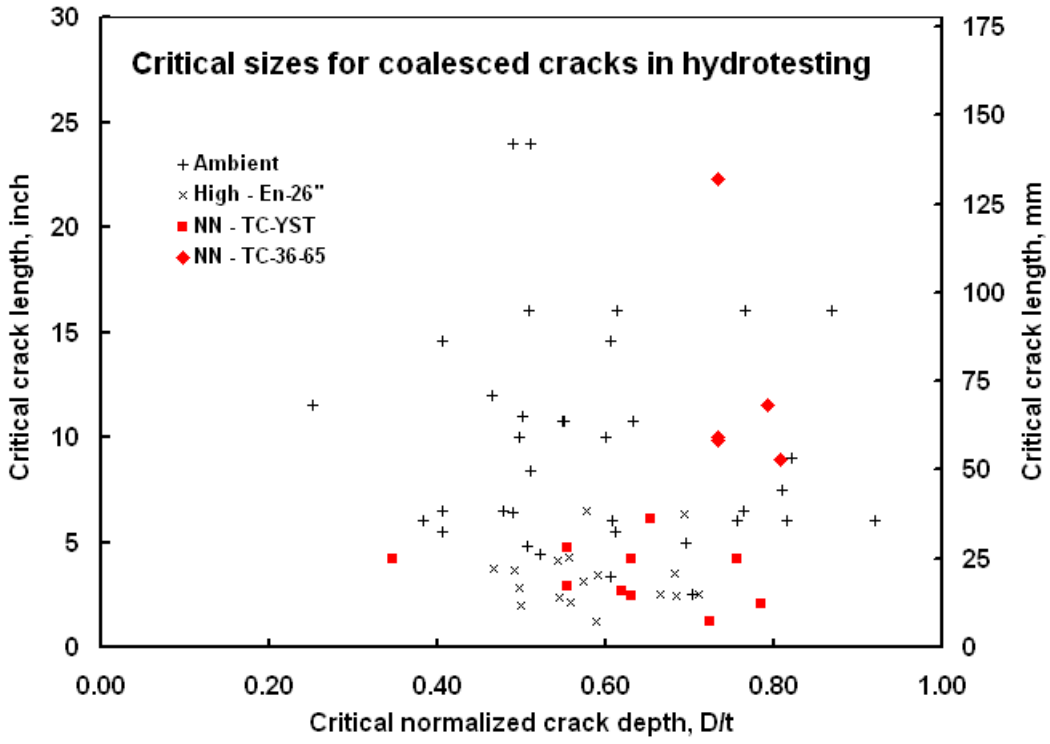


**a) L as a function of D/t**

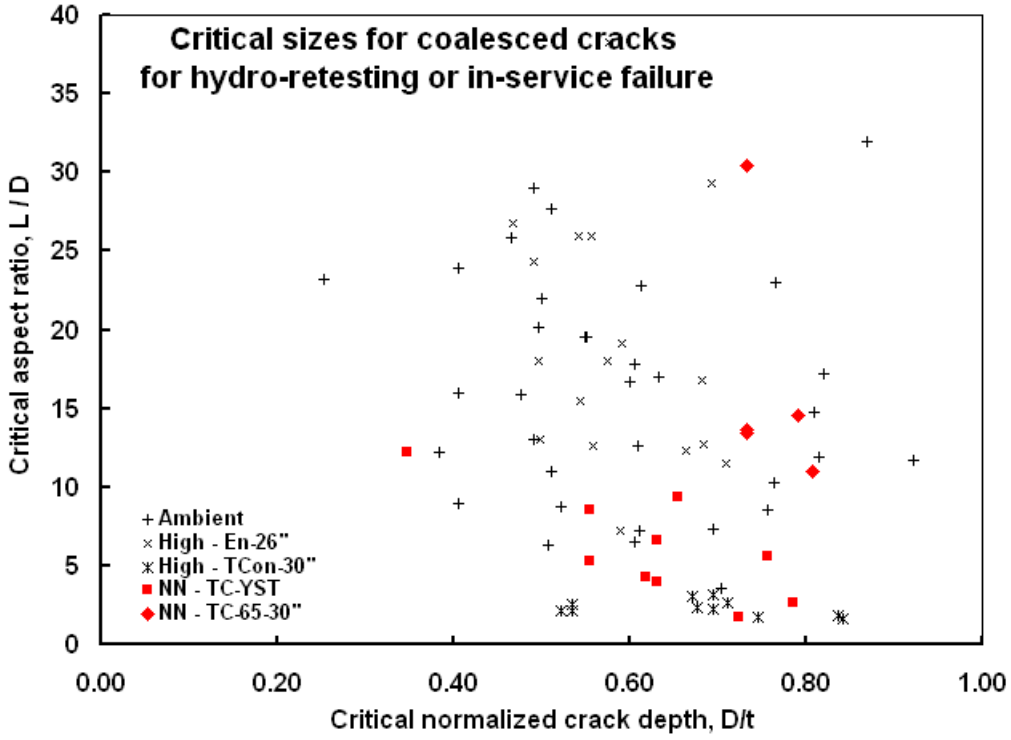


**b) L/D as a function of D/t**

**Figure 14. Cracking characteristics for failures in service or hydro retesting**

# Develop Field Validation for Severity Assessment

As part of usual practice documenting field digs for SCC, photographs and measurements are made of the cracking colonies. Such work has occurred in Canada, the US, as well as Europe and elsewhere leading to statistically large samples of typical SCC found on a wide range of large-diameter high-pressure pipelines.

Tables 5 and 6 summarize a variety of results for a large number of colonies of SCC. No attempt has been made to match operating pressure, pipe grade, diameter, or other such metric in assembling these results, nor was there any selection to bias the outcome. Suffice it to state they represent line pipe whose diameter was equal or greater than 20-inches (508-mm), in high-

**Table 5. SCC colonies in large-diameter pipelines: length and depth**

**a) crack length**

| *Result* | *Isolated cracks, mm* | | *Coalesced cracks, mm* | |
|---|---|---|---|---|
| | *High-pH* | *NN-pH* | *High-pH* | *NN-pH* |
| ***Average*** | *4.8* | *9.7* | *17.7* | *36.6* |
| ***Range*** | *1 to 40* | *2 to 46* | *4 to 46* | *5 to 190* |

**b) crack depth**

| *Estimated crack depth,% wall* | *Relative frequency* | |
|---|---|---|
| | *High-pH* | *NN-pH* |
| *7-10* | *0.00* | *0.03* |
| *10-15* | *0.27* | *0.35* |
| *15-20* | *0.22* | *0.16* |
| *20-25* | *0.41* | *0.13* |
| *>25* | *0.10* | *0.10* |
| *Unknown* | *0.00* | *0.23* |

**Table 6. SCC colonies in large-diameter pipelines: location and role of corrosion**

**a) crack location**

| *Location* | *Relative frequency* | |
|---|---|---|
| | *High-pH* | *NN-pH* |
| ***Body*** | *0.49* | *0.39* |
| ***Girthweld <10mm*** | *0.08* | *0.03* |
| ***Girthweld*** | *0.00* | *0.00* |
| ***Longseam <10mm*** | *0.44* | *0.28* |
| ***Longseam*** | *0.00* | *0.07* |
| ***Unknown*** | *0.00* | *0.23* |

**b) role of corrosion**

| *Near corrosion* | *Relative frequency* | |
|---|---|---|
| | ***High-pH*** | ***NN-pH*** |
| *Yes* | *0.14* | *0.37* |
| *None* | *0.86* | *0.43* |
| *Unknown* | *0.00* | *0.20* |

pressure service. The tabulations reflect two sequentially compiled datasets that were selected simply based on the observation that one set was labeled classical while the second was noted near-neutral. These two datasets represented 283 colonies found in NN-pH environments and 78 colonies found in high-pH environments. These data reflect colonies of coalesced cracking on pipe stripped in field digs to evaluate typical cracking, and so are not characteristic of failures.

Results summarizing trends in crack length are presented in Table 5a based on surface measurements of coalesced cracks. The average length in the colonies is reported as is the maximum length. It is apparent from these results that the average crack as well as the maximum crack length in these colonies is similar for NN-pH and high-pH SCC.

Table 5b presents results characterizing crack depth. For present purposes, crack depth is an estimated metric based on the physical appearance of the "yawn" or opening of a crack as a function of its length. Fracture mechanics indicates this crack mouth opening displacement (CMOD) is a unique function of crack depth in comparable steels (similar grade and flow-response) for cracks of the same length in pipe of comparable wall thickness. Such results reflect the skill and experience of the observer, which for the present estimates is calibrated by grinding crack depths in colonies to remove cracking as part of the rehabilitation of the pipeline. While, such estimates are neither precise nor accurate, the empirical calibration and skill-based estimate of depth is viable for pooled data in statistically large samples where the purpose is a relative comparison between NN-pH and high-pH SCC. Table 5b shows similarities as well as differences exist for these data, although given the range of pipe grades and wall thicknesses being compared in the pooled data, the differences are unlikely significant.

Consider now the similarities and differences in cracking location, results for which are shown in Tables 6a and 6b. Table 6a considers crack location referenced to the pipe body versus in or near long-seam and girth-welds, while Table 6b considers proximity to corrosion. All tables show similarities as well as differences based on cracking location relative to weld seams and corrosion. From a fracture mechanics perspective, cracking in a weld seam could require consideration of different fracture-resistance properties or a locally elevated crack driving force, the latter also applying to cracking in corrosion pits. However, the nucleation of both forms of SCC is sensitive to stress, and cracking becomes possible where the cracking environment develops. As tented tape coating and the corrosivity of the environment could be as likely a cause for variance in these pooled data, the differences are unlikely significant.

# Establish Typical Flow and Fracture Properties of Line Pipe Steel and Histories Representative of Usual Pipeline Service in Support of High-pH SCC Service Simulations

Prior to simulating SCC in later sections and comparing those results to field data to assess the viability of the model for high-pH SCC to be delivered by this project, data for typical line-pipe properties and operational scenarios for pipelines are required. This section presents such data.

Table 7 presents trends for several of the early NN-pH SCC failures based on Battelle file data. As all entries in this table represent pipelines in gas-transmission service, and the majority of the available data to validate simulations involve gas-transmission service, the focus of this section is such pipelines[7].

Note from Table 7 that some failures occurred at locations experiencing rather high temperature that through the early research[(e.g., 2)] was identified as a key driver for these failures. With this recognition, gas-compression practices have changed and some companies have installed after-coolers to reduce discharge temperatures. Before SCC was recognized as a potential problem and the role of temperature understood, discharge temperatures often exceeded 150ºF. But, as the role of temperature was understood a marked reduction in discharge temperature has occurred for pipelines susceptible to high-pH SCC. Temperatures the order of 110ºF now can be taken as more typical for major transmission companies with pipelines known to suffer SCC. Such a temperature can be taken as representative of many gas-transmission pipeline operations. However, where SCC is a consideration a range of temperatures should be evaluated relative to this more typical service temperature.

**Table 7. Data trends useful to guide simulations for high-pH SCC**

**a) complete data sets for some early incidents (gas-transmission pipelines)**

| Diameter Inch | Thickness inch | Grade ksi | Years to first Incident | Conditions at failure | | Distance Downstream Miles |
|---|---|---|---|---|---|---|
| | | | | Temperature ºF | Pressure %SMYS | |
| 30 | 0.355 | 52 | 18 | 120 | 64.4 | 2 |
| 30 | 0.325 | 52 | 17 | 109 | 69.8 | 4.7 |
| 22 | 0.275 | 52 | 13 | 142 | 72.7 | 1.1 |
| 24 | 0.312 | 52 | 7 | 115 | 71.0 | 3 |
| 26 | 0.281 | 52 | 21 | 70 | 71.6 | 14 |
| 26 | 0.303 | 52 | 22 | 100 | 61.9 | 16 |
| 24 | 0.281 | 52 | 19 | 135 | 65.7 | 0.8 |
| 26 | 0.312 | 52 | 20 | 90 - 170 | 69.3 | 9.8 |
| 30 | 0.335 | 52 | 18 | 120 | 68.3 | 2.28 |
| 26 | 0.281 | 52 | 20 | 120 | 70.6 | 3 |

[7] This is not to say failures for other scenarios cannot be addressed, but rather indicates that because the data gathered in this section are subsequently used to generate trends to compare with field data this process is most effective if it focuses on scenarios with significant databases – which presently target gas-transmission systems.

**b) Property distributions for X52 line-pipe steels (selected file data)**

| Parameter | Distribution | Mean Value | Standard Deviation |
|---|---|---|---|
| **Ultimate Strength, ksi** | Normal | 75.0 | 3.39 |
| **Yield Strength, ksi** | Normal | 55.0 | 2.49 |
| **CVN Energy, ft-lb** | Weibull | 33.7 | 10.5 |

As is implied by the trends in Table 7a much of the data available for SCC is for pipelines made of X52 line-pipe steel, and involves cross-country transmission built from the late 1940s into the early 1960s – the period when much of the pipeline was constructed. Accordingly, mechanical and fracture properties typical of the late 1940s into the early 1960s have been gathered for X52. While the focus here is delivery of a deterministic model to help understand operational effects on high-pH SCC, it was difficult to broadly validate this model in a deterministic setting in reference to field data or tendencies. This is because all such situations involve the reality of an operating pipeline. Recall that SCC requires the concurrence of a microstructure susceptible to a cracking environment in the presence of a tensile stress, which for anodic dissolution to function requires continued exposure of bare surface at a local stress raiser and passivated flanks. On this basis, high-pH SCC develops on a pipeline only where the local conditions admit nucleation. Nucleation can only occur on free surfaces in microstructures that favor microplastic response under the nominally elastic stressing of a pipeline – which reflects the susceptible microstructure requirement. This can only occur where the cracking environment has formed, which can only occur where the coating has failed and disbonded. These coupled conditions satisfy the cracking environment requirement. Continued growth will only occur at sites where microstructurally the adjacent grains lead to mismatch sufficient to limit repassivation at crack tips, while admitting repassivation on the flanks of those grains. This satisfies the coupled tensile stress and related passivation requirement, during nucleation. Nucleation of SCC can only occur where these probabilistic requirements for nucleation are satisfied. Growth of the nucleated cracks can only continue if neighboring coparallel cracks are sufficiently remote to limit stress-shielding, thereby creating a "sparse" colony of cracks. This satisfies the tensile stress and related repassivation requirement beyond nucleation. Sparse colonies formed remote to other colonies can only threaten integrity through sympathetic nucleation of co-linear cracking within the colony. This can only occur if over time conditions that favor SCC drives that cracking through-wall (causing a leak) or leads to coalescence with other cracking in that colony leading to a critical length (causing a rupture). Alternatively, if conditions continue to favor SCC then adjacent colinear colonies of sparse cracking could nucleate close enough to this colony to interact and grow such that the larger cracks between these colonies eventually coalesce, causing a leak or a rupture. These aspects occur first within sections along the pipeline for which the strength and toughness properties lie in the lower tails of these distributions. Nominally higher specified properties indicate greater survivability – all else being equal. As all such scenarios involve a sequence of statistically unlikely events, field cracking that continues to failure is a statistically unlikely event that can only be simulated my modeling each event in a framework that addresses this uncertainty.

Because of the need subsequently to address field scenarios where this sequence of statistically unlikely events leads to failure or stable field cracking the properties are presented in Table 7b in terms of distributions parameters. Specifically, Table 7b indicates the distribution type and provides the first and second moments for yield stress, ultimate stress, and full-size equivalent Charpy V- notch (CVN) plateau energy. As required, other distribution properties are calculated from these moments. The specific mechanical properties presented are obtained from mill-certification sheets for heats representing a 1000-mile (1609-km) cross-country pipeline built of typical of early-vintage X52 line pipe. The toughness distribution is specific to X52 line-pipe steel made in the 60s.

Recognizing that the majority of the data available to subsequently validate high-pH simulations represent natural-gas transmission pipelines, operational data were sought and characterized for such pipelines. As such pipelines have typically operated at or near capacity in the US and Canada, often with a daily pack and draft cycle matched to demand – with this demand-induced pressure cycles occurring typically once per day. Even though this cycle is demand driven, gas is compressible such that this daily pressure cycle leads to a pressure ratio the order of 0.80 or higher. Because of their minimum regulatory-based burial depth, thermal cycling is neither frequent nor severe. Because the amplitude of the cycling is infrequent and small, there is little to no possibility for fatigue in such operation[(40)]. It remains to determine the variation of key operational parameters as a function of distance downstream of compressor stations to include the role of this factor, which is clearly evident in Table 7a.

Because gas-transmission pipelines operate over long distances transporting a compressible fluid that experiences frictional losses compressor stations are distributed along the length of the pipeline to boost the pressure and maintain the gas-flow. The heat of compression increases the gas temperature[8], the extent to which depends on the degree of compression and whether or not chillers are used. It follows that the gas at discharge is much warmer than at suction at the next compressor station. There is an associated pressure drop, which also reflects frictional losses in-route, as is apparent for typical operation in Figure 15. Figure 15 is taken as typical of the operation of such pipelines. These results reflect the discharge temperature and pressure as a function of the distance downstream from the compressor station, normalized by the distance between stations. It follows from Figure 15 that the average pressure and gas temperature along a typical natural-gas transmission line varies with the normalized distance downstream of the compressor station.

In reference to pipelines transporting liquids that are incompressible, these pipelines tend to experience much larger cycles, which opens the door to fatigue or fatigue coupled with SCC, possibly in a synergistic fashion as seen with the interaction between corrosion and fatigue. In some cases the operators of liquid pipelines draw down the lines to quite low pressures during the day, and push the lines to quite high pressures to fill their storage tanks at night through a cycle that depends on both demand and the cost of energy, which for large power consumers can vary significantly over the period of a day.

In evaluating the effects of loading history, Fessler[(11)] found there have been about twice as many NN-pH SCC service *failures* on gas pipelines as on liquid lines, but there are about four times as

[8] Scenarios where LNG is transported differ from this description – but as they were not a factor when SCC was recognized as a problem their unique operation is not considered.

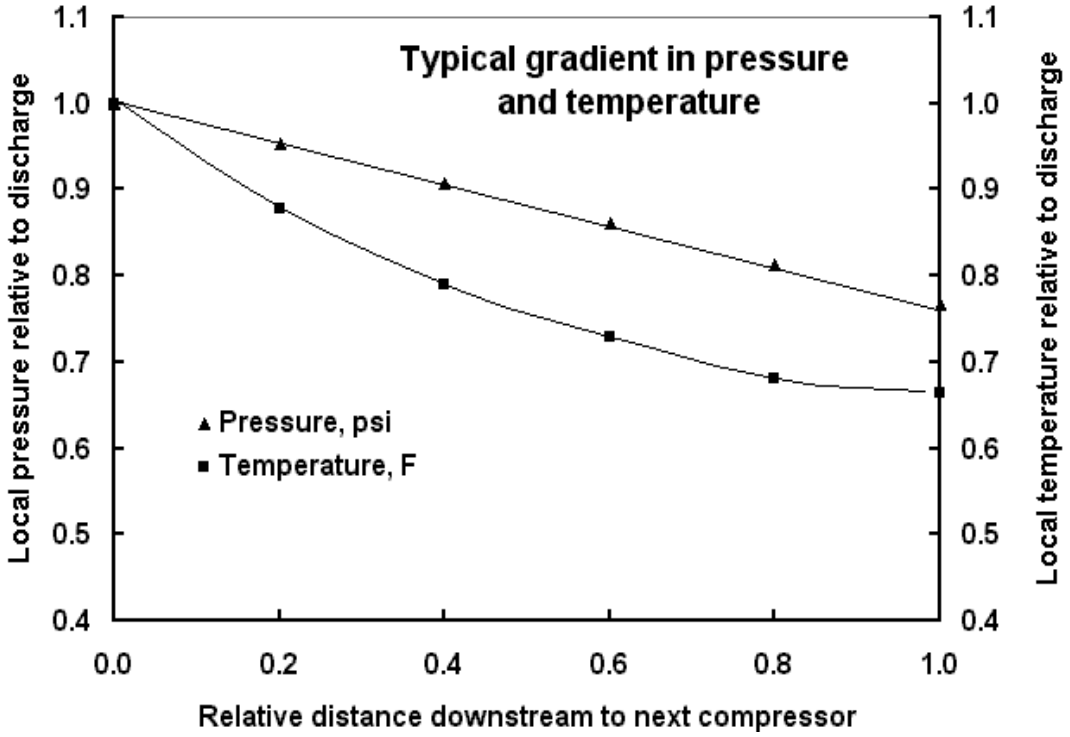


**Figure 15. Typical pressure and temperature gradients between compressor stations**

many miles of tape-coated gas pipelines than tape-coated liquid lines. Thus he concluded on a per-mile basis it appears that the probability of NN-pH SCC failures is twice as high for liquid lines, which have larger pressure fluctuations, than for gas pipelines, which rarely have large pressure fluctuations. Further he commented "that the mechanism of crack growth on the liquid lines may have been a combination of corrosion fatigue and SCC, whereas the mechanism of crack growth on the gas pipelines probably was primarily or entirely SCC." In related analysis of a recent study of the effect of pressure fluctuations on NN-pH SCC he noted "Beavers found distinct combinations of frequency and pressure (stress) ratio, R, in which corrosion-fatigue-type behavior was observed and other combinations where SCC-type behavior was observed." In analyzing those data Fessler[11] again discriminated between the cycling experienced by gas pipelines as corresponding to the SCC-type behavior, whereas the cycling experienced by liquid pipelines was noted to more closely reflect corrosion-fatigue type behavior. Finally, Fessler[11] noted "liquid lines have experienced twice as many failures per mile than gas pipelines, on that same per-mile basis, there have been at least twice as many SCC colonies found on gas pipelines than on liquid lines," commenting that "these data are typical for the entire industry, it would suggest that crack initiation is favored on gas pipelines, which tend to operate at higher temperatures, higher discharge pressures, and lower pressure drops per mile, while crack growth is favored on liquid lines that experience larger pressure fluctuations."

In summary, Fessler's analysis suggests that care must be taken in identifying mechanisms for NN-pH SCC and in formulating related models focused on gas-transmission for broader usage such as liquid operation. This aspect needs to be addressed in future development of models for SCC regardless of the cracking environment.

# Evaluate Practices to Quantify Hydrogen Effect on Microplasticity

NN-pH SCC is a phenomenon as described earlier that includes buried pipelines when they are exposed to aggressive underground environments while used for hydrocarbons transmission lines applications; the ionic species that surround the structure might form atomic and/or molecular hydrogen as a product from homogeneous and heterogeneous reactions as suggested by the reactions shown as Reactions 3 and 4. Hydrogen ion is a species that is transported through the bulk solution-electrolyte and the corrosion products formed thermodynamically mainly of iron carbonate and iron oxides depending on the pH, potential and temperature conditions. Mass transport of the ionic species involves migration and diffusion within the porous corrosion product layer. Because this physical barrier decreases the flux of the ionic species to the metallic surface, some ions will accumulate within the pores of the layer and others will react at the metal surface-layer. The physical magnitude that quantifies the transport rate of the ionic species and the atomic hydrogen is the diffusion coefficient, this later parameter introducing proportionality to the concentration gradient of ionic and transported species, therefore the magnitude influences the mass transport resistance and physical conditions of a particular ionic species exposed in that environment. The hydrogen ion and molecular hydrogen can be followed in terms of the transport properties by means of diffusion coefficient. There are two different approaches for hydrogen quantification and the effects of the metal under static and load conditions. The first method is experimental by means of hydrogen permeation, and electrochemical polarization measurements, while the second method is theoretical modeling to solve the transport equation in terms of the flux density equation[41].

## Hydrogen Permeation Test

The experimental form for hydrogen quantification within the metallic structures is hydrogen permeation. These measurements are performed by charging a metallic structure, which is a common practice for assessing hydrogen diffusivity by use of the Devanathan- Stachurski cell[42, 43]. This cell has two chambers to facilitate diffusion through a metallic sample that is exposed to different media and electrolytic conditions on either side. The experimental set up provides for measuring the current that generates the hydrogen for diffusion from the chamber on the cathodic side to the anodic side where detection occurs. For this work focused on NN-pH SCC, the anodic (detection side) chamber contained NaOH 0.1M solution while the cathodic (input side) chamber contained deareated NS4 solution. The input (cathodic) side initiates the hydrogen reaction at the metal-electrolyte interface where hydrogen ions convert to atomic hydrogen and finally to molecular hydrogen, via adsorption, recombination and electrochemical reactions processes. Molecular hydrogen evolves to the upper path of the chamber whereas atomic hydrogen that is not reconverted starts to diffuse through the metallic structure.

Dissociation of $H_2CO_3$ from $CO_2$ (aqueous) produces the hydrogen ion, as shown in the homogeneous Reactions 3 and 4 as previously explained. The dissociation of water is another source of hydrogen ion, however the concentration of hydrogen ions is very low, on the order of 1E-7M and so is not considered in the formation of atomic hydrogen. The heterogeneous reactions (electrochemical reactions at the electrode) that are considered for the formation of molecular and atomic hydrogen are as follows:

$$2H^{+}+2e^{-} \rightarrow H_2 \qquad (5)$$

$$HCO_3^- + H_{ads} + e^- \rightarrow H_2 + CO_3^{2-} \quad (6)$$

These reactions quantify the number of moles that the hydrogen evolution reaction forms as molecular hydrogen, by calculating the current generated to form a mole of hydrogen.

Considering the combination of processes, chemical discharge-recombination mechanism, the hydrogen reaction occurs in two steps as described by F. M. Al Faqeer[44] et al , where the hydrogen ion is adsorbed at the metal surface and converted into hydrogen atoms. The complete adsorption reaction with the steel structure is given as Reaction 7:

$$H^+ + e^- + Fe \rightarrow Fe\text{-}H_{ads} \quad (7)$$

with the recombination of two adsorbed hydrogen atoms forming molecular hydrogen gas that evolves to the surface and out of the electrolyte, as in Reaction 8:

$$Fe\text{-}H_{ads} + Fe - H_{ads} \rightarrow 2Fe + H_2 \quad (8)$$

where $Fe\text{-}H_{ads}$ refers to an adsorbed hydrogen on the metallic structure.

The total hydrogen adsorbed at the surface of the metallic structure can be monitored and characterized with the impedance measurements at low frequencies [45] as explained subsequently, which facilitates determining the permeation current.

## Experimental Procedure and Setup

To measure experimentally the hydrogen permeation characteristics through a metallic material, the Devanathan[42] method considers two electrochemical cells that are separated by a metallic membrane. The current produced for the hydrogen permeation is recorded with a potentiostat that is set for positive potentials on the anodic side of the membrane [46-49]. The metallic membrane on the cathodic side can be polarized or held to the open circuit potential (OCP) in order to generate hydrogen at the surface of the electrode and compare polarization conditions with the OCP. Reactions 3 and 4 consider the formation of hydrogen under open circuit conditions due to the ionic species present in the electrolyte and the electrode reactions that might be active at the surface. Atomic hydrogen is formed and diffuses through the metallic membrane. After some time the atomic hydrogen can accumulate sufficiently to influence the mechanical properties of the structure. Because of the design of this Devanathan- Stachurski cell, these permeation experiments reflect unstressed conditions. However, this cell can be adapted to active loading conditions considering the results at the detection side of the hydrogen permeation, with the same electrochemical DC technique and AC measurement procedures used to quantify the outcome.

Figure 16 shows the configuration of the cell, wherein the cathodic side considered the different ionic species that comprise the NS4 solution like $CaCl_2$, $NaHCO_3$, KCl and $MgSO_4$ with a view to assess their role in the permeation current,. The anodic side contained 0.1M NaOH solution to facilitate the consumption of hydrogen ions. The anodic potential was set at 250 mV (referenced to saturated calomel electrode (SCE)) from OCP. The cathodic side was set at OCP because the hydrogen formation included only the atomic hydrogen formed without polarization conditions.

**Figure 16. Electrochemical cell for hydrogen permeation experiments through a metallic membrane**

## Theoretical Formulation and the Mathematical Model

The theoretical formulation considers the transport of the hydrogen ion through the corrosion products and the metallic structure, with the formation of iron carbonate as the main corrosion product when the pH is near neutral (about pH~7.5), but otherwise iron oxide in form of $Fe_3O_4$ or $Fe_xO_y$ when the electrolyte is alkaline (pH>9.5). The mass transport processes considered in the model include diffusion due to the ionic concentration gradient between the bulk electrolyte and the reactions occurring at the interface. Migration is considered due to the electrical neutrality that prevails in the electrolyte. Mass transport and continuity equations are used for each ionic species, such as $H^+$, $HCO_3^-$, $Cl^-$ and $SO_4^{2-}$, and the ions that will not have any reaction other than concentration accumulation, but do participate in the electrical neutrality and diffusion process within the electrolyte like $Mg^{2+}$ and $SO_4^{2-}$. It is assumed that the ions will be transported through the bulk solution to the metal-electrolyte interface and that the corrosion product will be formed after $HCO_3^-$ reaches the surface of the electrode and the saturation index is reached to form the correspondence corrosion product. The transport properties will change depending on the layer formed, for high pH iron oxide and neutral pH iron carbonate. Diffusion coefficient, volumetric porosity, and surface permeability are the parameters that control the transport characteristics of the ionic flux throughout the layer formed. Electrochemical reaction will be considered at the interface and chemical reactions will be considered either for the bulk of the solution or the porous corrosion product. Finally the concentration of hydrogen ion formed at the surface of the electrode is taken proportional to the amount of molecular hydrogen formed and the permeation concentration within the metallic structure.

By dividing the system into equal segments, where the nodes in the array represent the system and any changes in the system, the electrochemical cell can be represented as a Cartesian plane,

as illustrated in Figure 17. The boundary conditions are those for a semi-infinite slab, where the bulk of the electrolyte is the infinite coordinate and the initial coordinate is the interface metal corrosion product, as illustrated in Figure 17.

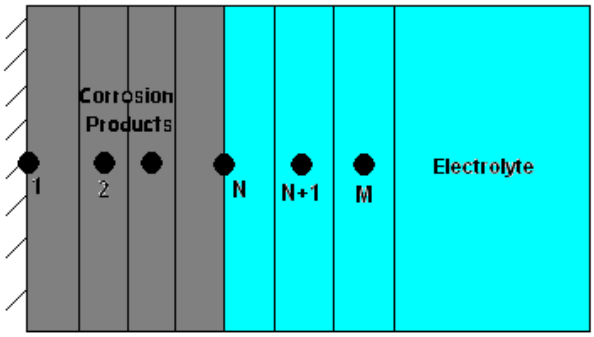


**Figure 17. Boundary conditions for the steel-electrolyte system**

The mass balance equation is taken as one dimensional in a Cartesian framework and is applied to each ionic species:

$$\frac{\partial \varepsilon C_j}{\partial t} = -\frac{\partial (\kappa N_j)}{\partial x} + \varepsilon R_j \tag{9}$$

where, ε and κ are the volumetric porosity and the surface permeability of the film, respectively. Nj is the flux of the ionic species j, Rj is the source or sink of species j due to all the chemical reactions, and C is the concentration of species j.

Equation 9 represents the flux term that considers three different process diffusion, migration, and convection – the latter not being considered because the electrolyte is static and so absent fluid motion. Therefore, the flux expression in terms of Nernst Planck is:

$$Nj = -D_j \frac{\partial C_j}{\partial x} - Z_j \mu_j F C_j \frac{\partial \phi}{\partial x}. \tag{10}$$

Nj is the flux of the species j that is considered in the electrolyte, Dj is the coefficient diffusion of the j species, Zj is the charge, μ is the conductivity Cj is the concentration of the species j and ϕ is the electric potential.

For example, by solving for the $HCO_3^-$ ion in the system we have three different conditions for the position and one more condition for the time,

The boundary condition for initial time is:

$C_{HCO3-}(t,0)=C_{HCO3-}$

Boundary conditions for the concentration according to position are:

At x=L (bulk electrolyte or semi-infinite condition); $C_{HCO3-}(L,t)= C_{HCO3-}$

At x=N (interface electrolyte corrosion product);$C_{HCO3-}(N,t)= R_{HCO3-}$

At x=0 (interface metal-corrosion product); $C_{HCO3-}(0,t)=0$.

This set of simultaneous equations can be solved for every node by a finite difference implicit method that approximates the transport equations for $HCO_3^-$ applied to Reaction 10.

The solution of the equations considers the concentration profiles with time, and the time at which a certain amount of hydrogen is obtained due to the concentration of hydrogen ion depending upon pH conditions in the solution. The calculated corrosion product thickness will depend on the electrolyte conditions with either iron carbonate or iron oxide being produced. Finally the accumulation of specific ionic species at the interface or within the corrosion product and the physical properties of the layer formed will determine the characteristics of the electrolyte and for the layer formed as the corrosion product – according to the initial concentrations, temperature, and potential. The total amount of hydrogen ions concentrated in a specific time is related either with hydrogen permeation or hydrogen recombination according to the Reactions 3 and 4 for hydrogen permeation, and the Reactions 6 and 7 for hydrogen evolution or recombination.

The hydrogen evolved can be extrapolated and validated to field conditions by combining electrochemical techniques with theoretical models under operational conditions.

# Characterize Effect of Field-Factors on NN-pH SCC Susceptibility

## Background

Buried transmission pipelines can be exposed to cracking environments that form from the soils and groundwater under operating conditions. As noted earlier, SCC occurs under the mutual presence and interaction of three factors – a cracking environment, a tensile stress, and a material susceptible to SCC for those conditions. This phenomenon is considered synergetic wherein the combination of these factors is much worse than their individual effect. Various studies of SCC for different material – environment systems[50-54] address the phenomenon in terms of anodic dissolution, often through sensitivity studies.

Hydrogen associated with the SCC process becomes an important factor for this phenomenology when dealing with near-neutral solutions[55-57]. Different ionic and dissolved species in the soil served as reactants for atomic hydrogen and constitute the basis for the formation of two forms of hydrogen – with atomic hydrogen diffusing into the metallic structure and interacting with the dislocation array, which can cause hydrogen embrittlement. Crack nucleation can ensue[57-58], however the nucleation time to the first pit or metallic defect and the initiation mechanism remains a matter for further study.

Once crack nucleation occurs, physical and numerical analysis including stress and hydrogen diffusion become important for life prediction as does analysis of crack propagation when there is exposure to hydrogen embrittlement and/or anodic dissolution conditions. Yokobori[59] et al considered a physical model that described the local stress field with hydrogen emission around a crack tip, as well as anodic dissolution. In this context, once stress raisers form all processes associated with crack nucleation and growth for NN-pH SCC occur synergistically in reference to mechanical stress in the presence of molecular hydrogen formation; where $CO_2$ (aqueous) is the main source of molecular and atomic hydrogen formation according to the previous mechanism suggested in Reactions 3 and 7. The formation of an active site involves the interaction between the environment and the steel, with the stress causing breakdown of the corrosion product developing additional active sites for electrochemical reaction. As cracking

continues, there is a transition from local stress control to fracture-mechanics control, with coalescences between cracking at active sites occurring until it reaches a critical size.

Chemical dissolution of steels exposed in near-neutral and high pH environments includes homogeneous processes (chemical reactions), heterogeneous processes (electrochemical reactions), and transport of the species that are in solution. The ionic species are transported from the bulk solution to the interface of the corrosion products; the ion hydrogen forms atomic hydrogen from homogeneous and heterogeneous reactions, once in the atomic form it diffuses to the bulk of the metallic structure. Some reactants presented in solution influence the corrosion process, like hydrogen ion that promotes a cathodic reaction; or the chloride that changes the local pH conditions in the pores of the corrosion product. Hydrogen ion forms as a homogeneous reaction decomposition product. $CO_2$ (aqueous) produces homogeneous reactions when is exposed in electrolytic aqueous solution. The Fe-$CO_2$-$H_2O$ system under equilibrium conditions establishes feasible electrochemical and chemical reactions for anodic dissolution under corrosion conditions. NN-pH SCC involves three concurrent phenomena: anodic dissolution competes with hydrogen embrittlement with both occurring on a background of dislocation mechanisms. The formation of corrosion products at the steel-environment interface will lead to a barrier layer between them, which could influence the anodic dissolution and embrittlement processes and could also locally impact the dislocation mechanisms. This could impact the corrosion rate when this layer is stable and thick. Likewise, the formation of layers with specific physical conditions could impact the hydrogen diffusion characteristics according to the motion of the ionic species into the layer, whereas an influence on dislocation movement could influence the formation of corrosion products layers. Logically the kinetics of the system suggest different transport mechanisms for atomic hydrogen formed under different pH, electrode potential, electrolyte composition conditions, as proposed by Misra[60] and Nesic et al[61] who describe the formation of atomic hydrogen and the transport through the bulk solution, respectively.

Thermodynamics for steel- $H_2O$-$CO_2$ aqueous solutions have been examined for high pH and near-neutral solutions under no stress conditions by some authors [55, 62], whereas stress in the steel induces random breakdown of the corrosion product breakdown as compared to the layer formed under static conditions. The initial layer formed spontaneously for steel exposed to NS4 solution (KCl, $NaHCO_3$, $CaCl_2$, $MgSO_4$) in the presence of $CO_2$ at different temperatures is iron carbonate ($FeCO_3$). On the other hand, the predominant compounds formed at different temperatures in the presence of $O_2$ and high pH solutions are $Fe_3O_4$ (Magnetite) and $Fe_xO_y$[63].

E-pH aqueous diagrams are excellent tools to assess the feasibility of chemical and electrochemical reactions in equilibrium for two or more species present in the media – which here addresses a buried steel pipeline exposed to soil and groundwater. As for all such scenarios a set of reactions, compounds, ions, temperature, concentrations, total and partial pressure can be evaluated. The plots that follow focus on potential versus pH and identify different regions or stable zones. For the pipeline in soil and groundwater of interest herein, the system Fe-$CO_2$-$Cl^-$-$H_2O$ is relevant – and so is considered at different temperatures in reference to $FeCO_3$, $Fe_2O_3$, $Fe_3O_4$, $FeCl_2^+$,$FeCl^+$, $Fe^{2+}$ and Fe as the main species. The underlying calculation considers the temperature, concentration of each species, and $CO_2$ pressure as independent variables to build the E - pH diagram. For higher temperatures the diagrams should contain the pH correction for the water equilibrium. The general reactions for the Fe-$CO_2$-$Cl^-$-$H_2O$ system are presented in Figure 18 in terms of equilibrium lines.

## Theoretical Feasibility and Experimental Results Applied to Field Conditions for NN-pH SCC

At 25ºC iron carbonate shows predominance over a region in the form of the Pourbaix diagram as shown in Figure 18a, where this corrosion product is stable in the region from pH 6.5 to 11.25 and potentials from 0.0V to -0.8V versus ENH. Accordingly, steel (~98%Fe) exposed in near-neutral solutions that have pH magnitudes of ~7.0 will have $FeCO_3$ as the main reaction product along with $Fe_2O_3$ depending on the half cell potential. Results for the experiments on the X52 and X65 grade steels showed -0.642V to -0.842V versus ENH, respectively, in NS4 solutions.

The scenario in Figure 18 considered $PCO_2$=1atm and $Fe^{2+}$=1e-6M. The ferrous iron concentration affects the corrosion process because dissolution of the metal increases, thus influencing the concentration of the ions released to the electrolyte. The reactions for iron carbonate formation are originated from the $CO_2$ (aqueous) decomposition reaction. The important reactions for NN-pH SCC in terms of homogeneous (chemical) and heterogeneous (electrochemical) reaction for the formation of iron carbonate formation were introduced earlier as reactions 3 and 4.

The predominance region for iron oxide, $Fe_2O_3$ in Figure 18b considers the influence of the pH magnitude with respect to $Fe^{2+}$ concentration in order to form this corrosion product (from 11.5 to 9). The dissolution of iron into the electrolyte increase the formation of $FeCO_3$ at constant temperature, therefore the dissolution process enhances the formation of the iron carbonate corrosion product layer.

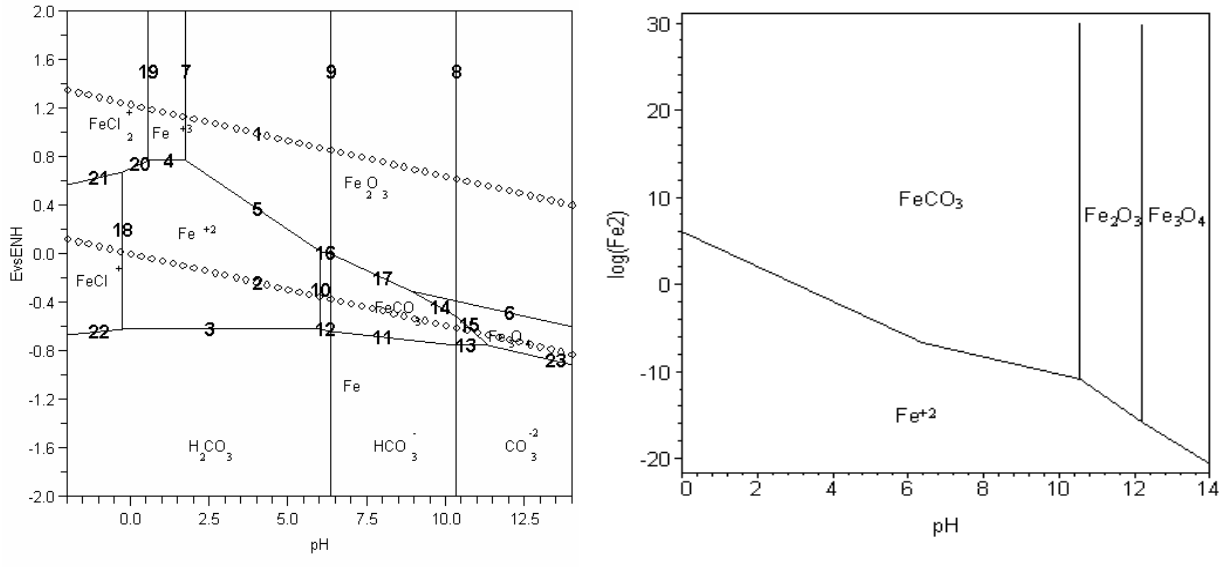


**a) E-pH equilibrium for the system Fe-CO2-Cl at 25C**

**b) Ferrous iron concentration versus pH**

**Figure 18. E-pH equilibrium and $Fe^{2+}$ versus pH diagram for 25°C (Fe-$CO_2$-$H_2O$)**

Equilibrium diagrams illustrate the characteristics of the system, such as predominance diagrams at constant temperatures, as shown in Figure 18. Figure 18b diagrams the stability region for iron carbonate versus ferrous ion concentration ($Fe^{2+}$) versus pH at 25°C. The precipitation of ferrous iron to iron carbonate considers high pH conditions and low concentration of ferrous ion.

The chemical reaction to convert iron carbonate to iron oxide considers high pH conditions at levels >10.2, as shown in Figure 18b. Another thermodynamic parameter that can impact the formation of corrosion products is the temperature of the system, with equilibrium at different temperatures reflected by the iron carbonate field on the E-pH representations. Accordingly, the formation of iron carbonate can be driven at higher pH levels by increasing the temperature as compared to the response at lower pH magnitudes and room temperature conditions. E-pH diagrams show the feasibility of forming corrosion products from an electrochemical system at different temperatures, with Figure 18 being specific to the $Fe\text{-}CO_2\text{-}Cl\text{-}H_2O$ system. Because of its impact on the thermodynamic properties, differences in temperature can play a major role in the timeline to establish steady state experimental conditions affecting SCC. For example, an iron carbonate film can be obtained in shorter times when the temperature is raised above 40°C, which reflects the enhanced precipitation rate as a function of temperature[62].

The reactions considered in these E-pH diagrams are half cell reactions, either anodic or cathodic. The anodic reaction is iron dissolution that forms the most stable corrosion product or ionic form of iron according to temperature, electrolyte composition and pH, existed in the electrochemical cell system. The cathodic reaction for near-neutral conditions in the absence of oxygen (anaerobic conditions) is the hydrogen formation, which occurs in two steps. First, atomic hydrogen is formed leading to molecular hydrogen as the second step via Reactions 8 and 9 for steel exposed in NS4 solutions.

Table 8 shows the corrosion products formed at the surface of the X52 steel as determined using the XRD technique for different combinations of temperature, ionic concentrations of species, and pH conditions under static solution. As can be seen there, the results of calculations based on thermodynamic predictions are in good agreement with the experimental data for the coupon testing involving exposure to different ionic solutions presented earlier. As anticipated, corrosion species and iron carbonate are observed to form under static exposure and with $CO_2$ (gas) injection.

As indicated above, E-pH diagrams for complex systems like the NS4 solution that is considered to simulate the near-neutral environment under buried conditions can be used to assess the feasibility of the layer formed under different circumstances. Likewise, such diagrams can be used to evaluate the effect of many environmental parameters, such as oxygen concentration, temperature, pH, in regard to the stability regions for the corrosion products, like the iron carbonate, or oxides, which are considered by some as keystones for crack initiation process for NN-pH SCC. The physical characteristics of the corrosion products influence the breakdown of the layer that eventually forms “active sites” and also the cracking behavior that continues beyond each site. In contrast, hydrogen ions will transport easily and favor the cathodic reaction and the formation of atomic hydrogen, such that the thermodynamic requirement for cracking is the reduction of hydrogen ion and the concentration of atomic hydrogen influence the stress in the microstructure.

**Table 8. Corrosion products at different temperatures and concentrations of NS4**

| Solution Composition [Bicarbonate g/L] | Temp oC | pH after 48 hours | Experimental Phases by XRD | Theoretical-Thermodynamic Prediction |
|---|---|---|---|---|
| 10 | 25 | 8.23 | $Fe_3O_4$, Fe | $FeCO_3$, Fe |
| 0.1 | 35 | 6.59 | $Fe_3O_4$, Fe | $Fe^{2+}$ |
| 0.5 | 35 | 6.75 | $Fe_3O_4$, Fe, $Na_2O$, $FeCO_3$ | $Fe^{2+}$ |
| 1 | 35 | 7.00 | $Fe_3O_4$, Fe | $Fe^{2+}$ |
| 5 | 35 | 8.01 | $Fe_3O_4$, Fe, FeO, $Fe_2O_3$, $FeCO_3$, $Na_2CO_3$, $Fe_3C$ | $Fe^{2+}$ |
| 10 | 35 | 8.43 | $Fe_3O_4$, Fe, $Fe_xO_y$, $FeCO_3$, $Na_2CO_3$ | $FeCO_3$, Fe, $Fe_3O_4$ |
| 5K | 35 | 8.09 | $Fe_3O_4$, Fe, $Fe_xO_y$, $Fe_2O_3$, $FeCO_3$, $Na_2CO_3$, $Fe_3C$ | $FeCO_3$, Fe |
| 5M | 35 | 8.08 | $Fe_3O_4$, Fe, $Fe_xO_y$, $Fe_2O_3$, $FeCO_3$ | $FeCO_3$, Fe |
| 5C | 35 | 8.03 | $Fe_3O_4$, Fe, FeOOH, $Fe_2O_3$, $Na_2CO_3$, $Fe_3C$, $Fe(OH)_2$, $CaCO_3$, $C_2CaO4{\cdot}H_2O$ | $Fe^{2+}$ |
| 5KMC | 35 | 8.04 | $Fe_3O_4$, Fe, FeOOH, $Fe_2O_3$, $Fe_3C$, $CaCO_3$, $C_2CaO_4{\cdot}H_2O$, $MgO{\cdot}H_2O$ | $Fe^{2+}$ |
| 10K | 35 | 8.35 | $Fe_3O_4$, Fe, $Fe_xO_y$, $Fe_2O_3$, $FeCO_3$ | $FeCO_3$, Fe, $Fe_3O_4$ |
| 10M | 35 | 8.39 | $Fe_3O_4$, Fe, $Fe_xO_y$, $Fe_2O_3$, $FeCO_3$ | $FeCO_3$, Fe, $Fe_3O_4$ |
| 10C | 35 | 8.40 | $Fe_3O_4$, Fe, $Fe_2O_3$, $Fe_3C$,$CaCO_3$, $C_2CaO4{\cdot}H_2O$, $Na_2CO_3$ | $FeCO_3$, Fe, $Fe_3O_4$ |
| 10KMC | 35 | 8.49 | $Fe_3O_4$, Fe, FeOOH, $C_2CaO_4{\cdot}H_2O$, $MgO{\cdot}H_2O$, $KMg(CO_3)_2$ | $FeCO_3$, Fe, $Fe_3O_4$ |
| 0.1 | 45 | 6.73 | $Fe_3O_4$, Fe | $Fe^{2+}$ |
| 0.5 | 45 | 6.8 | $Fe_3O_4$, Fe | $Fe^{2+}$ |
| 1 | 45 | 7.01 | $Fe_3O_4$, Fe, $FeCO_3$, $Fe_2O_3$, , $Fe_xO_y$, $Fe_2(OH)_2CO_3$ | $Fe^{2+}$ |
| 5 | 45 | 7.99 | $Fe_3O_4$, Fe, $Fe_xO_y$, $Fe_2O_3$, $FeCO_3$ | $FeCO_3$, Fe |
| 10 | 45 | 8.24 | $Fe_3O_4$, Fe, $Fe_xO_y$, $Fe_2O_3$, $FeCO_3$ | $FeCO_3$, Fe |

Note: for the composition of NS4, K=KCl solution, M=$MgSO_4$ solution, C=$CaCl_2$ solution. This notation is adopted in the following sections.

## Near-neutral and High pH conditions under Cyclic Softening Conditions with Hydrogen Permeation

Thermodynamics considers the feasibility for SCC to occur by anodic dissolution and the properties of the corrosion product and trends. However, without a corresponding understanding of the kinetics via the crack growth mechanism, the characterization of conditions for SCC is insufficient, because the life of structures depends on the rates for crack initiation and propagation. Such mechanisms can be categorized as metallic dissolution for initiation and fracture mechanics for crack propagation.

The anodic dissolution models consider the charge transfer rate to be the rate-controlling step, so the rate is calculated based on the kinetics of the dissolution reactions. In contrast, where cracking occurs under mechanical fracture control, the total crack advance is faster than the dissolution rate. The exposure of bare steel to the environment increase the active-passive ratio from anodic dissolution, the bare area becomes the anode and the passivated area the cathode. The formation and breakdown of the corrosion product and the cathodic reaction are the two variables to consider in assessing kinetics.

High pH and near-neutral pH SCC environments involve different corrosion products according to the thermodynamics of the system. The high pH solution is considered to be formed by the carbonate-bicarbonate concentrations that lead to a pH of ~9, for which cracking predominantly occurs on intergranular paths leading to cracks with a characteristically sharp tip. Near-neutral solutions involve a higher concentration of $CO_2$ or dilute concentration of ground water with a pH near 6.5, which results in corrosion coupled with transgranular cracking sometimes with a cleavage-like morphology.

The nucleation of a crack beginning with the formation a surface defect involves the time at which the coating fails followed by the formation process that initiates the defect. Once the corrosion cell or bare steel is exposed under a disbond on a buried pipeline, transport mechanisms become involved, moving the ionic species to the pipeline's surface. Thermodynamic calculations as discussed previously quantify the equilibrium reaction products across the range of pH, $CO_3^{2-}$, and $HCO_3^-$. This determines the corrosion products that form at the interface, which as discussed in light of Figures 18a and 18b leads to $Fe_3O_4$ is the most feasible compound to form at the steel's surface for high-pH SCC. Near-neutral pH environments lead to different corrosion products because the solution chemistry and electrochemical conditions that simulate those soil-groundwater conditions favor the formation of $FeCO_3$.

Calculation of the time at which the species in solution transfer from the bulk to the surface, and then into the microstructure, is related to the kinetics of the micromechanism(s) interfacial reactions and mass transfer processes that drive this process, which for the present is taken as embrittlement[9]. Hydrogen ions reach the surface after which the atomic hydrogen is adsorbed

[9] While the term embrittlement is used here, Lynch[(64)] notes there are three high-level mechanistic views for the role of hydrogen in the deformation and cracking response of metals, including steel. These include hydrogen-enhanced decohesion (HEDE)[(e.g.65)], adsorption-induced dislocation-emission (AIDE)[(e.g.66)], and hydrogen-enhanced localized-plasticity (HELP)[(e.g.67)]. Combinations of these mechanisms, with the dominant mechanism depending the material, microstructure, strength, environment, stress-intensity factor, and other variables, have been proposed by Lynch[(68)]. He states "there appears to be some consensus emerging that cleavage-like fractures are mainly promoted by AIDE, brittle intergranular fractures probably occur mainly by HEDE, and slip-band fractures probably involve HELP,"

and diffuses into and accumulates within the metallic structure. Concurrently, the corrosion rate is considered through the kinetics of anodic dissolution and the hydrogen permeation-cathodic process.

The rate of dissolution can be formulated in terms of Faradays Law, as was done by Ford[63] assuming that the surface is locally dissolved at preferential sites exposed by film rupture, with dissolution at the exposed free surface occurring proportionally to the charge at the interface due to electrochemical reactions, as follows:

$$Vt = \frac{M}{z\rho F}\frac{Qf}{\varepsilon f}\varepsilon_{ct} \tag{11}$$

where M and ρ are the atomic weight and density of the metallic structure that is corroding, F is the Faradays constant, and z is the number of exchange electrons in the reaction. Q is the oxidation charge density, and εf as the fracture strain of the film that considers the rupture of the corrosion product film formed due to the environment that exposed.

## Experimental Evaluation for NN-pH SCC – Microplasticity and Hydrogen Permeation

Potential sites for hydrogen permeation and microplastic strain for NN-pH SCC in the laboratory are limited in scope in comparison to the field conditions. One aspect involves the active area exposed to the environment. For example, the area used for hydrogen permeation experiments involves just 1 inch$^2$ (6.45cm$^2$) whereas the surface area of a pipeline, or more appropriately the surface area associated with disbonds and other local conditions essential to formation of the cracking environment is for some pipelines suffering SCC larger by a factor of $10^5$ or more . If one assumes that the pipeline has coating damage typical of some sites where severe SCC has been observed, then the number of potential sites for SCC approaches the order of $10^6$ times that for cracking and hydrogen permeation in the laboratory.

Susceptibility to SCC can be enhanced as compared to field conditions by a variety of experimental procedures that consider specimen size and shape, or be accelerated via testing at higher stress, temperature, or electrochemical drivers, or their combinations. Regardless of the choice made, the constraints of typical laboratory facilities and use of glassware as in Figure 16 impose limits on the size and shape of the specimen geometry to assess hydrogen permeation in a stressed state. Likewise, the procedure deployed as for the unstressed tests dictates use of thin plate specimens to characterize the hydrogen permeation within the metal. For such reasons, the specimen used is flat with 1mm thickness. As for the unstressed tests, two steel grades were evaluated (X65 and X52), with the stressing axis oriented along the length of the pipe. The exposed area involves one face as the remaining three faces were coated to focus the process in the thickness direction. Figure 19 illustrates the geometry and specifications of the specimens used for these experiments, which were cut from 24-inch diameter line pipe.

---

with consensus apparently coming in reference to the work of Hänninen[69]. Of these three, the HELP mechanism reflects a somewhat ductile microstructure and fracture process, which makes it as plausible as an embrittlement process for this application. Further work is needed to resolve this aspect for SCC on pipelines, discussion of which can be found in Reference 70.

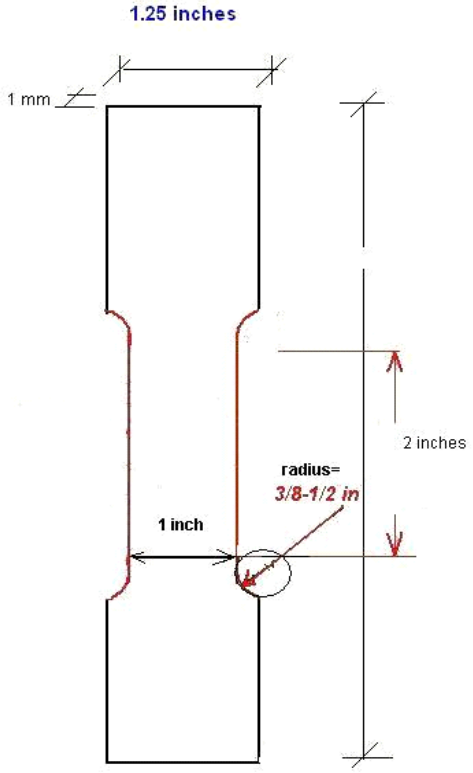


a) plan-form and dimensions

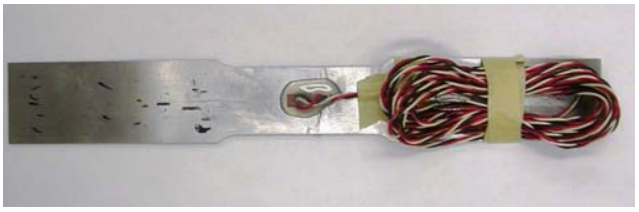

b) example used in ambient testing with strain gage

c) exposed side used in NN-pH SCC testing

d) unexposed side used in NN-pH SCC testing

**Figure 19. Specimen geometry used for the ambient and NN-pH SCC testing**

## Experimental Design

The effects of stressing considered both monotonic and cyclic loading, the later designed to represent the service conditions typically experienced by pipelines, as discussed for example in regard to Figure 15. Under such cycling with strain (displacement) control, steels typically exhibit phenomena known as cyclic hardening or cyclic softening[71,72], depending on the steel, its processing, and the magnitude of the cyclic strain[e.g., 72,73,74]. Parallel phenomena develop due to the same mechanism under load (force) control[72], which when instability ensues is known as ratcheting. Cyclic softening has for some time been suggested as the source of microplasticity that motivates SCC in pipeline applications[e.g., 21].

Cyclic softening was achieved by load-control cycling on samples prepared from the same two steels considered above under ambient conditions. Samples of X65 and X52 line pipe steels were cycled at a frequency of 1Hz, over a range of stress cycles with respect to specified minimum yield strength (SMYS), with the percent-SMYS magnitude taken as the reference for the upper limit in the cycle. Cycling up to a limit of 20,000 was done for the high stress-amplitude case (upper limit at 65-percent of SMYS with lower limit at 10-percent).

## Experimental Set Up For NN-pH SCC Testing

Figure 20 is a photograph of the complete setup of the electrochemical cell developed for NN-pH SCC testing. This testing involved concurrent exposure of steel specimens to the NS4 synthetic groundwater solution and axial loading. As noted above, the NS4 solution contained (in g/L):

0.122 potassium chloride (KCl); 0.483 sodium bicarbonate, ($NaHCO_3$); 0.181 calcium chloride ($CaCl_2.H_2O$) and 0.131 magnesium sulfate ($MgSO_4.7H_2O$)). As is apparent from Figure 21, this synthetic groundwater environment was contained in a glass chamber designed to both contain the test solution while it also exposed the flat steel specimens shown in Figure 20. For this testing one side of the test section was prepared using 600-grit paper, with the remainder of the specimen coated using coal tar enamel to expose only a 1-inch square area, as was shown in Figures 19b and 19c. Figure 20, which presents an overview of the test setup shows that wedge-grips under hydraulic load were used to transfer slow strain rate tension-tension cycling into the test specimen. This cycling was introduced in stages, as follows. To limit the time involved and also maximize the available microplasticity for time-dependent response in the slow strain testing, the initial loading to a target level below the yield stress was applied via a high-speed ramp. Once this ramp was completed, slow strain rate cycling at 1E-6 $sec^{-1}$ was started using the setup shown in Figure 21.

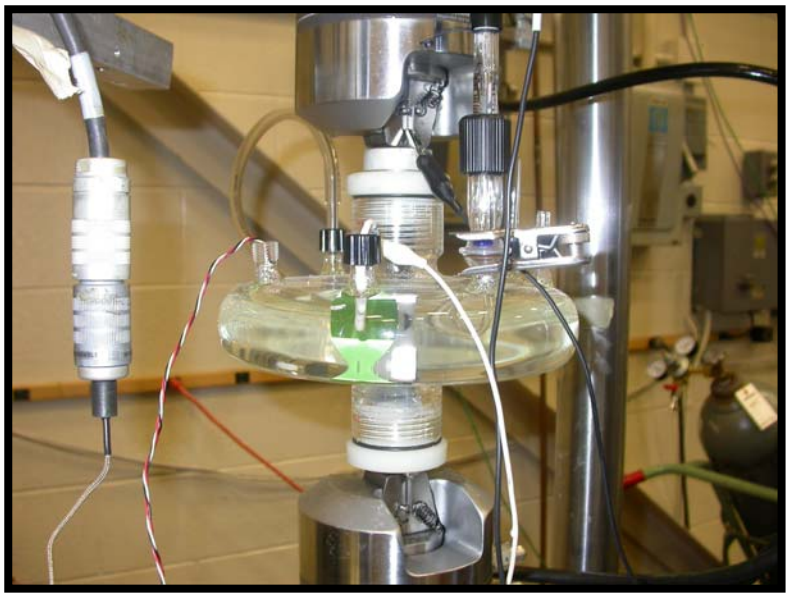

**Figure 20. NN-pH SCC chamber designed for cyclic loading with environmental exposure**

**Figure 21. Experimental set up for the NN-pH SCC testing**

Figure 22 presents a close-up of the cell configuration used to contain the environment and provide for the electrochemical measurements during slow strain rate testing. The working electrode was the flat steel X52 or X65 test specimen whereas the counter electrode was a gold-platinum alloy (95%Pt-5%Au) and the reference electrode was a calomel saturated SCE. The glass chamber contained five different ports for gas injection and sample probes location and was designed to hold a metallic band-heater that allows control of the temperature.

**Figure 22. NN-pH SCC test chamber with three electrode system (reference electrode, SCE, and counter electrode, Pt-Au alloy)**

## Electrochemical Impedance Spectroscopy Techniques to Track System Response under NN-pH SCC Conditions

Electrochemical techniques have evolved as powerful tools for corrosion rate estimations and mechanistic analysis of the metal dissolution in specific environment in terms of the operation conditions and with respect to time, that helped to characterize the interfaces and follow multivariable processes in real time. Electrochemical techniques based on AC electrochemical impedance spectroscopy (EIS) can characterize the interfacial mechanisms while different conditions are developed in an electrochemical cell. Accordingly, such techniques can help to understand the SCC phenomenon, which herein considers the near-neutral environment. DC principles can be used to characterize the interfacial phenomenon while hydrogen permeation is taking place within a metallic structure, and so likewise can be useful in understanding NN-pH SCC. The wide range of frequencies for EIS AC technique allows the separation of each element of the electrochemical cell associated to electrical elements in "real time." Both techniques can be used for different applications from sub-micro scale systems (nanometric scale) to macro electrochemical systems (field conditions scale).

EIS monitors in "real time" are the interface for an electrochemical system while it is subjected to different conditions such as the loadings characteristics of pipeline SCC. The output variable of EIS technique is the impedance magnitude that can be represented quantitatively in a mathematical expression by following two different approaches – via electrical analogs that represent the physical characteristics of the electrochemical system with passive electrical elements – and via mechanistic models that describe the transport properties occurring in the electrochemical system. This section uses the EIS technique applied to the electrochemical cell formed with steel to evaluate causal factors for the SCC process considering the slow-strain rate loading coupled parametrically with various NN-pH conditions.

# Develop Parametric Results Quantifying Evolution of Hydrogen

## Calculate Mass Transport Characteristics for Hydrogen Permeation and the Evolution of Hydrogen

The hydrogen permeation rate (HPR) and diffusion coefficient ($D_{eff}$) can be estimated from the results of permeation experiments using the following expression [64,6574,75]:

$$HPR = J_{ss} L = \frac{i_{ss} * L}{n * F} \tag{12}$$

where

- $J_{ss}$ is the steady state atomic hydrogen permeation flux in mol H .$s^{-1}$ $cm^{-2}$,
- $L$ is the specimen thickness (cm),
- $i_{ss}$ is the steady-state atomic hydrogen permeation current density (A/$cm^2$),
- $F$ is the Faraday´s constant (96500 C/mol), and
- $n$ is the number of transfer electrons for hydrogen reduction reaction.

In contrast, the effective atomic hydrogen diffusion ($D_{eff}$) is calculated via Equation 13:

$$D_{eff} = \frac{L^2}{6t_{lag}} \quad (13)$$

where

- $t_{lag}$ is the time lapsed to achieve a value of $i(t)/J_{ss}=0.63$ (s),
- $i(t)/J_{ss}$ the normalized flux of atomic hydrogen, and
- $J(t)$ = time dependent atomic hydrogen permeation flux as measured on the oxidation side of the specimen (mol of H.s$^{-1}$ cm$^{-2}$).

Tables 9 and 10 present results of the hydrogen permeation experiments and calculations, including the diffusion coefficient, current density and time lag in terms of the concentration of ionic species that formed NS4 solution, for two different pipeline steels grades and two temperatures. These tables illustrate the magnitude of the diffusivity of the hydrogen transported in atomic form within the metallic structure. It can be seen that the magnitude range is from 1E-07 to 1E-08 cm$^2$/seg, which depends on the temperature, steel composition, and ionic concentration.

The hydrogen current density favors atomic hydrogen formation at the surface of the steel. However, the physical properties of different steels influence the magnitude of current density associated with the corrosion product layer that is formed when different combinations of electrolyte and ionic solution are in contact with the metallic structure. Temperature is an important variable that contributes to the magnitude of the diffusion coefficient; whose dependence is proportional to the corrosion product formation. The diffusion and concentration influence the transport of ionic concentration from the bulk to the metallic structure, such as hydrogen, magnesium, and sulfate. These species in solution decrease the hydrogen diffusion coefficient parameter and the current density; therefore, these ionic species can be considered as a hydrogen reaction inhibitor. On the other hand, bicarbonate ion influences the transport properties of hydrogen ion within the electrolyte solution, the proportionality for the X65 steel in terms of diffusion coefficient is shown in Table 11 where the higher the concentration of bicarbonate ion, the lower the diffusion coefficient magnitude. Therefore the concentration increment of bicarbonate decreases the transport of atomic hydrogen to the metal-electrolyte interface and further accumulation of this species within the metallic structure.

**Table 9. Hydrogen diffusion coefficients in X-52 steel for different conditions**

| Electrolyte Composition and Temperature (C) | Time Lag (seconds) | Diffusion Coefficient (cm$^2$/seg) | Current Density (Amp) |
|---|---|---|---|
| 0.1 HCO3 T=25 | 5550 | 3.00E-07 | 1.14E-07 |
| 0.1 HCO3 T=45 | 4500 | 2.8$^E$-07 | 1.07E-07 |
| 0.5 HCO3 T=25 | 9300 | 1.79E-07 | 3.40E-07 |
| 0.5 HCO3 T=45 | 2075 | 8.03E-07 | 1.37E-07 |
| 1 HCO3 T=25 | 11550 | 1.44E-07 | 2.39E-08 |
| 1 HCO3 T=45 | 9800 | 3.01E-07 | 8.3E-08 |
| 0.5 HCO3+KCl T=25 | 8475 | 1.96E-07 | 7.68E-08 |

| Electrolyte Composition and Temperature (C) | Time Lag (seconds) | Diffusion Coefficient ($cm^2$/seg) | Current Density (Amp) |
|---|---|---|---|
| 0.5 HCO3+KCl T=45 | 4450 | 3.74E-07 | 2.46E-07 |
| 0.5 HCO3+CaCl2 T=25 | 13520 | 1.23E-07 | 1.40E-07 |
| 0.5 HCO3+CaCl2 T=45 | 3000 | 5.55E-07 | 4.10E-07 |
| 0.5 HCO3+MgSO4 T=25 | 9620 | 1.73E-07 | 8.66E-08 |
| 0.5 HCO3+MgSO4 T=45 | 10340 | 1.61E-07 | 9.60E-08 |
| 0.5 HCO3+NS4 T=25 | 8225 | 2.02E-07 | 2.98E-08 |
| 0.5 HCO3+NS4 T=45 | 11200 | 2.3E-07 | 1.30E-07 |

**Table 10. Hydrogen diffusion coefficients in X-65 steel for different conditions**

| Electrolyte Composition and Temperature (C) | Time Lag (seconds) | Diffusion Coefficient ($cm^2$/seg) | Current Density (Amp) |
|---|---|---|---|
| 0.1 HCO3 T=25 | 16200 | 1.028E-07 | 1.46E-04 |
| 0.1 HCO3 T=45 | 15200 | 1.096E-07 | 4.76E-05 |
| 0.5 HCO3 T=25 | 11360 | 1.467E-07 | 1.60E-04 |
| 0.5 HCO3 T=45 | 6640 | 2.510E-07 | 1.09E-04 |
| 1 HCO3 T=25 | 6820 | 2.443E-07 | 2.61E-06 |
| 1 HCO3 T=45 | 5400 | 3.086E-07 | 1.03E-04 |
| 0.5 HCO3+KCl T=25 | 12380 | 1.346E-07 | 5.00E-08 |
| 0.5 HCO3+KCl T=45 | 5240 | 3.180E-07 | 2.08E-07 |
| 0.5 HCO3+CaCl2 T=25 | 14720 | 1.132E-07 | 1.20E-04 |
| 0.5 HCO3+CaCl2 T=45 | 6640 | 2.510E-07 | 1.10E-04 |
| 0.5 HCO3+MgSO4 T=25 | 19780 | 8.426E-08 | 4.40E-05 |
| 0.5 HCO3+MgSO4 T=45 | 7720 | 2.158E-07 | 2.26E-05 |
| 0.5 HCO3+NS4 T=25 | 20900 | 7.974E-08 | 2.13E-07 |
| 0.5 HCO3+NS4 T=45 | 48200 | 3.457E-08 | 5.40E-05 |

## Theoretical Model to Calculate Current Permeation and Discharge Parameters

Consider now the combination of processes, such as chemical discharge-recombination in regard to molecular hydrogen formation reaction in the two step process as proposed by Al Faqeer[44] et al. This mechanism involves the adsorption of hydrogen ion on the metal converted in atomic form, as represented in Reaction 8. This recombination involves two adsorbed hydrogen atoms that evolved at the surface from the electrolyte, as in Reaction 9, where Fe-$H_{ads}$ refers to adsorbed hydrogen.

The total hydrogen adsorbed at the surface of the metallic structure can be estimated via impedance measurements at low frequencies [45], which facilitate quantification of permeation current via ACDC measurements.

The amount of hydrogen adsorbed can be obtained from EIS potentiostatic measurements and theoretical calculations, the latter estimated by considering the "cover factor"[45], which can be determined with the impedance magnitude of the lowest frequency in the impedance spectra by assuming adsorption control mechanism. The impedance developed over a given frequency range provides the parameters needed to quantify hydrogen evolved at the interface, where the current permeation with respect to concentration of hydrogen ion at the interface is estimated from EIS measurements. This approximation is described later in this report.

**Table 11. Hydrogen permeation magnitudes for different $NaHCO_3$ solutions**

| Electrolyte Composition (g/L @25C) | Diffusion Coefficient ($cm^2$/seg) | Maximum Experimental Current Density (Amp/$cm^2$) | Calculated Permeation Current Density (Amp/$cm^2$) |
|---|---|---|---|
| 0.1 NaHCO3 | 1.02881E-07 | 1.46E-04 | 2.37244E-11 |
| 0.5 NaHCO3 | 1.46714E-07 | 1.60E-04 | 3.38322E-11 |
| 1 NaHCO3 | 2.44379E-07 | 2.61E-06 | 5.63538E-11 |
| NS4 | 7.97448E-08 | 2.13E-07 | 2.91448E-12 |

## Quantifying Mass Transport Characteristics for Hydrogen Diffusion in Steel under different NN-pH SCC and High-pH Conditions

The theoretical approach formulated in Equation 9 is used now to illustrate profiles of hydrogen ion concentration. These concentration profiles are considered from the bulk to the metal-electrolyte interface based on an algorithm programmed in Matlab. From this calculation we determine the time when a specific concentration of hydrogen reaches the interface as a function of different initial conditions. Theoretical simulation of the concentration profiles is included in Figure 23 based on the data shown in Table 12, where the kinetic model is used to determine the hydrogen concentration profiles by assuming the formation of iron carbonate at the interface.

**Table 12. Input and Output parameters for near-neutral pH solutions via the kinetic model**

| Input | Output |
|---|---|
| Initial Concentration of $C_{Cl}$=0.2; | Time for concentration profile after 1000 sec |
| $C_{HCO3}$=0.15 | |
| $C_H$=0.1 | |
| $C_{CO3}$=0.1 | $C_H$=0.45 |
| $C_{H2CO3}$=0.1 | $C_{Cl}$=0.025 |
| $C_{SO4}$=0.15 | $C_{SO4}$=0.05 |
| Diffusion Coefficients, $D_{SO4}$=1E-5 | $C_{HCO3}$=0.001 |
| $D_{HCO3}$=2e-4 | |
| $D_H$=1E-04 | |
| | Relation for atomic initial-ion hydrogen content with instantaneous hydrogen concentration before atomic hydrogen formation within the metallic structure: |
| Constant rates for FeCO3 formation, | |
| Kfca=0.000001 | $C_{Hcr}/C_{+}/C_{H+in}$=4.5 |
| Kbca=0.000001 | |
| Kfbbi=0.000001 | Time to reach critical aspect ratio T=1000 sec |
| Kfbi=0.00001 | |
| Temperature 20 C | |

The theoretical results shown in Figure 23 qualitatively describe the concentration profile for specific initial conditions, with profiles shown for different times. Figure 24 illustrates the experimental $H^+$ profile in terms of pH magnitude at different times and positions. Results of the theoretical formulation presented in Figure 23 illustrate the transport characteristics of hydrogen ions within the bulk and at the electrode interface, and show the accumulation of the species as a function of time. This latter magnitude represents the conversion to atomic hydrogen and the capacity to transport it into the metallic structure. Note that the aspect ratio set in the hypothetical conditions for $C_{Hcr}/C_{in}$ reaches $4.5C_{Cl}$ after 1000 seconds.

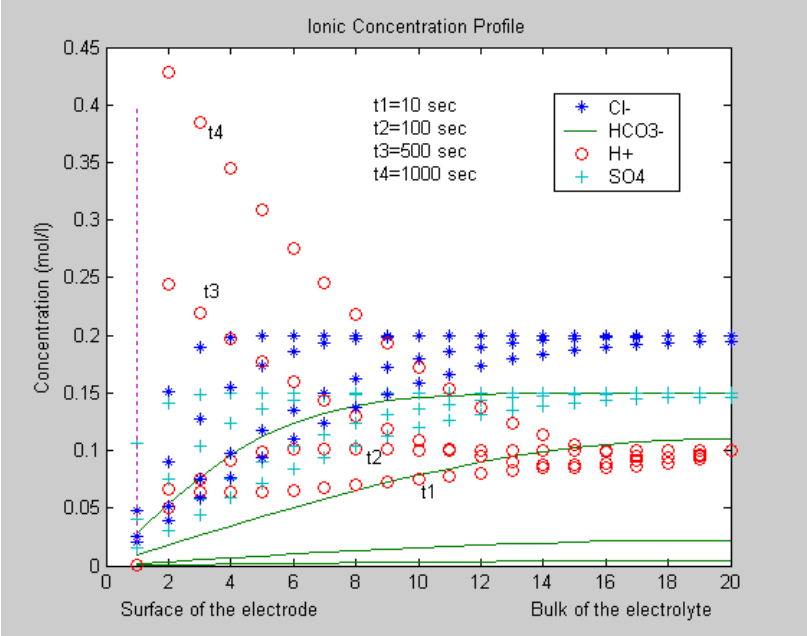


**Figure 23. Concentration profile for ionic species presented in the NS4 solution with time**

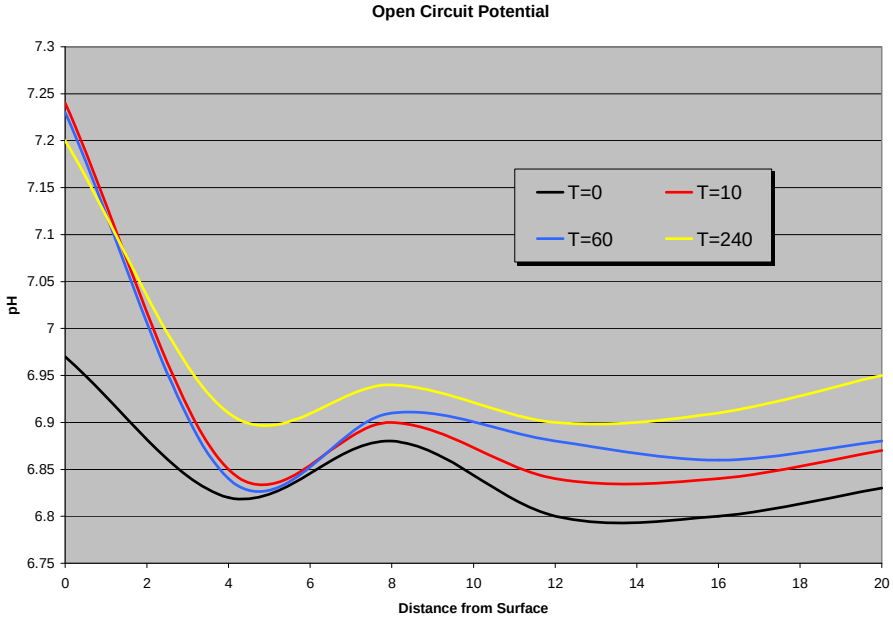


**Figure 24. Experimental results for hydrogen ion content in terms of the pH measurements**

## Illustration: Kinetics Model Applied to High pH Environment

If anaerobic conditions prevail and $CO_2$ (aqueous) is present, the decomposition products, such as $HCO_3^-$, lead to near-neutral solutions with iron carbonate forming as the main corrosion product, as indicated in Reactions 3. In this case, the iron carbonate ($FeCO_3$) promotes the formation of atomic hydrogen at the metal-electrolyte interface as part of the cathodic reaction. If this atomic hydrogen diffuses within the metallic structure, additional stress is induced. In

contrast, where aerobic conditions prevail combined with $CO_2$ (aqueous) the decomposition equilibrium reaction promotes high pH conditions with the carbonate ion being the main species resulting from the decomposition of $CO_2$ For this situation the cathodic reaction is the reduction of oxygen with the corrosion product in high pH solutions being iron oxide which in presence of OH- leads to iron hydroxide. This is the scenario depicted by the Reactions 4.

The algorithm programmed for near-neutral solutions was used to calculate the concentration profile under high pH conditions, with the expectation that the characteristics of the corrosion product will differ for the reactions considered. Figure 25 illustrates typical results simulated via this kinetics model, which as noted for this figure represent high pH conditions and also the effect of oxygen in the electrochemical cell. This figure shows the theoretical concentration profile for oxygen over time as it diffuses throughout the bulk and corrosion product layer. The result is concentration accumulated at the interface or the formation of the corrosion layer due to the anodic dissolution and electrolyte conditions that lead to $Fe_3O_4$ under high pH conditions. The results in Figure 25 indicate the depletion of oxygen at the interface due to cathodic reduction reaction and the formation of the corrosion product layer with time.

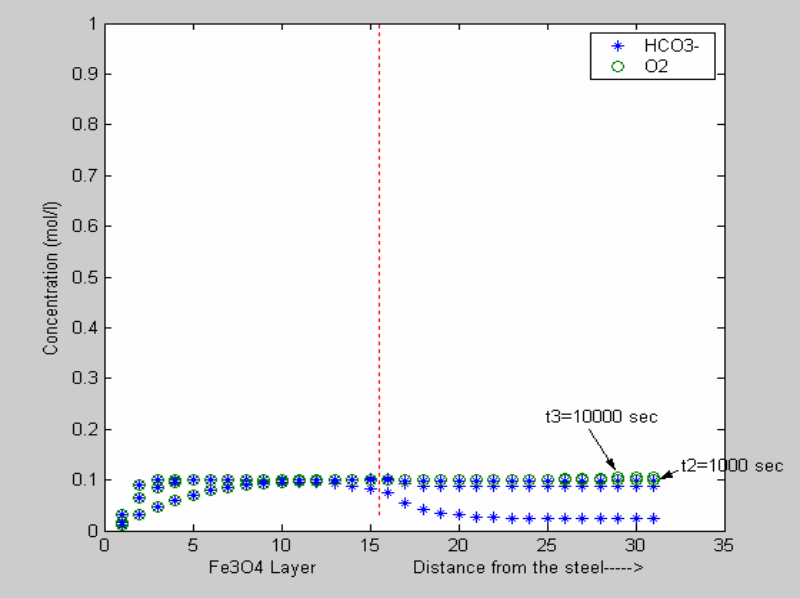


**Figure 25. Ionic concentration profile for high pH environment in the presence of oxygen**

## Correlate Hydrogen Evolved and its Effect on Microplastic Response

The section evaluates relationships between electrochemical properties and factors controlling near-neutral SCC over a range of experimental conditions. Electrochemical parameters, like charge transfer resistance and electrical aspects associated with the interfacial physical parameters of the electrochemical cell, should be sensitive to parameters such as the extent of hydrogen formation and its influence on the microplastic response and/or cyclic softening

response[10]. Accordingly, the AC technique EIS has been coupled with bias polarization experiments to explore parametric relationships between hydrogen formation as a function of electrochemical parameters, such as cathodic reaction and its effect on microplastic response.

EIS coupled with potential bias (polarization) under near-neutral conditions facilitates study of atomic and molecular hydrogen formation at the interface between the steel and the near-neutral solution. Atomic hydrogen is formed at this interface as a metal-corrosion product and in that form can diffuse within the metallic structure and integrate into the microstructure. Differences in the properties of the interface change the impedance response, which depends on the characteristics of the surface. Cyclic softening is a phenomenon that introduces microplastic deformation, which for the nominally elastic loadings experienced by pipelines localizes due to the "free-surface" effect within surface of the metal structure in grains favorably oriented for slip. Therefore, interfacial reactions between the environment and the metal surface can be expected to develop different corrosion products or morphology as compared to non cyclic softened conditions. The EIS technique was used to characterize the parameters that influence differences in the formation of corrosion products while NN-pH SCC develops.

## Use of Electrochemical Techniques and Their Interpretation

Polarization and permeation magnitudes show the formation of corrosion products and the influence in the transport properties through use of DC basis electrochemical techniques as compared to the reference condition where line pipe steel samples are exposed to near-neutral environment while unstressed. The important assumption is the cathodic reaction introduced earlier in Expressions 9 and 10. These expressions are the basis to estimate the hydrogen current density and diffusion coefficient that show the influence of each ionic species that formed the electrolyte.

The key parameter to quantify the ionic species at the interface is the cover factor, results for which are shown for $HCO_3^-$ in Table 13. The magnitude of the cover factor motivates bicarbonate ion interaction with the active sites left by the iron carbonate (corrosion product formed). As indicated in the expressions that follow below, the cover factor is directly proportional to the ionic concentration and permeation current. This relationship allows the implementation of electrochemical techniques to quantify the ionic species and the atomic hydrogen formed without use of the permeation experiment setup.

**Table 13. Cover factor and kinetic magnitudes from polarization tests of X-65 in $NaHCO_3$**

| Electrolyte Composition (g/L @25C) | a | $i_o$ ($A/cm^2$) | $k_1$ ($s^{-1}$) | $\theta H$ | HCO3- |
|---|---|---|---|---|---|
| 0.1g/L NaHCO3 | -0.021917648 | 2.69891E-05 | 1.00278E-13 | 0.15 | 0.85 |
| 0.5g/L NaHCO3 | -0.038149343 | 0.000510199 | 1.89565E-12 | 0.1 | 0.90 |
| 1g/L NaHCO3 | -0.027490206 | 0.002372008 | 8.81323E-12 | 0.03 | 0.97 |

[10] As discussed earlier, cyclic softening has for some time been suggested as the source of microplasticity that motivates SCC in pipeline applications[(e.g., 21)].

Table 13 shows the adsorption magnitudes that relate DC and AC techniques that help to estimate hydrogen evolution and permeation in presence and absence of load conditions. Successful use of these electrochemical techniques indicates it is feasible to measure interface properties and to determine the charging current electrode (ic), which is the sum of the recombination current (ir) and the steady state permeation current (iα) – (ic=ir+iα) due to hydrogen cathodic reaction.

The cathodic reaction includes processes that describe the interaction of measurable variables with theoretical modeling. The hydrogen ion diffuses and interacts with the surface of the electrode. After the initial conversion of hydrogen ions into atomic hydrogen at the surface there are two possible further paths for the atomic hydrogen that are the atomic permeation and the recombination reaction, which reflect either atomic or molecular hydrogen interaction with the metal, respectively. The recombination reaction leads to evolution of molecular hydrogen out of the electrolyte, while the permeation of hydrogen produces the atomic accumulation in the metallic matrix.

The cathodic reaction can be expressed in terms of electrochemical measures such as cathodic current produced for the hydrogen evolution reaction. The magnitudes that relate experimental conditions with the current for our parametric analysis include the cover factor and concentration of hydrogen ions. Therefore the cathodic current can be expressed in terms of the overpotential parameter, as follows:

$$i_c = Fk_1 CH^+ \ (1 - \sum \theta - \theta_H) \exp(-a\alpha\eta) \tag{14}$$

where F is the Faradays constant, $k_1$ is the constant reaction rate; $C_{H+}$ is the hydrogen concentration, θ is the cover factor, η is the overvoltage and α is the symmetry factor.

The recombination reaction is expressed in terms of cover factor of the hydrogen as given by Equation 15:

$$i_r = Fk2\theta_H^2 \tag{15}$$

where F is the Faraday's constant, k is the constant reaction rate, and θ the cover factor of hydrogen calculated from the DC polarization expressed in Equation 14.

The hydrogen permeation current is expressed in terms of the model of Iyer et al[(6676)] where the permeation current generated by the permeation flux or current is given by the following expression:

$$i_\infty = FD\frac{C^0{}_H}{L} \tag{16}$$

where D is the bulk diffusivity of hydrogen in the metal, L=the thickness of the metal membrane (or metallic plate), and $C^o_H$ is the concentration of hydrogen in the metal adjacent to the surface.

The hydrogen permeation current can be expressed in terms of directly measured variables determined by DC electrochemical techniques, such as the time that the hydrogen current stabilizes with time.

Note: The total cathodic reaction current comprises the permeation and the recombination currents. The hydrogen permeation experiments quantify important parameters such as the permeation current and diffusion coefficient, while the recombination reaction determines the

hydrogen cover factor. These expressions are used for static conditions and the permeation testing, with similar procedures proposed for cyclic load conditions. The Hydrogen Evolution Reaction (HER) can be used to estimate the total hydrogen evolved when NN-pH SCC occurs. Electrochemical techniques, such as EIS and polarization, quantify the experimental characteristics of the steel-electrolyte interface and the hydrogen current density for the different hydrogen processes.

## Correlation between Electrochemical-Parameters and NN-pH SCC Test Results via EIS

EIS is an electrochemical tool that has been used for the analysis of corroding mechanisms, such as localized attack[77,78], coating defects, and crack detection[79,80]. The EIS technique correlates frequency response analysis (using a small single AC sine perturbation) to the electrochemical system and measurement of the resultant current and voltage, via a potentiostat. This enables repeatable and accurate determination of the relationship between input and output with Linear System Theory (LST) analysis used to model the outcome. LST is used to test the validity of experimental data using linear equations rather than second order differential equations. If the applied potential is an AC sine signal across a range of frequencies, the corresponding current will be a sine wave signal for same number of frequencies. The impedance of the system is quantified by the phase shift between the input voltage and the output current in the frequency domain; therefore if a small sine signal amplitude is applied across a simple electrochemical cell, the changes in transport phenomena, electrochemical reactions, and physicochemical properties due to that perturbation and current distribution can be described in terms of passive electrical elements.

The approach adopted involves comparison of results developed for samples of line pipe steel pretreated with microplastic deformation (cyclically softened) with results developed on samples that were either not pretreated or otherwise stressed in NN-pH solutions, at different polarization levels. Such data were developed for monotonic tension as well as for cyclic loading comparable to that experienced by pipelines and compared to results developed for the reference unstressed condition.

Figure 26a associates electrical passive elements with the components of an electrochemical cell, i.e., low carbon steel exposed in NS4 solution. In this figure, a resistor ***Re*** represents the electrical resistance of the electrolyte, with the parallel resistance in the circuit, ***Rct***, associated with the charge transfer resistance, or the kinetics of the electrochemical reactions that exist at the interface (cathodic and/or anodic reactions), such as a corrosion process. The term ***Cdl*** represents the double layer capacitance at the electrode/electrolyte interface. The magnitude of ***Cdl*** determines the physical characteristics of the corrosion products interacting with the metal and the electrolyte. The electrical characteristics of the elements of the circuit are described according to the frequency range. At high frequencies the magnitude of the capacitance (***Cdl***) makes the charge transfer easily due to the low impedance characteristics of this passive component, therefore leaving the influence of the electrolyte resistance (***Re***) at this frequency limit. As the frequency approaches zero the capacitor ceases to conduct and the charge goes to the lowest resistance path (low impedance) leaving the influence of ***Rct*** and ***Re.*** Finally, as the frequency remains between finite limits, the capacitance magnitude influences the electrical circuit, having the influence of the components illustrated in Figure 26a. The electrical passive

elements can be expressed as a network of capacitors, inductors or resistances to quantify and characterize the processes that describe the electrochemical cell, like in Figure 26a.

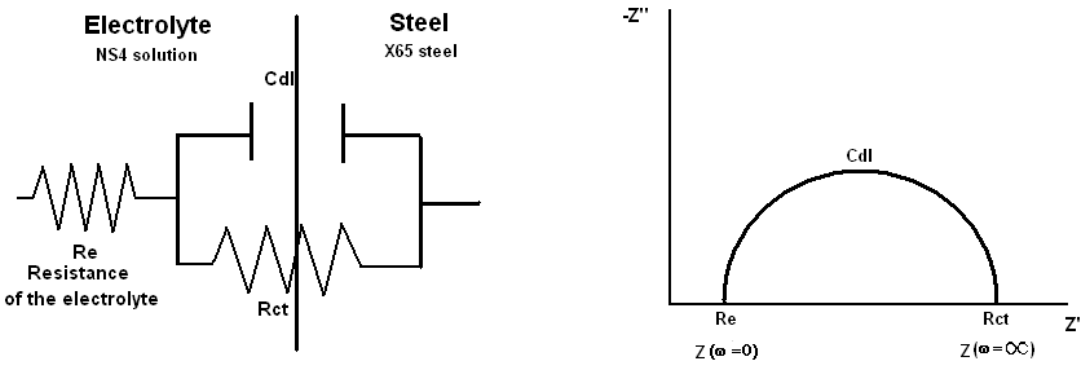


**Figure 26. a) – RC circuit describing a simple electrochemical cell interface and elements and b) – the complex representation due to this electrochemical cell**

The impedance results are plotted in three different formats. The phase angle format represents the phase shift changes at different frequencies due to the relation between input and output signal in the frequency domain. The complex representation or Nyquist format represents the real and imaginary components that describe the characteristics of the system as complex vectors at different frequencies, as shown in Figure 26b. The third representation, the total impedance representation or Bode plot, displays the characteristics of the physical conditions in terms of an independent variable (frequency).

In this work, the EIS technique is implemented as a monitoring and diagnosis tool for the NN-pH SCC initiation phenomena by assuming that we are able to follow the response of electrochemical reactions. This work monitors the physicochemical properties of X65 steel exposed in NS4 solutions after different electrolyte concentrations and NN-pH SCC sensitive variables, such as cyclic softening (mechanical pretreatment). The electrochemical parameters that can follow the dissolution characteristics of the metal exposed in near-neutral solutions and the influence of the mechanical pretreatment under SCC conditions are the electrolyte resistance, the impedance at the interface, and the porous resistance from the corrosion products formed with respect to time. The EIS results associate each element of the electrochemical cell with passive electrical properties that describe the system as shown in Figure 26a.

**EIS Results at Zero Stress**

The reference unstressed condition was developed using samples of X-65 steel exposed to the NS4 solution without cyclic softening pre-treatment and without polarization bias. This zero external loading situation serves as the reference state for the adsorption process of the ionic species using EIS characterization.

Figures 27 and 28 contrast the impedance response for the unstressed reference condition to the same circumstance developed in samples after cyclic softening pretreatment. It is apparent from this comparison of unloaded specimens evaluated over a range of values of potential bias that cyclic softening pretreatment changes the impedance response characteristics of the interface. Impedance analysis in terms of passive electrical elements characterizes the general trends and parametric relationships developed in the electrochemical cell with the X65 steel and the NS4

electrolyte. Table 14 shows the magnitudes of the electrical elements associated to the elements of the electrochemical cell formed when no mechanical pretreatment and unload conditions existed. The electrical circuit associated to this condition is an electrolyte resistance represented by R1, a corrosion product that forms a cover layer at the steel surface, acting as a semiconductor or pseudo-capacitor material and magnitude associated to this layer is associated to CPE1 magnitude, and the resistance of the porous formed in the layer represented as magnitude R3. The transport phenomena occurred at the interface can be followed by the magnitude represented as CPE2 magnitude, and the charge transfer resistance that considers either the anodic or cathodic reaction kinetics of the corrosion product-steel interface is represented by R2.

**Table 14. Different polarization conditions for X-65 steel for no pretreatment or stress**

| Bias mV(SCE) | R1 (ohm) | R2 (ohm) | R3 (ohm) | L1 | CPE1-T (Farads) | CPE-P | CPE1-T (Farads) | CPE-P |
|---|---|---|---|---|---|---|---|---|
| OCP | 1532 | 1779 | 1779 | 1704 | 2.1E-4 | 0.791 | 2.1E-4 | 0.791 |
| -200 | 1492 | 10991 | 10991 | NA | 2.5E-4 | 0.669 | 2.5E-4 | 0.669 |
| -250 | 1480 | 5590 | 5590 | NA | 2.1E-4 | 0.681 | 2.1E-4 | 0.681 |
| -500 | 1463 | 586.6 | 586.6 | NA | 1.79E-4 | 0.860 | 1.79E-4 | 0.860 |
| -800 | 1359 | 145.8 | 145.8 | NA | 1.36E-4 | 1.045 | 1.36E-4 | 1.045 |
| -1000 | 1298 | 101.6 | 101.6 | NA | 1.72E-4 | 1.059 | 1.72E-4 | 1.059 |

The electrical impedance associated with the interface and the resistance associated with the electrolyte reflect the characteristics of the layer formed (the corrosion product), which for the present involves iron carbonate precipitation (described via the thermodynamics and kinetics of NN-pH SCC) at the surface of the steel. Table 14 shows the magnitude of R3, which characterizes the porous resistance within the iron carbonate layer when no mechanical pretreatment exists on the steel sample. There it is evident that the magnitude of R3 decreases as the potential bias increases, which is attributed to the current increase at the corrosion product-steel interface. The open circuit potential condition shows adsorption of ionic species that are in the electrolyte. Assuming that hydrogen ion is the main species for the metal-electrolyte interface interaction, then the electrical passive element associated to the interface is an inductor or negative capacitance, such as the role of L1 illustrated in Figure 14. The ionic species increases its transport properties as the potential increases – therefore the formation of atomic and molecular hydrogen is feasible as the current capacity in the system (polarization condition) is increased. The cathodic reaction is potential dependent, therefore the rate and probability of atomic hydrogen diffusing within the metallic structure is proportional to polarization conditions.

The microplasticity phenomenon affects a few microns below the steel surface by changing the microstructure due to grain to grain interaction subject to compatibility requirements after the mechanical pretreatment. The surface changes promote changes in the film formation according to differences in electrical and physical characteristics that develop at the interface.

As is apparent from Table 15, the sample that has mechanical pretreatment (cyclic softening) and is exposed to NS4 solution without external stressing illustrates the impact on the impedance when different polarization conditions are applied. The EIS results in this table indicate this impact in terms of R2, which represents the porous resistance of the corrosion product, and R1,

which quantifies the kinetics of the cathodic reaction. Note that R2 increases when a negative potential of 200mV is added to the system, while R1 representing the polarization resistance (the cathodic or hydrogen reaction rate) remains steady. Note that the porous resistance, R2 includes the total hydrogen transport process throughout the corrosion product layer and the total hydrogen reaction, which is the combination of atomic formation and molecular formation.

**Table 15. Different polarization conditions for X-65 steel for microplasticity (cyclic softening) and static load conditions**

| Polarization (mV vs SCE) | R1 (ohm) | R2 (ohm) | CPE-T Farads | CPE-P |
|---|---|---|---|---|
| OCP | 419.6 | 474.8 | 1.08E-3 | 0.579 |
| -200 | 402 | 30000 | 1.61E-3 | 0.449 |
| -250 | 407 | 7829 | 1.22E-3 | 0.521 |
| -500 | 448.5 | 354.1 | 9.69E-4 | 0.542 |

The highest potential magnitude at 500mV vs. OCP applied to the cell shows the critical potential bias that starts to increase the kinetics of the hydrogen reaction. R1 and R2 magnitudes changed when 500mV bias is added to the system, with the resistances are decreased under the highest magnitude polarization bias. As becomes evident shortly, cyclic softening alters the surface condition leading to its susceptibility to the evolution of cathodic reaction sites for the hydrogen reaction.

The reactions that take place at the interface of the material with no mechanical pretreatment involve the adsorption and active processes with the related electrical magnitudes illustrated in Table 14. As becomes evident shortly, the response when cyclic softening is included in the metallic structure shows that the influence of the mechanical treatment on the free-surface and the related mechanisms differ – as becomes apparent in the inductance magnitude when cyclic softening is introduced. Likewise it becomes apparent that the magnitude of the resistance R3 is lower when mechanical pretreatment via softening is compared to mechanical treatment associated with service.

Figures 27 and 28 present the tabulated trends, respectively considering results without and then with polarization. Using these static conditions as a reference, we now consider differences in impedance measurements and mechanisms that develop as a result of dynamic cycling as compared to this reference. EIS is used as the tool to detect surface changes under otherwise similar NN-pH SCC conditions.

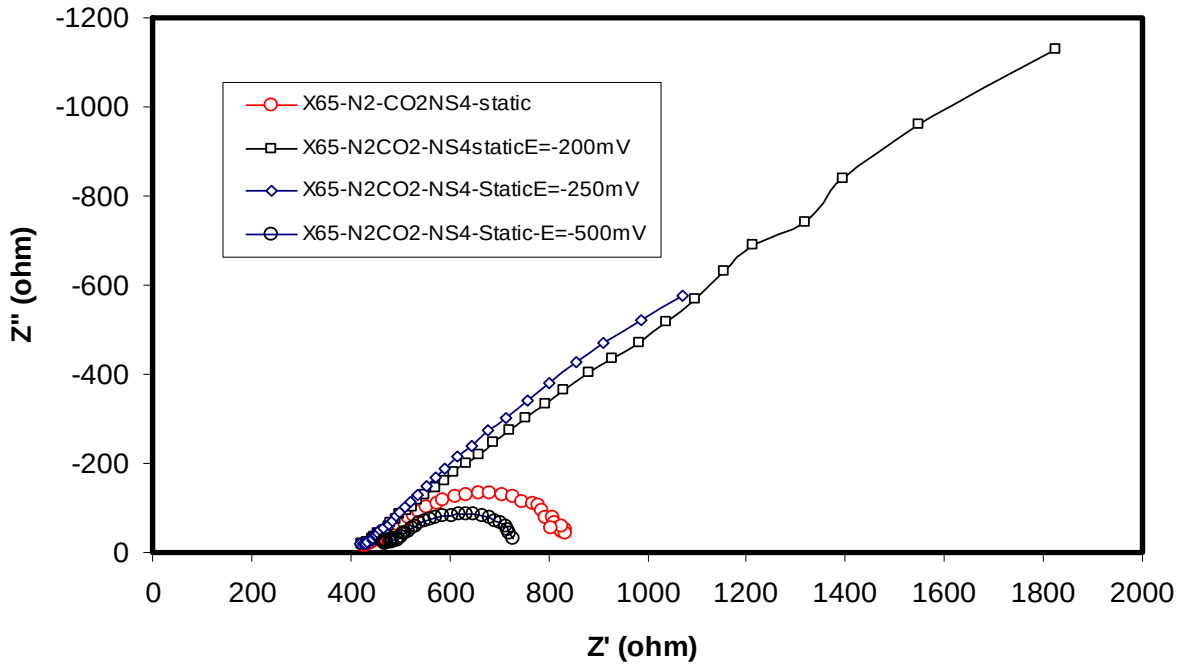


**Figure 27. Results in complex form for X-65 steel (no softening / no stress condition)**

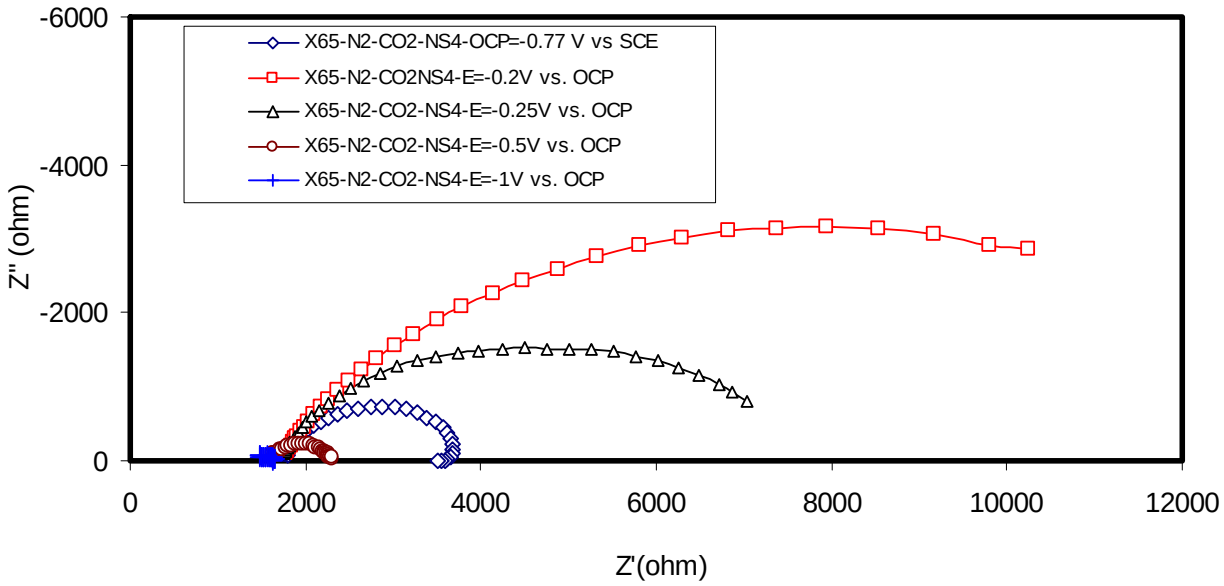


**Figure 28. EIS for X-65 steel as in Figure 27 for a range of different potentialsAC Impedance Characterization for NN-pH SCC over a Range of Polarization Conditions**

**Zero Polarization Reference State**

The utility of AC Impedance as a monitoring technique was evident in the prior section that developed reference conditions for the steel-electrolyte system considered to simulate field conditions involving line-pipe steel exposed to near-neutral cracking solutions under static conditions. As outlined earlier, this technique detects and tracks changes in the electrochemical cell as well as their evolution in the cell over time.

The slow strain cyclic testing considered in this section introduces small changes in the metal that can be detected at the interface with the electrolyte. Table 16 and Figure 29 present results for X65 samples subjected to cyclic loading with a period of 16 minutes per impedance spectra for testing in the same NS4 near-neutral environment. OCP (zero polarization) conditions are considered first contrasting the impedance parameters due to the effects of mechanical pretreatment and cyclic loading as compared to Figure 27. Thereafter differences in hydrogen generation will be considered over a range of polarization conditions in contrast to Figure 31. Key differences in the EIS spectra for these conditions become evident when these results are compared to the above reference data developed for static conditions.

**Table 16. EIS results for slow strain rate testing in NS4 at OCP conditions**

| Time (intervals) | R1 (ohm) | R2 (ohm) | CPE1-T (Farads) | CPE-1P |
|---|---|---|---|---|
| 1 | 434 | 877 | 5.12E-4 | 0.59 |
| 3 | 400 | 750 | 5.82E-4 | 0.63 |
| 7 | 412 | 672 | 6.2E-4 | 0.60 |
| 9 | 427 | 723 | 6.3E-4 | 0.63 |
| 11 | 425 | 716 | 6.5E-4 | 0.63 |
| 15 | 407 | 758 | 7.0E-4 | 0.62 |

Table 16 shows the impedance response in terms of electrical magnitudes for OCP conditions with time. The R1 magnitude describes the resistance of the electrolyte or the related ohmic-drop resistance. The parameter R2 cited therein represents the charge transfer resistance for this condition, and how the hydrogen reaction changes with time. It is evident that the kinetics is more favorable with time due to a decrease in this electrical magnitude and the increased time for the ion hydrogen to reach the surface of the steel.

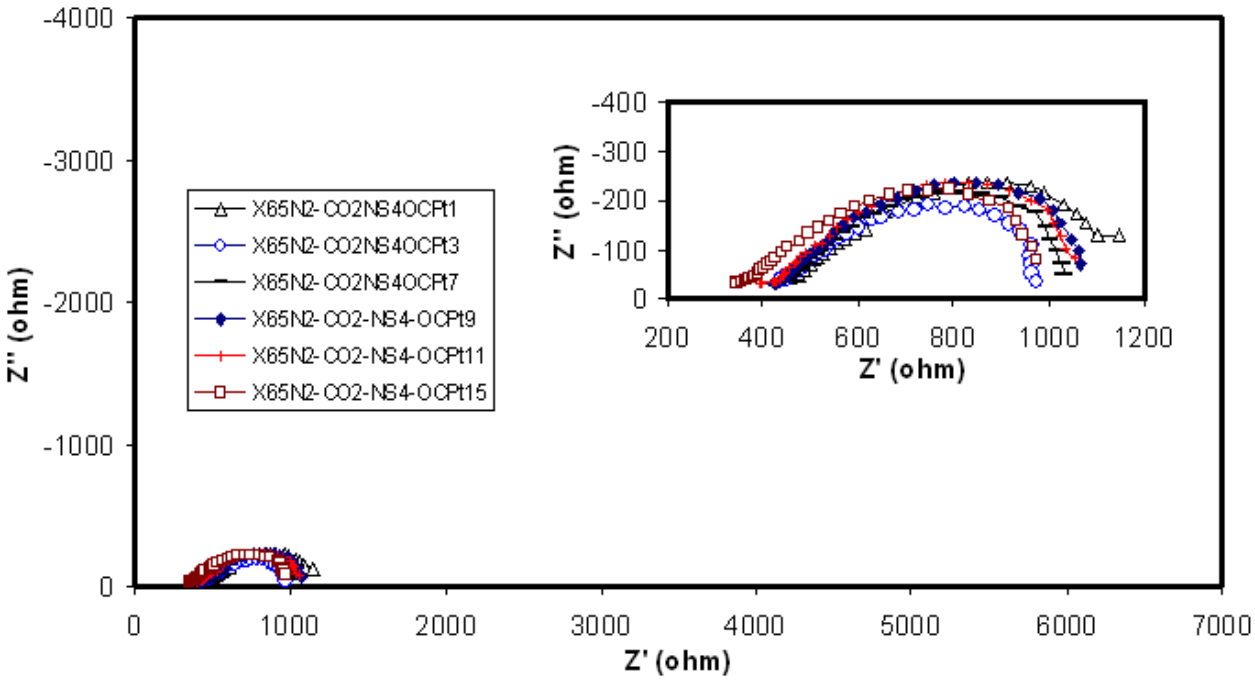


**Figure 29. EIS complex diagram for X-65 steel under NN-pH SCC conditions at OCP for different time intervals**

## NN-pH SCC simulated under protective conditions

The effects of polarization are evident in two characteristics of the steel-electrolyte interface exposed to near-neutral solution and cyclic loading. The first is the continuous growth of the corrosion product layer due to the increase in the porous resistance parameter, as is evident from Table 17 as the magnitude of R2 begins to decrease after the 4$^{th}$ measurement (time) interval. This latter change can be attributed to the breakdown of the corrosion product caused by the cyclic loading and the additional hydrogen stress induced due to polarization. The R1 magnitude represents the resistance of the electrolyte. The behavior of the parameter CPE indicates that this occurs as a pseudo-capacitance condition, which involves the formation of a dielectric (corrosion product). The response of the parameter CPE1, which shows continuous decrease over time, is attributed to the less conductive properties of the corrosion product under load conditions and the ionic or charge accumulation at the active sites.

**Table 17. EIS results for slow strain rate for E=-0.9V vs SCE**

| Time (interval) | R1 (ohm) | R2 (ohm) | CPE1-T (Farads) | CPE-1P |
|---|---|---|---|---|
| 0 | 575 | 4845 | 7.40E-04 | 0.61 |
| 1 | 567 | 5642 | 5.37E-04 | 0.63 |
| 2 | 579 | 6135 | 4.18E-05 | 0.664 |
| 5 | 574 | 4559 | 2.80E-05 | 0.68 |
| 9 | 567 | 3987 | 2.00E-05 | 0.7 |
| 13 | 574 | 3642 | 3.50E-05 | 0.68 |

Figure 30 shows the evolution of the impedance properties with time under polarization conditions (E=-0.9V vs. SCE) as represented on the complex plane. Electrical passive elements associated with the electrochemical interface describe the characteristics of the interface with time under polarization conditions, i.e. the charge transfer or R2 magnitude represents the hydrogen reaction. The response of R1 magnitude under polarization conditions indicates an increment of about 100ohm as compared to OCP conditions attributed to the addition of dissolved species from the anodic reaction (steel corrosion) to the electrolyte.

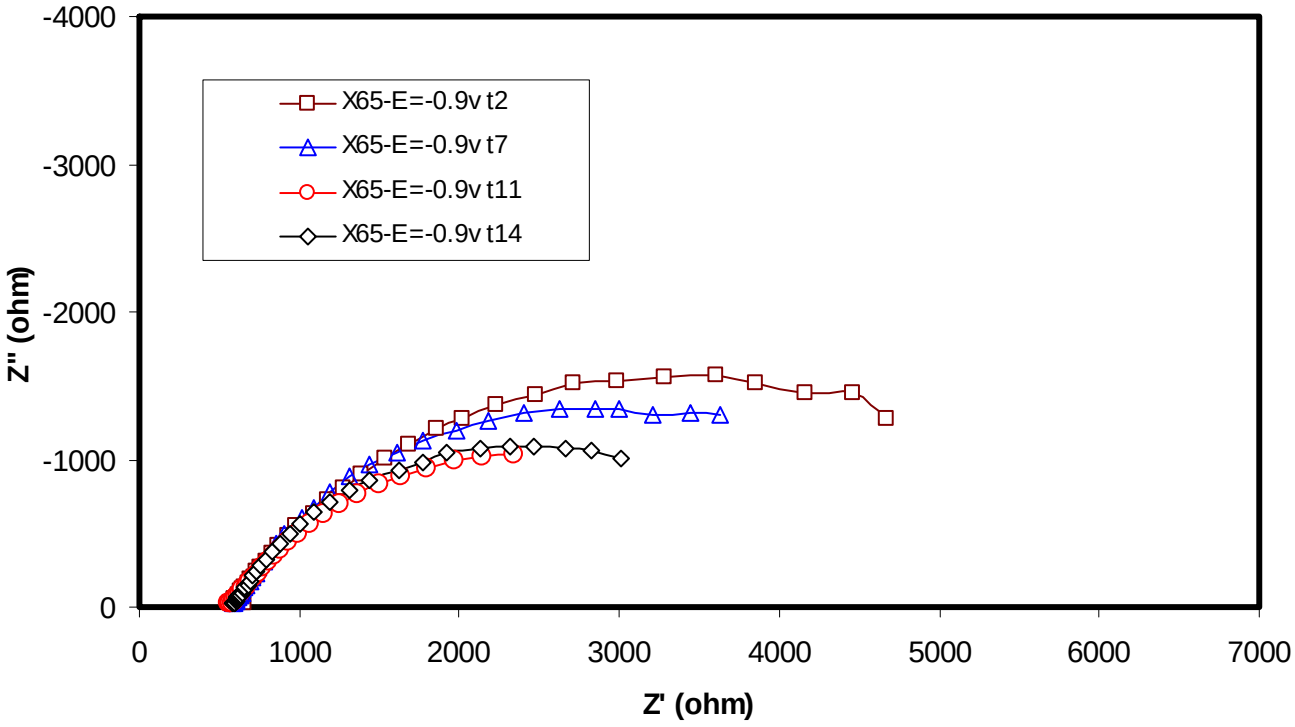


**Figure 30. Complex presentation format for X-65 steel under NN-pH SCC conditions after different exposure time at cathodic-polarization conditions (E=-900 mV vs. SCE)**

Figure 31 presents the response of the electrical parameters that describe the kinetics of the hydrogen formation when the highest polarization magnitude (E=-1.2V vs. SCE) is considered for this NN-pH SCC testing. The charge transfer resistance (magnitude of R2) decreases with time as expected in view of Table 18. This response resembles cathodic overprotection conditions for a buried steel pipeline, as the cathodic reaction is kinetically favorable at this potential due to the current added to the electrochemical interface, so the probability to form atomic and molecular hydrogen increases. Cyclic softening is the physical parameter that affects changes at the electrochemical interface in terms of the charge transfer resistance magnitude due to the corrosion product formation and subsequent breakdown – which accounts for the increase active area as compared to non-cyclic softening conditions.

Electrochemical components are associated to electrical passive elements (resistances, capacitors and inductors) to describe the process and transport phenomena at the interface. However one simple electrical circuit can not describe the localize behavior of the entire steel surface exposed to the electrolyte conditions, just the general characteristics as described earlier. Therefore,

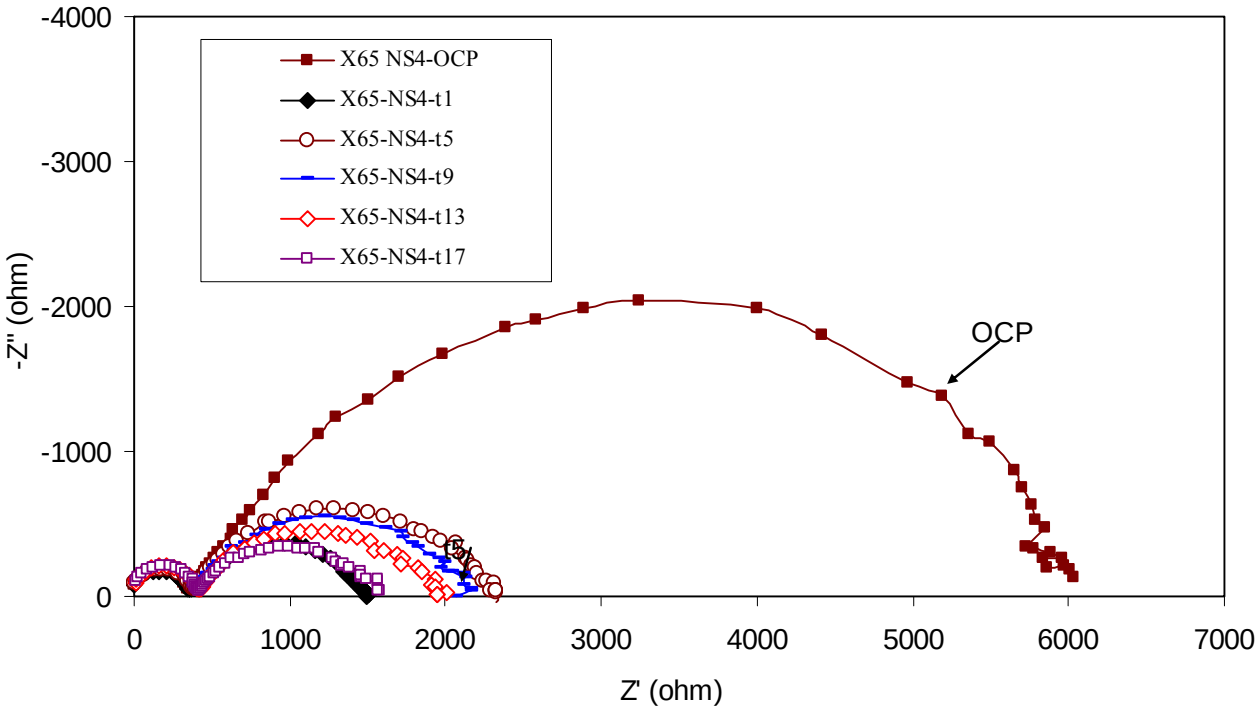


**Figure 31. EIS complex diagram for X-65 under NN-pH SCC conditions at different times and overprotected conditions, E=-1.2V vs. SCE**

deterministic models for impedance profiles are used to describe the electrical and physical distribution characteristics of the electrochemical interface when corrosion products are formed, such as Transmission Line Modeling that has been used to study high impedance, porous or long distance systems.

**Table 18. EIS results for slow strain rate E=-1.2V vs. SCE**

| Time (interval) | R1 (ohm) | R2 (ohm) | CPE1-T (Farads) | CPE-1P |
|---|---|---|---|---|
| OCP | 343 | 6072 | 2.89E-5 | 0.705 |
| 1 | 329 | 1216 | 4.18E-5 | 0.664 |
| 5 | 360 | 2221 | 2.64E-5 | 0.714 |
| 9 | 385 | 1741 | 2.67E-5 | 0.716 |
| 13 | 390 | 1637 | 3.20E-5 | 0.697 |
| 17 | 386 | 1247 | 4.49E-5 | 0.66 |

## Mechanical-Electrochemical Relationships for NN-pH SCC with Different Hydrogen Formation Conditions

As outlined above, the AC response has been obtained continuously over broad range of frequencies (7 decades) the results of which can be associated with the effects of variables such as cyclic softening or mechanical pretreatment at the surface due to corrosion product formation

and breakdown. The electrochemical parameters that can characterize the NN-pH SCC process and the physical changes of the steel interface over time include corrosion rate, electrolyte resistance, and the charge transfer resistance.

The corrosion rate corresponding to these conditions can be determined from the impedance response at intervals of 16 minutes. Table 19 presents results for cyclic slow strain rate test in regard to OCP conditions whereas Table 20 presents results for E=-900 mV vs. SCE considering corrosion rate calculations based on EIS results, and other parameters such as porous resistance response (Rpo), which relates to the microstructural changes occurring on/near the surface of the line-pipe steel. This last parameter can indicate the evolution of strain developing through grain to grain interaction within the microstructure, as well as the stress induced in the corrosion product layer, which drives failure of this layer and exposes a greater more reactive steel surface area. The active surface area is associated to the parameter Rpo (porous resistance, previously R2), which reflects the properties of the corrosion product layer formed as described earlier.

Contrasting the results in Table 19 to those in Table 20 shows the evolution of Rpo with time and the load conditions associated to corrosion rate for open circuit conditions and polarization conditions respectively. In comparison to results reported earlier it is apparent that polarization increases the magnitude of Rpo due to the current drain into the surface. Thus, the corrosion rate increases as the potential is increased (for E=-900 mV vs .SCE).

**Table 19. Parameters that recreate (theoretically simulate) OCP conditions**

| Testing time (hr) | Rct (ohm) | Icorr | Corrosion Rate (mpy) | Load (psi) | Potential Vs. SCE | %Yield Strength |
|---|---|---|---|---|---|---|
| 1 | 877.5 | 2.97E-05 | 1.06E-01 | 49107.03 | -0.758 | 70.15 |
| 3 | 759.6 | 3.43E-05 | 1.23E-01 | 51889.69 | -0.743 | 74.13 |
| 5 | 672.2 | 3.88E-05 | 1.39E-01 | 55105.72 | -0.744 | 78.72 |
| 7 | 721.1 | 3.61E-05 | 1.29E-01 | 56316.57 | -0.744 | 80.45 |
| 9 | 723 | 3.60E-05 | 1.29E-01 | 58568.04 | -0.744 | 83.67 |
| 11 | 716.3 | 3.64E-05 | 1.30E-01 | 60760.38 | -0.746 | 86.80 |
| 13 | 740.8 | 3.52E-05 | 1.26E-01 | 61521.91 | -0.746 | 87.89 |
| 16 | 758.3 | 3.44E-05 | 1.23E-01 | 63568.76 | -0.748 | 90.81 |
| 19 | 819.6 | 3.18E-05 | 1.14E-01 | 65009.91 | -0.749 | 92.87 |
| 21 | 834.8 | 3.12E-05 | 1.12E-01 | 66736.35 | -0.750 | 95.34 |
| 25 | 844.5 | 3.08E-05 | 1.10E-01 | 68567.18 | -0.750 | 97.95 |
| 28 | 872.1 | 2.99E-05 | 1.07E-01 | 68248.70 | -0.749 | 97.50 |
| 29 | 874 | 2.98E-05 | 1.07E-01 | 67984.61 | -0.749 | 97.12 |

**Table 20. Parameters that recreate (theoretically simulate) E=-0.9V vs. SCE**

| Testing time (hr) | Rct (ohm) | Icorr | Corrosion Rate (mpy) | Load (psi) | Potential Vs. SCE | %Yield Strenght |
|---|---|---|---|---|---|---|
| 1 | 5642 | 4.62E-06 | 1.66E-02 | 26538.71 | -0.90 | 32.43 |
| 7 | 6135 | 4.25E-06 | 1.52E-02 | 38231.20 | -0.90 | 46.71 |
| 12 | 5137 | 5.07E-06 | 1.82E-02 | 46193.19 | -0.90 | 56.44 |
| 16 | 4791 | 5.44E-06 | 1.95E-02 | 52239.88 | -0.90 | 63.83 |
| 21 | 4559 | 5.72E-06 | 2.05E-02 | 57659.95 | -0.90 | 70.45 |
| 25 | 4456 | 5.85E-06 | 2.10E-02 | 63160.77 | -0.90 | 77.17 |
| 29 | 4438 | 5.87E-06 | 2.11E-02 | 67058.10 | -0.90 | 81.94 |
| 35 | 4342 | 6.00E-06 | 2.15E-02 | 73021.74 | -0.90 | 89.22 |
| 41 | 3987 | 6.54E-06 | 2.34E-02 | 75138.00 | -0.90 | 91.81 |
| 47 | 4011 | 6.50E-06 | 2.33E-02 | 79191.67 | -0.90 | 96.76 |
| 50 | 3892 | 6.70E-06 | 2.40E-02 | 82163.26 | -0.90 | 100.39 |
| 55 | 3677 | 7.09E-06 | 2.54E-02 | 82232.14 | -0.90 | 100.48 |
| 61 | 3642 | 7.16E-06 | 2.57E-02 | 83089.33 | -0.90 | 101.53 |

Figure 32 illustrates the difference in the stress-strain response of the X-65 line-pipe steel exposed to NS4 near-neutral solution under slow strain rate loading for two electrochemical potential levels. Testing in this solution provides for carbonate and chloride ions and the breakdown of the iron carbonate passive layer respectively under static conditions and cyclic conditions. Differences in the evolution of microplasticity for static versus cyclic conditions are evident in the interfacial characteristics of the electrolyte-electrode system in terms of passive film growth and the frequency with which this film breaks down. Hydrogen permeation provides an additional stress factor that develops when the critical concentration condition is reached within the metallic structure. Anodic dissolution from a passive breakdown could induce a significant defect at the surface under loaded conditions, which like the other processes can be monitored by the EIS technique. EIS is viable in this context under the assumption that all components formed in the electrochemical cell during NN-pH SCC can be detected among the set of frequencies scanned and can be associated to an element of a passive electric circuit.

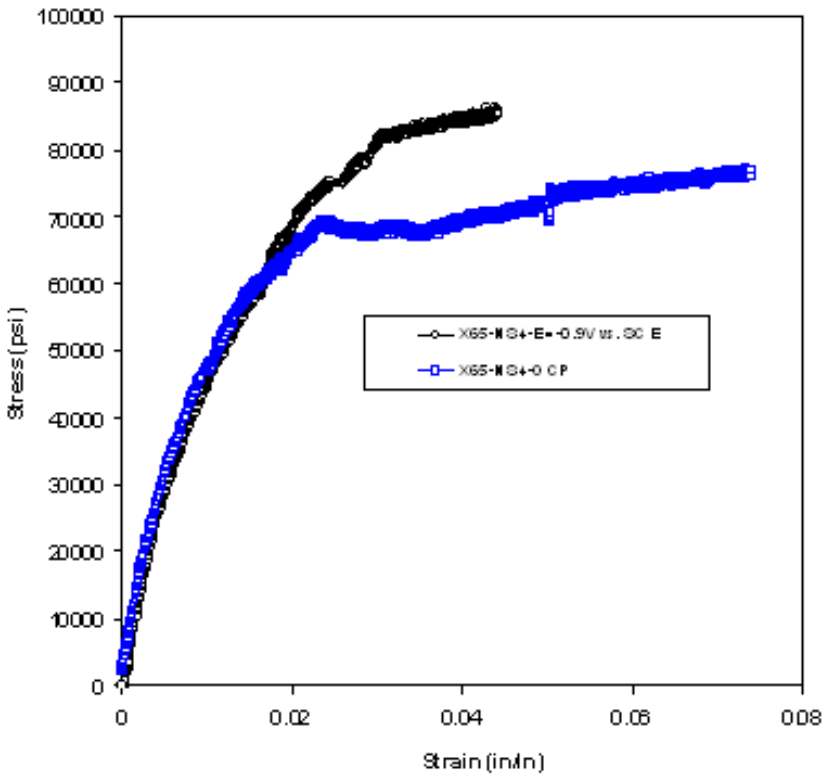


**Figure 32. Effect of potential on stress-strain response for X65 in NS4 solution**

# Develop Functional Relationships Characterizing NN-pH SCC Kinetics

## Theoretical Modeling – the Transmission Line Concept

A transmission line represents the subdivision of elements that form part or all of an electrical system that sends the transmission of electrical current from one place to another, such as an AC sine signal, through conducting media. The components of a transmission line can be discrete electrical elements distributed homogeneously or heterogeneously along the electrochemical steel-NN-pH system.

Transmission Line Modeling (TLM) has been applied successfully to electrochemical systems that show current distribution characteristics at the interface and within the electrolyte. The transmission of energy in the form of current is dissipated by the impedance distribution and the conduction characteristics of the whole system. Low and high impedance sites can be detected and described from equivalent circuit analogs distributed in a homogeneous or heterogeneous network along the transmission line. The impedance distribution is considered uneven due to the electrical and physicochemical characteristics of the interface of an electrochemical cell. TLM utilizes discrete or continuous passive electrical elements (resistance, capacitance and inductance) distributed normal to the interface considered. These models have been successfully used to explain the nature and characteristics of an interface, like porous and rough electrodes.[81, 82] Due to the flexibility of this model concept, this concept can be applied to micro and/or macro-scale heterogeneities, like corrosion products growth, dissolution and breakdown. By considering the steel-NS4 solution system as an interface that can be divided in equal and finite

number impedance segments, the impedance signal at the interface can be described with high accuracy in order to describe each element of an electrochemical cell, as in Figure 33. Theoretically the impedance profile can detect and characterize the sites for different impedance regions and locations of the electrochemical cell. The current distribution leads to the sites for different mechanisms according to the location at the interface of the working electrode.

The one-dimensional TLM has been developed for this project for which the interface is perpendicular to the impedance elements added as impedance segments, where the number of segments is as illustrated in Figure 33. These impedances are passive electrical elements

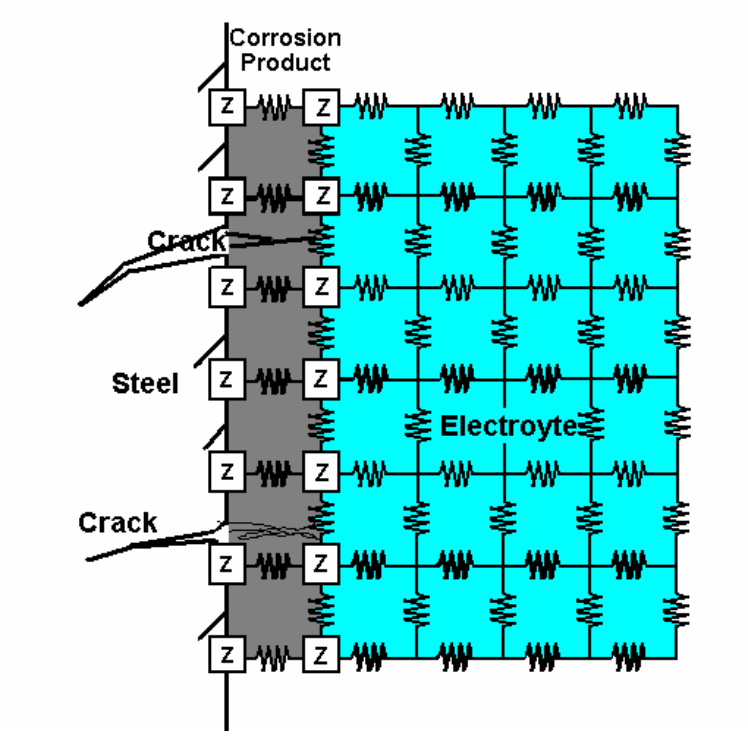


**Figure 33. Transmission Line Modeling to detect and follow in real time for surface defect**

arranged as capacitance in parallel with resistance. Each element has current distribution that allows the AC signal transported through different paths depending on the array. The current distribution and impedance in each element can be calculated leading to the final impedance spectra in terms of current distribution or from the following expression for total impedance and from Ohm's and Kirchoff's laws. The total impedance can be calculated as follows:

$$Ztot(\omega) = Z(1) + \left[(n-1) \times Rs\right] - \left\{ \frac{Rs \sum_{1}^{n-1} (I(n,1) + (I(1,1) \times Z(1))}{Ib} \right\} \quad (17)$$

Where the Z (1) and Z(n) are the impedance expression for each box, I(1) and I(n,n) are the currents for each current distribution box, Rs is the electrolyte resistance. Steel exposed in near-neutral electrolyte under load conditions is characterized by the equivalent circuit considered in Figure 29a, with the expression that represents this circuit being:

$$Z = \mathrm{Re} + \left( \frac{Rct}{1 + (j\omega CdlRct)} \right) \tag{18}$$

Equation 18 can be introduced into Equation 17 leading to a general expression that describes the electrochemical cell as a network of impedance components that describe the distribution of the system in terms of subdivided elements.

Equation 17 considers the spatial array of the impedance magnitudes according to the above-noted one dimension TLM. The experimental conditions can be recreated theoretically by determining valid curve-fit values for the parameters of the model, as illustrated for example by the trends in Figure 34. For this example representing E=-0.9V vs. SCE the characteristics of the elements that fit the dynamic frequency signal were determined by considering 100 different elements comprise the array. This model description of the interface fits the experimental conditions and so can be used to detect lower impedance sites, or make adjustments for changes in the corrosion products or when the critical site defect might appear. Such an outcome is shown in the predictions presented as Figure 34.

Impedance changes discriminate the different variables that can affect control over dissolution and defect appearance. Low impedance sites will be represented in the magnitude of Rp over time, as in Table 21 wherein changing conditions at the interface are evident in either Rp or the number of porous or active area that increase over time due to NN-pH SCC phenomenon. By changing the spatial conditions of the total impedance as a result of cyclic effects, hydrogen permeation, and/or slow strain conditions, the location of the breakdown of the passive layer in the formation of the active sites can be predicted, and once such active sites appear the failure process begins.

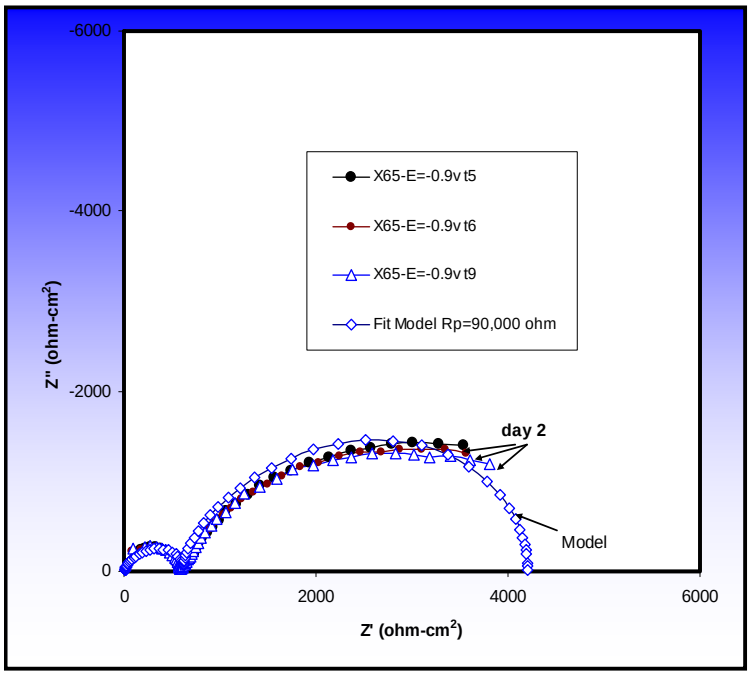


**Figure 34. Characterization of low impedance sites in one dimension using TLM and curve-fitting (for E=-0.9V vs. SCE and NN-pH SCC conditions via NS4)**

**Table 21. Parameters for Transmission Line Modeling, including Cracking**

| Number of elements | Re (ohm) | ZNC (ohm) | Cdl | Rct (ohm) |
|---|---|---|---|---|
| 100 | 1000 | 3E4 | 1E-06 | 90,000 |
| 100 | 1000 | 3E4 | 1E-06 | 100,000 |
| 100 | 1000 | 3E4 | 1E-06 | 130,000 |

Figure 35 shows the surface of an X-65 steel sample that was tested under cyclic slow strain rate conditions while polarized at E-1.2V vs. SCE. This view is following the breakdown of the corrosion product layer and the formation of defects. Tables 19 and 20 presented the parameters that characterize the corrosion rate, the protective layer, and the formation of active-passive states under kinetic favored hydrogen conditions at less negative potential levels.

Figure 35a shows the surface of an X-65 steel sample that was tested under cyclic slow strain rate conditions while polarized at E-1.2V vs. SCE. This view represents the situation following the breakdown of the corrosion product layer and the formation of defects. Tables 19 and 20 present the parameters that characterize the corrosion rate, the protective layer, and the formation of active-passive states under kinetic favored hydrogen conditions at less negative potential levels.

Figure 35b show the porous layer for NN-pH SCC conditions after steel X65 exposure to slow strain testing and E=-.09V vs. SCE.

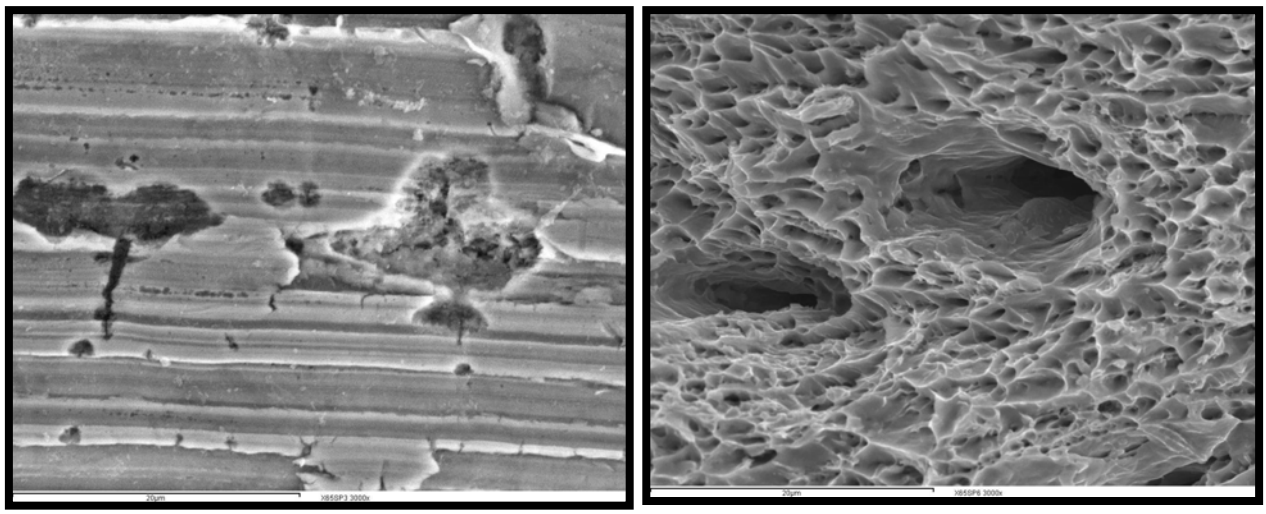

**a) Surface of the X 65 sample following the SCC slow strain test at E=-1.2V vs. SCE**

**b)SEM image of the layer with the porous formed within the corrosion product layer**

**Figure 35. SEM image of the layer with the porous formed after slow strain test and exposed to NpH SCC environment.**

## Mapping Trends in Hydrogen Effects into a Field-Useable Format

Different approaches have been suggested to relate NN-pH SCC mechanisms and phenomena to the testing parameters through experimental measurements and theoretical consideration of the role of pH and the presence/effects of the constituents in the near-neutral environment. For

example, Figures 18a and 18b presented the view of thermodynamics perspective that described the relationship between pH, potential, and the equilibrium species present as a function of the temperature. Such results can be developed for either high pH or near-neutral pH environments, which experimental observations validate via characterization of the corrosion products formed at the metal-environment interface. Kinetics characterizes the homogeneous reactions, while measurement of the corrosion products formed has droved the mechanism of atomic hydrogen formation according to the homogeneous reactions presented earlier, which has been supported by measurements of the accumulation of atomic hydrogen that diffused within the metallic structure under different testing conditions as reported earlier. Such results and analyses provide the basis to predict the corrosion products formation at the interface for different conditions, like pH, electrolyte concentration, and temperature.

Tables 19 and 20 illustrate trends in several parameters that characterize the role of hydrogen in the electrochemical reactions, such as the hydrogen formation and anodic dissolution and other factors evident throughout the experiments done in this project. Such results reflect the role of stressing conditions and their influence on the microstructure and the evolution of microplasticity under slow cyclic stressing conditions typical of operating pipelines. The evolution of microplasticity at a level sufficient to support nucleation and continued growth of either high or near-neutral pH SCC is evident for each of the pipeline steels evaluated over the last decade, and develops for these steels under laboratory testing over a range of loadings typical of real pipelines.

Because microplasticity is essential to nucleating and supporting continued SCC, understanding the trends evident in Tables 19 and 20 is critical to quantifying when and why SCC occurs on pipelines, and how to mitigate it. The EIS technique is uniquely capable of following these parameters and their influence on SCC – and in real time. While electrochemical AC impedance is a novel technique applied to SCC[34,35], some DC testing results do show the trends when the system is polarized and for different electrolyte concentration. Equation 17 shows the ability to recreate the trends evident via EIS, such that models can be developed once results such as the present are more broadly characterized and understood.

Clearly, as SCC on pipelines involves a reversible environment that can shift back and forth from low to high pH depending on field conditions and the seasons, it is critical to fully understand anodic dissolution and conditions that drive the breakdown and formation of a passive layer. It is equally critical to understand and quantify hydrogen concentration profiles as they evolve in the pipeline, reaching critical concentration levels and causing hydrogen to influence in the local stressing conditions. Finally, it is essential to address the transport properties of the various environments including the role of polarization conditions. While trends in the interface were successfully tracked theoretically using the transmission line model across a specific range of frequencies, this concept must be more broadly adapted to be of practical value in the format of an algorithm that can effectively discriminate the impact of the many parameters involved.

While much remains to be done to account for the reversible interplay between high and near-neutral pH SCC field environments and to integrate 40 years of work on high pH SCC with 20 years of work on near-neutral pH SCC, there is a clear path forward apparent now in the predictive context of the experiments and analysis reported herein. This is illustrated easiest in regard to corrosion, which dominates the lower-pH aspects of the near-neutral SCC process – and comprises the simplest element of the otherwise complex SCC phenomenon. Corrosion and

corrosion rate can be predicted directly from the fundamentals of AC impedance, which has played a central role in this project, as illustrated next.

## Corrosion rates predicted for different interface potential conditions and mechanical effects

Corrosion rates have been calculated using the parameters measured in the NN-pH experiments, with the results presented in Figures 36 and 37. These results contrast differences in surface condition due to differences induced by mechanical loading as well as differences in the potential. Figure 36 presents these predictions as a function potential on the x-axis value while Figure 37 presents such data as a function of time over the duration on the test, which could be adapted to reflect the timeline in the field. Figure 36 contrasts results for the static stress-free without microplasticity preconditioning with results for conditions involving preconditioning but without stress or slow-rate cycling. It is apparent there that samples exposed to inelastic deformation either as preconditioning or cycling experience similar corrosion rates that are about four-times faster than conditions absent the microstructural effects of inelastic deformation, with such rates from the order of 0.05 up to 0.1 mpy that remain more or less constant across the range of polarization magnitudes evaluated. For the samples absent the effects of inelastic deformation on the metal surface the current drained to the interface increases and favors the

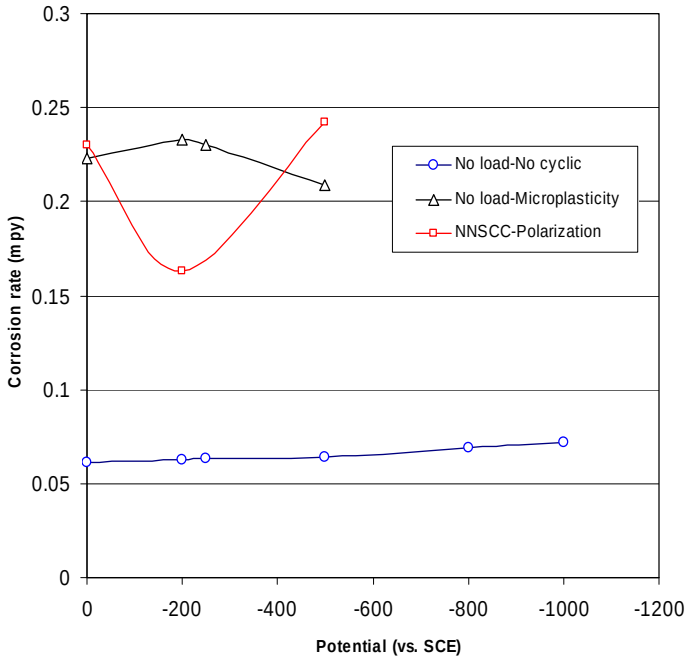


**Figure 36. Calculated corrosion rates as a function of potential and mechanical effects**

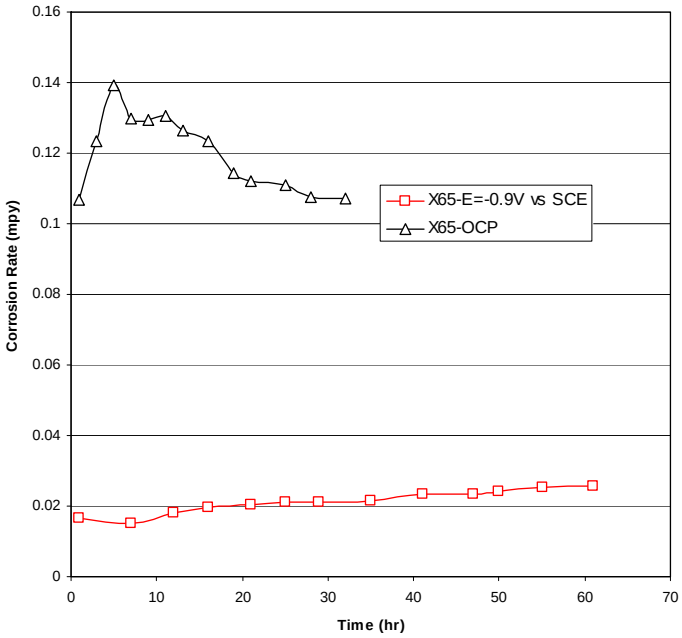


**Figure 37. Calculated corrosion rate for slow strain rate testing at different potentials**

kinetics of the molecular hydrogen formation, while active sites on the surface are homogeneous absent inelastic effects so the corrosion rate remains constant. However, for samples exposed in their history to microplasticity its effects modify the surface, leading to breakdown of the iron carbonate layer and a corresponding increase in the number of active sites each with a locally larger active area. For such cases, the corrosion rate tends to decrease as polarization increases while the current drained to the surface favored the cathodic reaction and mitigation of anodic dissolution.

The trends in Figure 37 for the static test show results similar to those in Figure 36, reflecting the fact that there is no external driver for change in the surface of the steel, or in the interface. In contrast, for samples subjected to cyclic loading segments of the microstructure at the free-surface favorably oriented for microplastic response experience the effects of cyclic softening and so have sites that are active until this softening saturates. Thereafter surface reactivity diminishes. Such effects are evident on hydrogen formation and evolution, and the corrosion products; as well as on the corrosion rate shown in Figure 37 while the NN-pH SCC test is running.

## Parametric Analysis Simulating High-pH Field Cracking

As noted earlier, while the focus here is delivery of a deterministic model to help understand and manage operational effects on high-pH SCC, broadly validating this deterministic model in that context is difficult because detailed cracking characteristics and similar detailed metrics reflect the probabilistic reality of SCC on an operating pipeline. While in a laboratory the concurrence of a microstructure susceptible to a cracking environment in the presence of a tensile stress is simply satisfied, such is not the case for field cracking. High-pH SCC develops in the field only

where the local conditions support crack nucleation and continued propagation within a colony of cracking that has the potential to grow to failure.

It was earlier noted that nucleation can only occur on free surfaces in microstructures that favor microplastic response under the nominally elastic stressing of a pipeline, satisfying the need for a susceptible microstructure. Unless this susceptible microstructure exists coincidentally with the cracking environment, which can only occur where the coating has failed and disbonded, SCC nucleation does not occur. Growth beyond nucleation can only occur where adjacent grains lead to mismatch sufficient to limit repassivation at the crack tip forming between them, whereas repassivation must be occurring on the flanks of those grains. Otherwise the crack tip blunts and a pit forms.

Assuming that the environmental and operational conditions continue to favor high-pH SCC, then growth beyond nucleation can only occur if neighboring coparallel cracks are sufficiently remote to limit stress-shielding[31,83]. On this basis, only "sparse" colonies of cracks can continue to grow and possibly threaten pipeline integrity, with the remaining colonies being benign. While sparse colonies pose a threat for eventual growth, eventual failure is only possible for sparse colonies that developed remote to other colonies through sympathetic nucleation of co-linear cracking. Such continued SCC could eventually grow through-wall (causing a leak) or coalesces within the colony to a size that is critical (causing a rupture). Alternatively, adjacent colonies of sparse cracking could develop whose axial spacing supports their interaction within the useful life of the pipeline. Such larger cracks could coalesce, leading a rupture, or grow independently leading to a leak.

Where the environmental and operational conditions continue to favor high-pH SCC, continued growth is possible, which as critical conditions are approached first threaten sections along the pipeline for which the strength and toughness properties lie in the lower tails of these distributions. Nominally higher specified properties possess greater survivability as critical crack sizes are larger – all else being equal. As all such scenarios involve a sequence of statistically unlikely events, field cracking that continues to failure is a statistically unlikely event that can only be simulated by modeling each event in a framework that addresses this uncertainty.

It follows that broadly validating the deterministic deliverable useful in trending operational sensitivities must be made within the probabilistic reality of SCC on an operating pipeline. The properties presented in Table 7b as distributions parameters support this probabilistic analysis, which used a Monte Carlo technique in the manner discussed in Reference 20. To limit the run-time for these analyses, simulations leading to so-called dense[(31)11] colonies wherein extensive closely spaced cracking networks predicted to become benign were terminated early in their simulation. In complement to the properties noted in Table 7b, typical service for high-pH SCC for purposes of these simulations considered operation at MAOP equal to 72-percent of SMYS, with the operational cycles normally distributed with a standard deviation taken at ten percent of MAOP. The corresponding maximum temperature was taken to represent values that ranged up to 140ºF (60ºC).

---

[11] As defined in Reference 31, a dense colony is one whose circumferential spacing is less than 20-percent of the wall thickness. As detailed in Reference 31, such cracking is predicted to become dormant because of stress shielding. Subsequent independent testing of dense colonies removed from the field confirmed this prediction[(84)].

Such simulations generate crack lengths and depths at some point in the future, which either is determined at the book life of the pipeline or some other arbitrary time, or upon failure of the first-to-fail colony of cracking for the pipeline. Results of both crack length and depth could be compared to field trends where this comparison is made of the length independent of the depth and vice versa. Such comparisons could match field distributions even though their coupled outcome in terms of aspect ratio did not. Accordingly, the present section tests the viability of the model by comparison to field data in terms of aspect ratio calculated for simulated pairs of length and depth.

Figure 38a presents typical results developed for simulations made absent simulated hydrotesting that is often used to control SCC in gas-transmission systems. The y-axis is the cumulative probability of occurrence whereas the x-axis presents the corresponding aspect ratio. A value of 1E-01 on the y-axis corresponds to one chance in ten, while a value of 1E-02 corresponds to one chance in one hundred, 1E-03 to one chance in one thousand and so on, to a negligibly small frequency of occurrence.

The trends in this figure show aspect ratios less than ~25 occur with a cumulative probability of about one chance in two, while aspect ratios less than ~10 are a common occurrence, whereas aspect ratios much greater than 50 are very unlikely. Because a hydrotest removes only one near-critical crack from one colony of cracking along a pipeline that might involve hundreds of colonies and many thousand cracks, the practice of hydrotesting does not appreciably change this distribution. Accordingly, data can be assembled from the field without concern for the effects of hydrotesting on this trend.

Results were developed in a previous section and presented in Figures 13 and 14 that can be used to assess the viability of the model that underlies the typical simulated trends in pairs of length and depth that underlie the cumulative probability of aspect ratio shown in Figure 38a. Because the results in Figures 13 and 14 include data for dense cracking simulations that were terminated in route to Figure 38a, results for the dense but shallow cracking have been culled and this field data and the results re-plotted. The culled data in the multiple parts of Figures 13 and 14 are combined in Figure 38b, with aspect ratio shown on the y-axis as a function of crack depth on the x-axis. The limit on the scale of the y-axis is this figure selected at 50 is consistent with the predicted trend that shows values of this magnitude to be very unlikely. The field data are bounded above by a value near 40, with a few field results found between 20 and 40, with the frequency of occurrence increasing toward values of 10, and values between 2 and 10 very common.

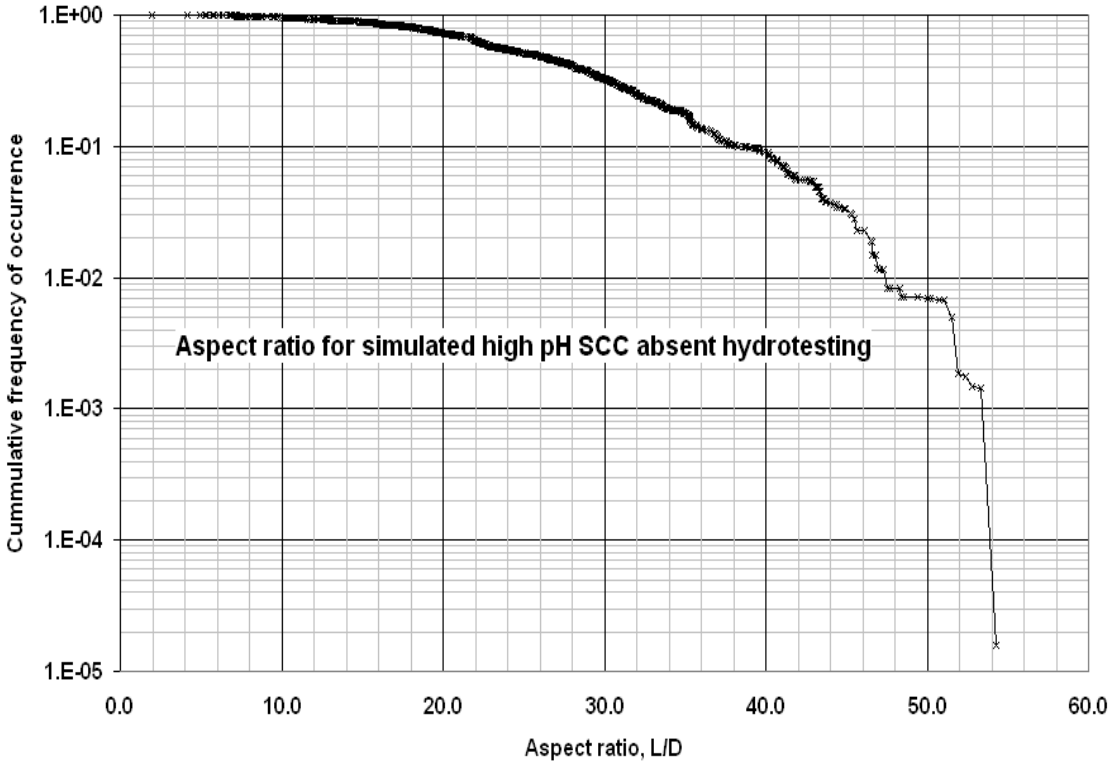


**a) predicted L/D as a function of D/t – focused on sparse colonies to manage simulation times**

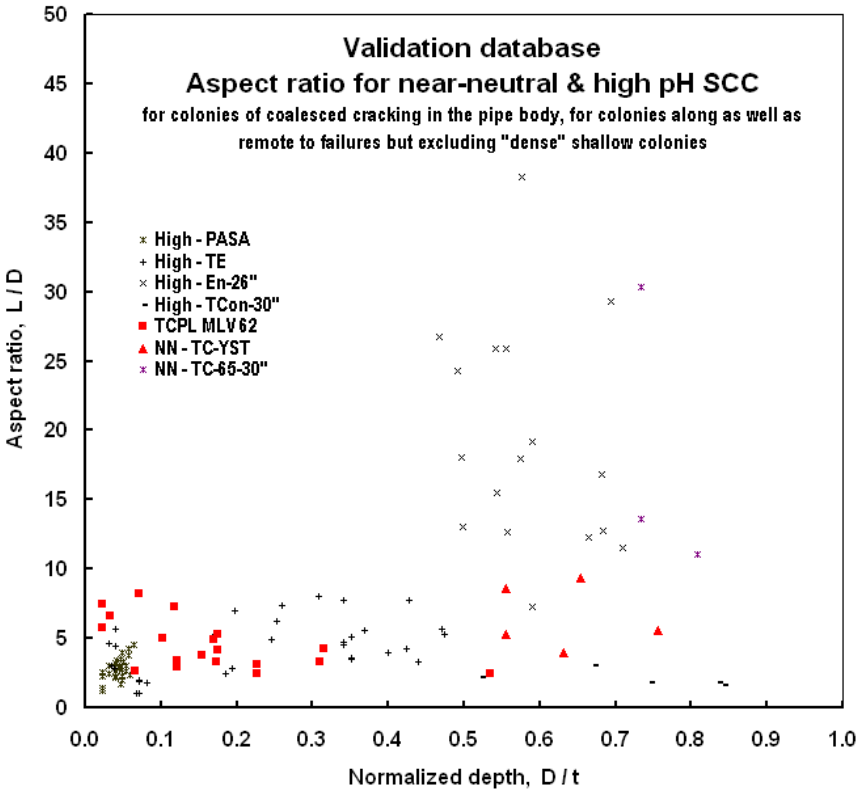


**b) field results for L/D as a function of D/t – focused on sparse colonies**

**Figure 38. Validation considering cracking characteristics**

Another good measure of the validity of the high-pH SCC model develops in terms of the frequency and location of the cracking, and its extent and severity. Typical trends from a series of simulations for cracking that occurs over the distance between two compressor stations are presented in Figure 39a. The y-axis in this figure is the frequency of cracking within a segment of the pipeline located between two compressor stations. A total of 20 such segments have been identified based on the decay of stress and temperature as shown on normalized axes relative to the levels at discharge, which for these results reflect a maximum pressure at 72-percent of SMYS and 115ºF (46ºC). Figure 39a shows the frequency of colony formation as a function of the relative position of each segment moving toward the next compressor station, which for the purpose of this analysis was taken as 60 miles (~97 km). For purposes of this analysis, a colony was taken as one or more cracks that grew beyond conditions associated with "dense"[(31)12] cracking.

It is apparent from Figure 39a that as the temperature and stress diminish moving downstream toward the next compressor station the frequency of colony formation diminishes sharply. As noted on the figure, the extent and severity of the cracking within a colony also diminish. While this frequency diminishes, there is still evidence of limited sparse cracking well downstream, and beyond distances often associated with the first valve section.

The tendencies in laboratory testing results which are shown in Figure 39b, are based on analysis of data reported in Reference 31. These TTT results represent tests done at 75°C and environmental conditions considered standard for high-pH SCC[(30)] with slow cycles at frequencies approaching the once-per-day cycling in the field, covering a range of stress (R) ratios chosen to bound field conditions. These results show larger cycles develop deeper cracks, as do higher stresses relative to the proportional limit for the steel. A similar tendency to deeper cracking is evident as the test temperature is increased. In contrast to laboratory data that show the incidence of nucleation diminishes rapidly with time for the TTT, the present simulations show that cracks continue to initiate over the life of the pipeline. This clear difference between simulations for pipeline SCC and laboratory data is due to the fact that the incidence of nucleation and the extent of early growth are strong functions of maximum stress level. As laboratory results tend to focus on the response at higher stresses that accelerate SCC, and higher stresses the cracks nucleate more frequently, causing dense cracking[(31)] that they eventually shield adjacent cracking from the applied stress, such dense cracking stops growing. In contrast, the field tends to develop more sparse colonies that support continued growth.

Analysis of TTT data in Reference 31 shows the incidence of cracking sharply decreases as the stress diminishes from near the proportional limit to a value approaching MAOP at 72-percent of

[12] Many more colonies would be indicated if the dense colonies that turned dormant were included.

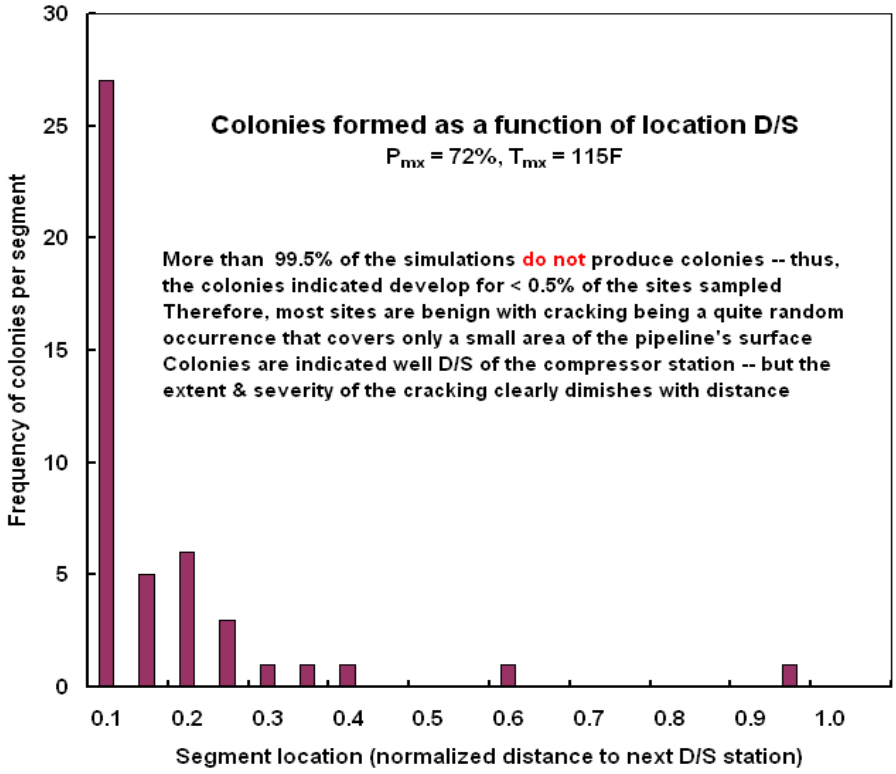


**a) simulated colony frequency and location relative to the compressor station**

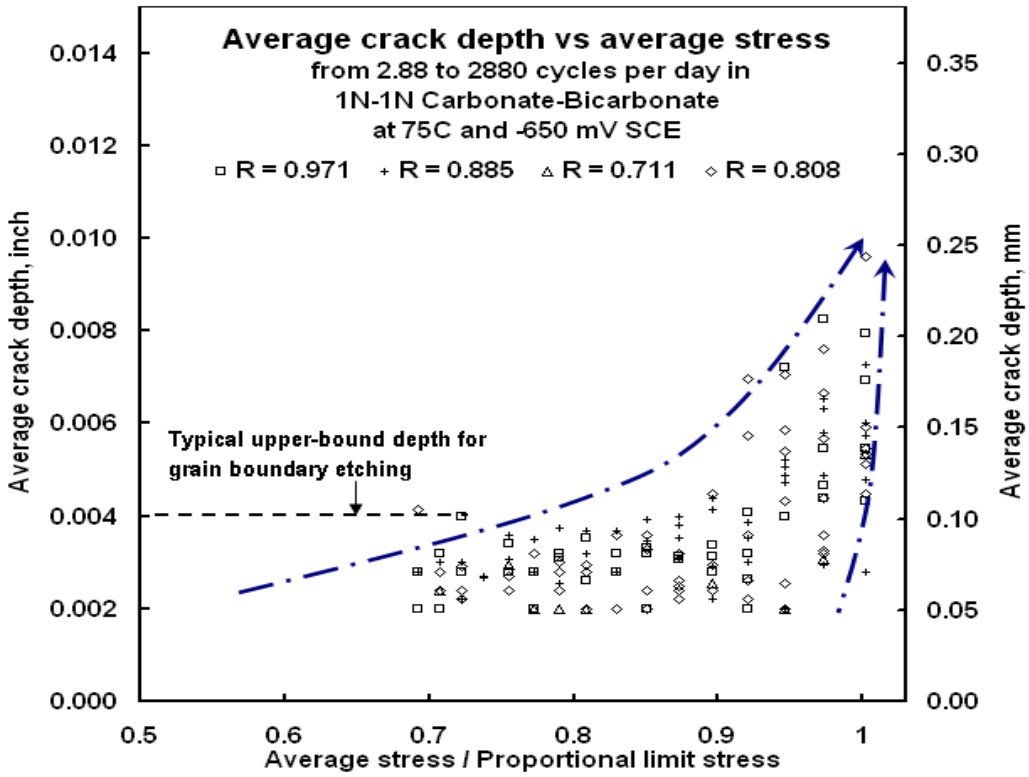


**b) laboratory trend with stress and stress ratio**

**Figure 39. Validation assessed via frequency and severity of cracking**

SMYS. Because the incidence of cracking diminishes, the spacing between cracks along the tension axis is increased, which is analogous to increased circumferential spacing. It follows that observations of pipeline cracking at MAOP can be anticipated to involve widely spaced cracking sites, with rather limited amount of cracking in any site. Unfortunately, comparison field data for the incidence of cracking are quite sparse, although there appears to be clear differences in the incidence of dense colonies for lines operated at 72-percent of SMYS as compared to that for lines operated at 80-percent of SMYS.

It follows that both the characteristics of cracking in terms of aspect ratio, as well as the severity and frequency of cracking are consistently predicted using the deterministic high-pH model to be delivered with this reporting when used according to Monte Carlo techniques. The next section considers the effects of hydrotesting interpreted via this model.

## Parametric Analysis Simulating Controls via Hydrotesting

The role of hydrostatic testing (hydrotesting) can be evaluated from two distinctly different viewpoints. The first involves hydrotesting of pipelines or valve-sections that have never experienced a hydrostatic test, or if previously tested the maximum pressure corresponded to the code-required minimum (1.25 times MAOP). The second involves hydrotesting of pipelines or valve-sections that have experienced a higher-pressure hydrostatic test to a level that approaches the actual yield stress (AYS) for the lower tail of this distribution, typically at least 100-percent of SMYS[13], as a function of retest interval and retest pressure to determine appropriate practices to control high pH pipeline susceptibility, as a function of service pressure and temperature, and the mechanical and toughness properties of the steel.

Hydrostatic testing to high pressure, regardless of when it occurs can have several beneficial effects(40). In its function as a "strength test" high-pressure testing can expose near-critical defects, enhancing the structural integrity of the pipeline. In its function as a "tightness test", which can be effective at reduced pressures, it can identify leak paths due for example to construction defects. The fact that the strength test requires higher pressures whereas a tightness test does not coupled with the desire to minimize defect growth during the test gave rise to the so-called "spike" hydrotest in the early 1990s(85). Under other circumstances, even high-pressure hydrotesting can be ineffective(40). For example, hydrotesting does not expose short defects, even if they are near through-wall. Likewise, hydrotesting is ineffective in applications involving very tough steels, as even large defects in such steels can survive very high pressure testing.

Absent cracking, high-pressure hydrotesting causes localized yielding at all locations where the yield strength falls below the stress due to the proof-pressure test. Such areas, which otherwise are the primary sites for SCC nucleation in regard to the "susceptible" microstructural

---

[13] Use of SMYS as a reference reflects the ideal scenario where the actual yield stress (AYS) and SMYS are coincident. The value of AYS considered here reflects the lower tail of its distribution in pipe form. The ratio AYS/SMYS is targeted in pipe production at values equal or greater than one to limit mill rejects because the pipe fails specification. Effective use of the hydrotest as a strength test requires stress levels approaching nominal yield(40), which for earlier grades with larger production variability could require testing at 110-percent of SMYS to brin AYS near yield. As mill controls have improved, distributions of AYS has tightened and mean values tend now to be closer to SMYS. Thus, the maximum test pressure should reflect consideration of the distribution of AYS/SMYS from mill sheet data.

requirement for SCC, are strain-hardened. Accordingly, lower-strength joints are effectively removed from consideration as SCC sites, as are portions of otherwise typical joints that for reasons such as microstructural variation or reduced wall thickness had slightly reduced strength. It follows that the effect of high-pressure testing is to increase in the proportional stress for pipe joints represented by the lower tail of the distribution of yield strength. This diminishes subsequent nucleation in all such areas, with the increase in proportional stress or the decrease in subsequent nucleation increasing as the retest-pressure increases. Modeling incorporates the effect of a higher-pressure hydrotesting by truncating the lower tail of the distribution of yield stress at a stress level corresponding that used in the hydrotest. As such, the potential benefit of hydrotesting is available from a SCC perspective only for the first high-pressure hydrotest. This is because subsequent hydrotesting does not appreciably alter the distribution of properties and their effect on susceptibility – except if and where cyclic softening[18,21,86] has occurred. At present, the complexity of cyclic softening and its service history dependence have been dealt with by "hard-wiring" its influence on the cracking kinetics based on the laboratory behavior of an X52 steel that was highly susceptible to high-pH SCC in service. This practice will cause the predicted failure rate to be overestimated as compared to the response pipelines.

Where sharp defects like those due to SCC or other cracking mechanisms are present, high-pressure hydrotesting acts to blunt such cracks. Blunted cracking must "re-sharpen" or "re-initiate" before it can resume its growth via SCC; the time for which could be significant. At present the mechanics of this re-sharpening are not well characterized. Suffice it to note that for the present the time for re-initiation is assumed the same as the time calculated for initiation. This interval varies randomly but typically the predictions indicate it takes the order of several years before cracking develops with lengths and depths large enough to grow according to the principles of fracture mechanics.

Finally, the model currently removes a colony of cracks from the pipeline after that colony leads to an in-service failure or is exposed by hydrostatic retesting, but it does not remove the related steel properties from the property distributions given in Table 7b. This decision reflects the observation that depending on how rehabilitation is done much of that joint of pipe can still remain in service, which requires continued consideration of its properties. However, where the affected pipe joint (and often adjacent joints) are removed from service, because the affected joint or adjacent joints usually contain other active colonies, sampling without updating the properties distributions could appreciably overestimate the likelihood of failure as compared to service situations. While an option to address this aspect could be incorporated, as yet it has not.

Consider first background for control high-pH SCC via hydrotesting in terms of control that can be achieved via compression ratio or the use of aftercoolers. Such data are presented in Figure 40a in terms of failure probabilities representative of the operation of a pipeline at average maximum discharge temperatures equal to 130ºF, 120ºF, 110ºF, and 100ºF (54ºC, 49ºC, 43ºC, and 38ºC), assuming as is reasonable that the steady-state temperature of the pipe wall is controlled by the gas. Because as Figure 15 indicates that pressure and temperature are coupled as a function of distance along the pipeline beyond the compressor station, for all simulations random variations in temperature are correlated to pressure as a function of position down the pipeline. Variations on that mean temperature are bounded by ± 5 F simulating the typical once-daily demand-induced cycle, with packed operation taken at a maximum pressure equal to MAOP with R taken as 0.95.

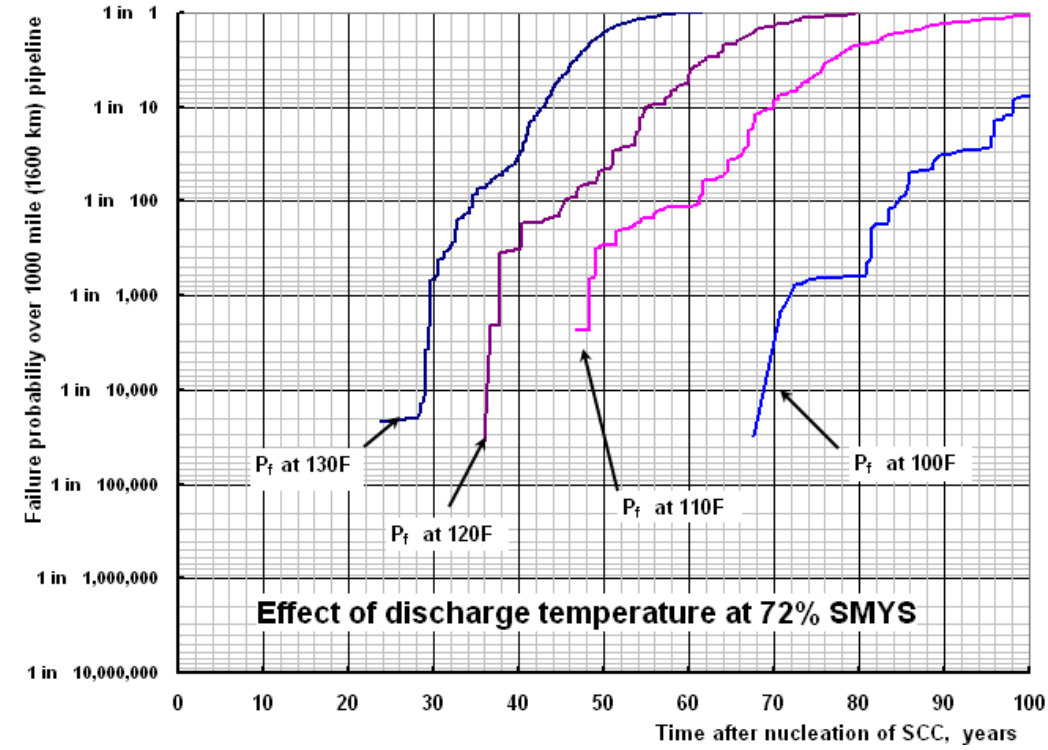


**a) relative effect of discharge temperature as a reference foe effect of hydrotesting**

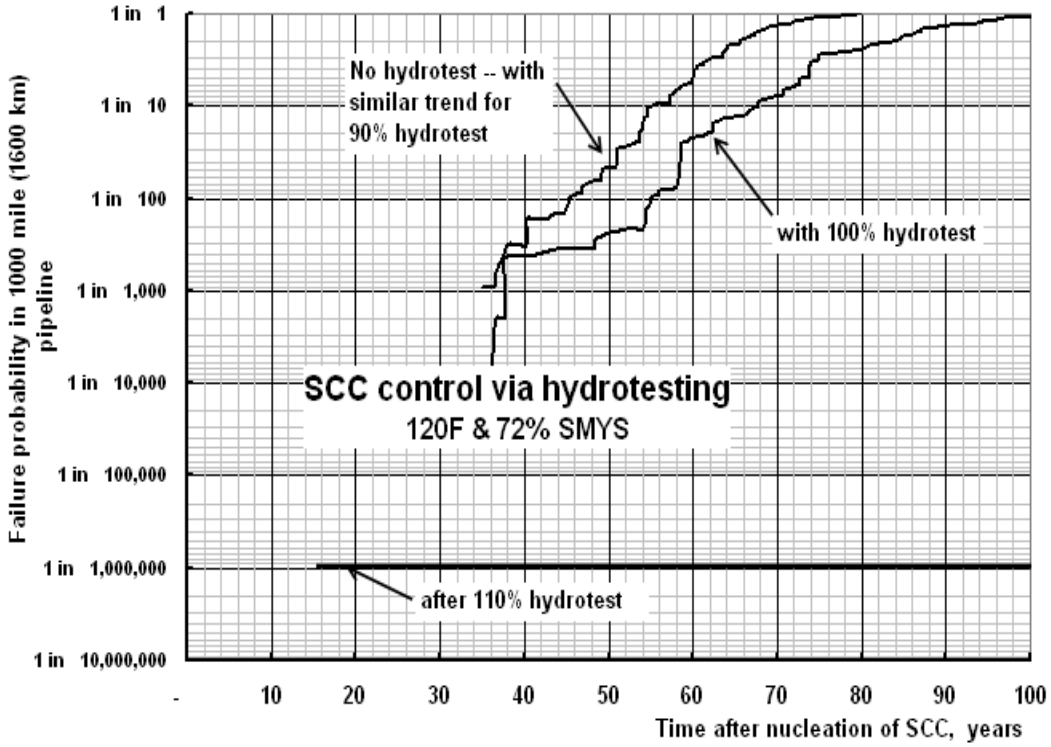


**b) control of SCC achieved by hydrotesting at 100-percent of SMYS**

**Figure 40. Illustrating the effect of hydrotesting as a control for SCC**

The simulations in Figure 40a show times to first nucleation of SCC the order of 23 years for the case at 130ºF (54ºC) up to about 65 years for the case at 100ºF (38ºC). These leading tails of their distributions correspond to the expected times for which the first evidence of field problems could be anticipated for such operation. These simulations show a strong effect of discharge temperature on the probability of failure throughout the book life of the pipeline, and indicate that a decrease in failure probability of about two-orders of magnitude (factor of 100) can be affected by a decrease in discharge temperature of about 10ºF over this interval of temperatures. This same 10ºF decrement in discharge temperature corresponds to a roughly 10-year increase in the time prior to first field evidence of high pH SCC. This dependence on discharge temperature is consistent with field observations that show a significant reduction in the incidence of SCC when aftercoolers were introduced to control in-service SCC. For discharge at 130°F (54°C), which was not uncommon before the significant effect of temperature on SCC kinetics was understood, the failure probability per 1,000 miles (1609 km) of pipe reaches $10^{-3}$ after about 35 years after the formation of the cracking environment and nucleation of SCC. It reaches a 50 percent failure probability at about 50 years. These simulated lower-bound lives are not too different as compared to the range of lives in Table 7a, which indicates the viability of this model concept.

In reference to the trends in Figure 44a, the gradual increase failure probability as a function of time indicates that near-critical defects could be periodically removed, which is essential to control of SCC via hydrotesting. Figure 44b illustrates the potential utility of hydrostatic testing in light of control via temperature reduction. This illustration is specific to service simulated at 120ºF (49ºC) and operation at 72-percent of SMYS, for a pipeline that did not experience a high-pressure pre-service hydrotest. This scenario is selected because many pipelines experiencing SCC were constructed prior to mandating pre-service testing to 1.25 MAOP, or the realization that higher-pressure testing could be beneficial. For these simulations, the first hydrotest occurred after 20 years, with retesting done thereafter on a 6-year interval.

As can be seen in Figure 44b, hydrotesting can be effective in control of SCC, as it shows about an order of magnitude decrease in failure probability at higher failure probabilities as a result of high-pressure testing at 100 percent of SMYS. Trends like this can be generated across a range of pipeline service conditions, addressing differing levels of inherent susceptibility to SCC. While hydrotesting is typically shown to have comparable effectiveness, it is clear that an initial hydrotest that reduces inherent susceptibility makes subsequent hydrotesting less effective. Key to the effectiveness of hydro-retesting is the presence of cracking large enough to respond to the maximum test pressure. This is apparent by inspection of changes to the populations of crack length and depth in scenarios where it is effective, as for example involving higher-pressure tests in lines run at higher discharge pressures tested later in their service life. However, while such circumstances make hydrotesting more effective, they also open the door to in-service failures, as these become more probable under such conditions.

Results from trending the effectiveness of hydrotesting are shown in Figure 45. The y-axis in the figure is the ratio of the number of defects exposed for testing at the indicated maximum pressure on the x-axis normalized in reference to the number of defects exposed by hydrotesting for the same scenario but using a maximum test pressure of 110-percent of SMYS. On this basis the value of one on the y-axis occurs for 110-percent on the x-axis. While there is scatter about this trend driven by the random nature of the SCC process, the results consistently indicated that hydrotesting at the code-required level at 90-percent of SMYS exposes relatively few defects in

comparison to both 100 and 110-percent tests. Such is also indicated to be the case for hydrotesting at 95-percent of SMYS. It follows from these results that while testing at 90-

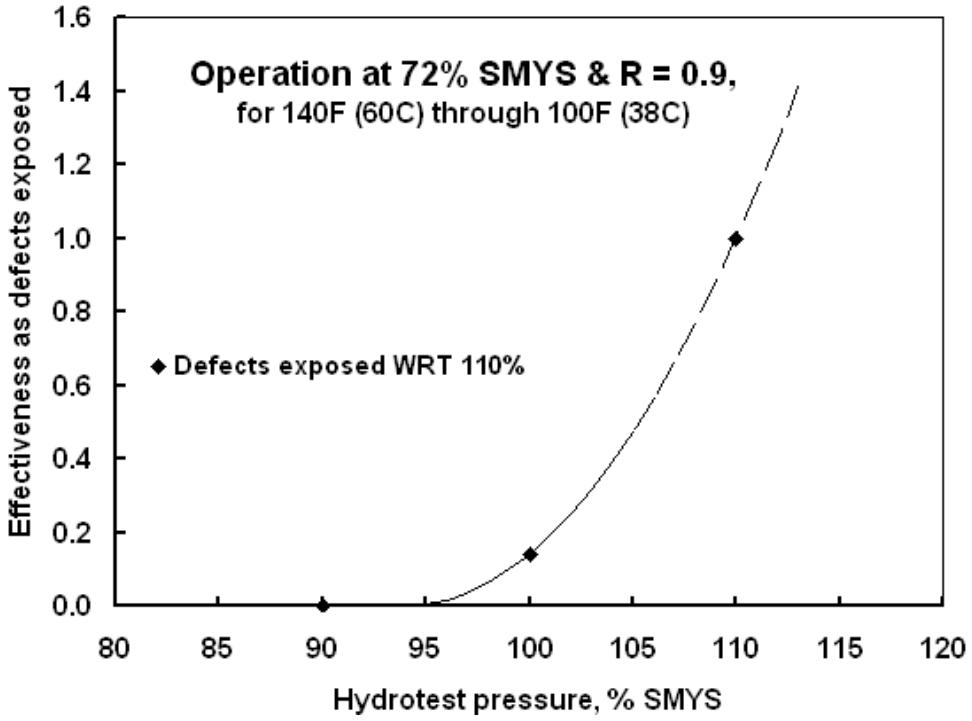


**Figure 41. Effectiveness of hydrotesting (referenced to testing at 110-percent SMYS)**

percent of SMYS satisfies code requirements it does little to affect integrity in contrast to hydrotesting at 110-percent of SMYS. It follows from such results that the retest pressure has a significant influence on the retest interval. Such results suggest that close intervals at higher pressures expose a larger number of defects than does testing at lower pressures. Moreover, because testing at lower pressures does little to affect integrity, the length of the retest interval should have little net effect on the integrity of the pipeline. These results indicate that retesting can be effective or rather ineffective depending on the test parameters chosen. The analysis process suggested by Fessler[87] could be useful in assessing this aspect on a pipeline-specific basis.

As noted earlier, the model of pipeline cracking evaluated does not consider failure of the coating or formation of the cracking environment. Consequently, the timeline for this discussion is relative to the time taken to nucleate SCC once the cracking environment develops. Further, because the kinetics depend on variables such as soil type, moisture content, potential, coating condition, which are generally unknown along the pipeline RoW, the present simulations consider a uniform distribution of average cracking speed (ACS) that lies below the maximum Farradaic rate for the temperature of concern. As such, in its present form this model is useful to assess the effects of changes made, for example to service pressure or temperature, to control cracking. Or it could be used to determine what hydrostatic retest parameters and retest frequency are best for a given mode of operation, to limit cracking without jeopardizing safety. It also could be used to evaluate purchase specifications involving related line-pipe properties to

limit the scope of cracking. But, without selected upgrades this model should not be used to infer absolute pipeline life.

## Parametric Analysis of Field Controls via Operational Changes

As indicated above, one viable use of this model is simulating the effect of changes in service temperature and service pressure history to evaluate possible practices to affect better control high pH pipeline susceptibility or assess how such dependencies affect susceptibility to high-pH SCC. Such comparisons must of course consider role of mechanical and toughness properties of the steel, and should reflect the effects of prior maintenance actions as for example a high-pressure hydrotest. For present purposes, use of the model is illustrated in an application considering some aspects involving SCC in the service conversion of a pipeline from gas to liquid transport, for a pipeline whose history involved no prior high-pressure hydrotesting.

### Conversion-Related Temperature Change

Gas pipeline systems where pressure is generated by compression operate at temperatures that range from a maximum at discharge to a minimum at suction, with a nonlinear decrease due to losses occurring between these sites, as was shown in Figure 15. For this hypothetical scenario past compression ratios coupled with use of aftercoolers lead to historical discharge temperatures on the order of 110ºF (43ºC). In contrast, liquid lines typically run at near ambient ground temperatures. Given that the pipeline is buried at least three feet, and the nature of the liquid service, this pipeline after conversion can be anticipated to operate at about 40ºF (5ºC).

The effect of temperature change due to conversion has been evaluated in regard to SCC for the past and future service temperatures, the results of which are presented in Figure 42a. The probability of SCC is presented on the y-axis in reference to the total length of this nearly 1000-mile long pipeline, with life presented relative to failure at 50 percent probability of occurrence referenced to operation at 110ºF. For this reason, the y-axis has a value of one at an x-axis value of 50 percent. According to the results shown in Figure 42a, a decrease in operating temperature from 110ºF to service at 40ºF leads to about an order of magnitude longer service life at higher probabilities for failure, whereas somewhat less benefit derives from service conversion at lower likelihood of failure. This means that control of SCC is much less problematic if the service is converted, with much less need to consider hydrostatic re-testing or other controls for SCC in that application.

### Conversion-Related Pressure Change

Gas service on the subject pipeline involved near-daily pressure cycles from a maximum pressure corresponding to about MAOP to a minimum pressure typically near 85 percent of the maximum pressure. In contrast to these slowly changing daily cycles, liquids/products service will involve more frequent, larger amplitude pressure cycles that can accelerate SCC (or promote corrosion fatigue or fatigue damage, which are beyond the current scope). The extent that SCC is accelerated depends on the amplitude of the cycles and their frequency, the presence of a cracking environment, and the chance that sites for future cracking lie under disbonds that also contain the cracking environment. Based on the service anticipated for this hypothetical pipeline after its conversion, its operation will involve pressure cycles from near 100-percent to about 60-percent of SMYS typically once per day.

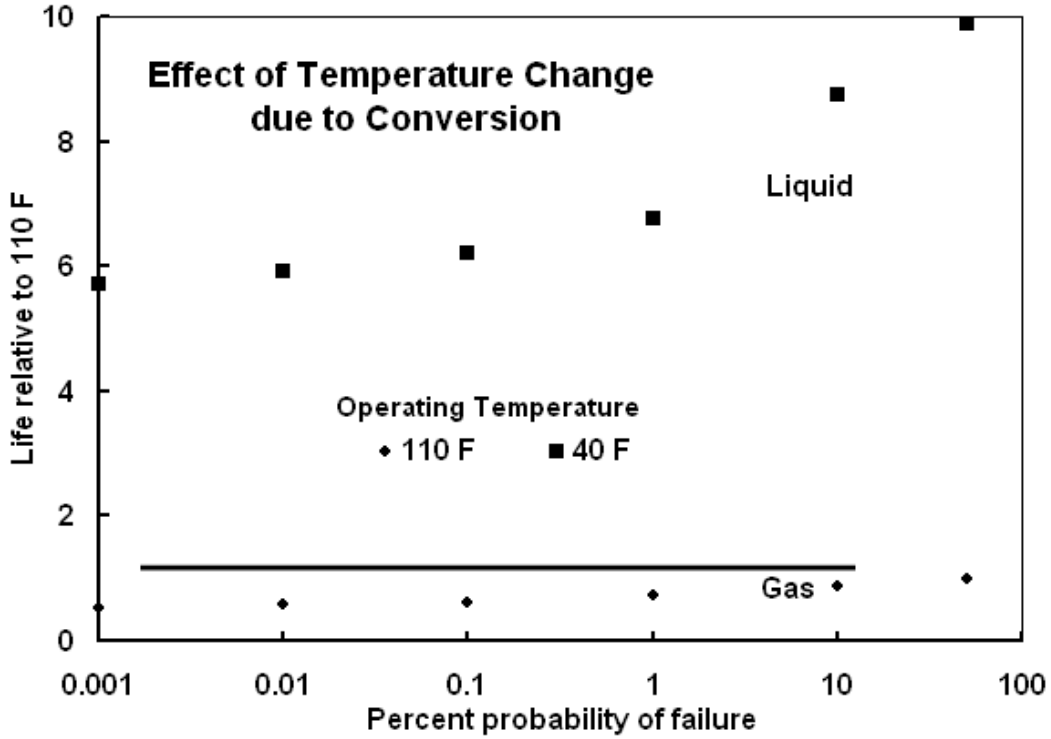


**a) effect of temperature change**

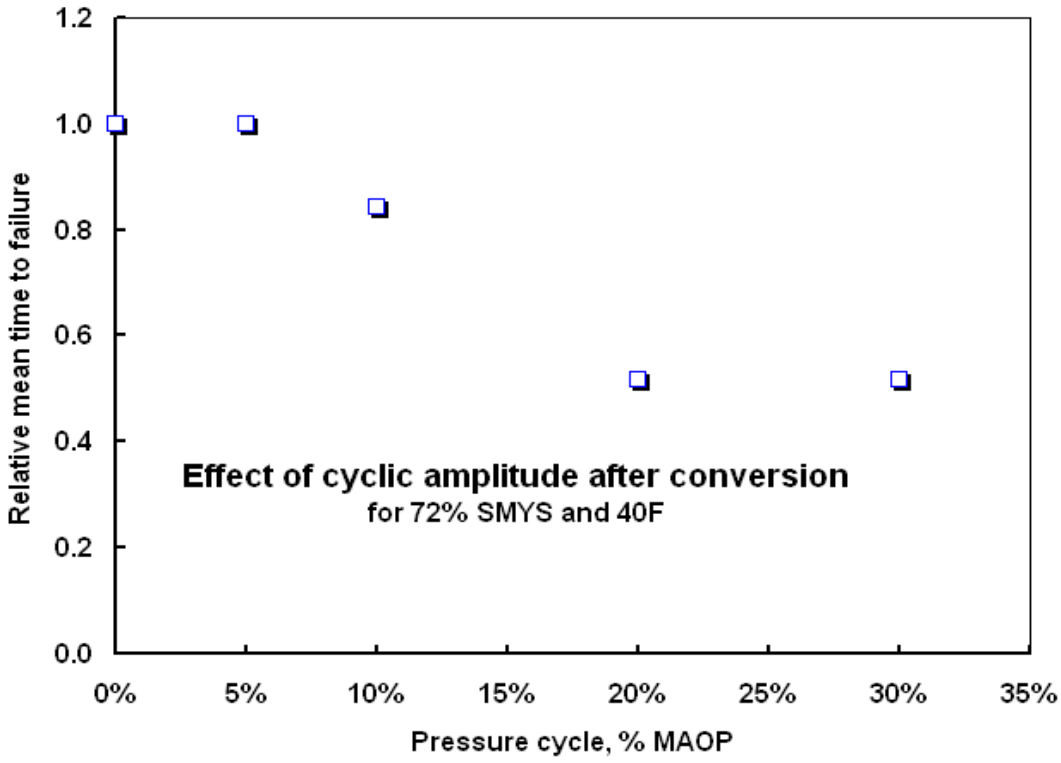


**b) effect of pressure change**

**Figure 42. Effect on SCC nucleation in a hypothetical service conversion**

The effect of larger pressure cycles on SCC susceptibility were calculated referenced to the case of zero pressure cycles, results for which are shown in Figure 42b. For this reason, the y-axis in this figure has a value of one at a value of the x-axis equal to zero. As is evident in Figure 42b, the results show only a modest reduction in service life occurs as a result of small pressure cycles, whereas larger pressure cycles cause a larger reduction. For the circumstances and line-pipe properties considered, the effect of this plausible service conversion leads to about a factor of two reduction in service life for operation at 40ºF (5ºC) with MAOP at 72-percent of SMYS. In conjunction with the 10-fold increase due to reduced temperature, these results indicate that control of high pH SCC could be achieved more easily after conversion to this anticipated liquid service. Clearly the above considerations reflect only a part of the many considerations in conversion of service. Such calculations address only the introduction of new cracking, without regard for the effects of the changes noted on the possible population of existing cracks. Likewise, they reflect only the response of SCC whereas other mechanisms such as corrosion-fatigue and fatigue may be more active under the changed history. While such aspects are beyond the present scope, they nevertheless must be addressed in practice.

## Develop I/O and Format High-pH SCC Model for Delivery

The objective of this task was to repackage an already existing file delivered to the PRCI membership as an ".exe" file compiled from a range of software platforms and delivered to run in an early Windows operating system (O/S) for delivery to run with a graphical users interface (GUI) – following its update to include the effect of hydrotesting. In turn this facilitates release of a more user-friendly high pH SCC model to the Government for their eventual release of the model to industry.

The original .exe-file known as SCCLPM for stress-corrosion cracking life prediction model provided user input through the usual on-screen live response as the file executed, with output in the form of ASCII strings that were written to files that in turn could be imported to any spreadsheet with provision to import comma-delimited character strings. The modest effort of this task simply restructured that input into a Visual Basic (VB) form that appears as a single screen that the same data are provided to. This screen provides for US units. This task also developed output format wherein the output is printed to a screen in a VB setting, as well as output as a *.csv file that is compatible with most spreadsheets. The output from each run of this code can be assembled in another spreadsheet as a function of the inputs to establish a basis for statistical analysis, or it could be embedded in other code to do this in an automated framework.

The screens developed for input address first the mechanical and fracture properties of the line-pipe steel, and then operation and the hydrotest scenario. SCC susceptibility is "hard-wired" to reflect the behavior of an early 1950s vintage pipeline whose properties, operation, and field environment led to recurrent high-pH SCC. This aspect of the underlying model could be changed to reflect the actual microplastic response of the steel involved, although the client that funded the evolution of that technology and SCCLPM did not exercise that option. Clearly it is now more feasible to quantify this aspect and its impact on SCC via the EIS technology.

# Discussion – Spectrum of Environments, Mechanisms, and Models

## Spectrum of Cracking Environments

The reactions leading to hydrogen generation postulated in the form of Reaction 3 provide a source of hydrogen whose capacity more than rationalizes crack nucleation on smooth surfaces such as pipelines in NN-pH environments. This postulate favors a solution pH that is buffered in the region of 6.4, which is preferentially apparent in field sampling associated with NN-pH SCC. The generation of hydrogen according to this postulate does not rely on hydrogen reduction from dissociated water, so the local pH on the steel surface does not become more alkaline as would occur during the normal corrosion of iron in acidic solutions. A contributing factor may be the presence of bicarbonate on the steel surface, which can act as a hydrogen recombination poison as does hydrogen sulfide, although this aspect has not yet been investigated to see if it plays this role. According to this postulate, given adequate concentration of the species involved this process is self-sustaining. This means that unless the environment promoting hydrogen generation according to the postulated mechanism is upset due to season or other changes, significant hydrogen will be available to drive any active hydrogen-related mechanism. The end result is the formation of hydrogen that if adsorbed can promote other hydrogen-related processes, such as embrittlement, that in turn can drive TG cracking provided the other microstructural and loading conditions necessary for SCC are also met.

Field results indicate the presence of shallow IG SCC typical of high pH SCC in association with TG NN-pH SCC, as for example that shown in Figure 1. This observation is not surprising as the reactions that underlie Figure 2 are reversible, such that IG SCC in high-pH environments is mutually expected with TG SCC formed in NN-pH environments. Whether IG or TG cracking occurs in this context depends on the species present in the ground water, as well as the CP level, the temperature, and other factors. The postulate for hydrogen generation is compatible with this scenario, and equally compatible with the classical form of SCC on pipelines. High-pH SCC simply lies at higher pH levels within this spectrum of compatible reversible reactions.

Field results also indicate corrosion occurs in the vicinity of NN-pH SCC. This scenario develops within the $CO_2 – H_2O$ environment at higher levels of $CO_2$, which when dissolved leads to a more acidic environment that favors corrosion rather than SCC.

Unfortunately pipelines tend to be buried in soils where depending on the RoW both carbonaceous material and groundwater may be present. Formation of the carbonate-bicarbonate solutions that are the cracking environment for high-pH SCC have been explained as a consequence of the CP, which promotes the formation of hydroxyl ions that, in turn, facilitate the absorption of carbon dioxide derived from decaying organic matter in the soil. The balance of the species present and the temperature and amount of water available control the pH of the environment, that can shift favor high-pH SCC, NN-pH SCC, or corrosion depending on its value. This scenario underlies the reactions noted above as Reactions 1 and 2, whose equilibria were shown in Figure 2.

It follows that the $CO_2 – H_2O$ environment that can form under coating disbonds can vary greatly along a pipeline, as well as seasonally, and is reversible. Conditions along the pipeline RoW where the $CO_2$ concentration is high and bicarbonate is low favor the left-side in Figure 2 and the reaction noted above as Reaction 1. In reference to Figure 2, this occurs for pH less than 8.4. This is the complementary scenario to that just discussed where the pH was high. At pH less

than 6.4, the environment can become very acid in highly concentrated $CO_2$ solutions. By reference to Figure 2 or Reaction 1 the bicarbonate concentration would be proportionately reduced as the concentration of $CO_2$ increases.

According to the reactions that underlie the postulated mechanism (Reaction 3), the proportional reduction in bicarbonate as pH decreases indicates less hydrogen is generated, because bicarbonate is the source of the hydrogen generation according to the postulated mechanism. Thus, a more acidic environment means the rate of cracking due to hydrogen-related mechanisms slows, whereas the rate of corrosion is increased. Under such circumstances, weight-loss corrosion occurs, as is the case for $CO_2$ pipelines. Such corrosion will broaden and deepen already existing crack-like features, although eventually down-crack conditions will dictate the response at the tips of deeper cracks. In contrast, corrosion will occur on the flanks of shallow cracking, obliterating characteristic traces of their origins, and corrosion focused at other stress raisers will promote the presence of pit-like features. Such results are consistent with the presence of pitting often observed with NN-pH SCC, and underscore why IG SCC when observed is typically limited to relatively shallow cracks.

At pH between 6.4 and 8.4, the process characterized by the postulated mechanism and the reactions in Reaction 3 occurs, but not as readily. As bicarbonate would initially be consumed to make iron carbonate, $H^+$ from the water must also be used in the reaction because only one $H^+$ is released from the bicarbonate and the electrons from the anodic reaction must be balanced. But, because the buffering capacity of such environments is not great, the pH will eventually drift to higher levels, becoming more basic and causing some carbonate to form. As this process continues, bicarbonate continues to decrease whereas carbonate increases. This creates the possibility that an initially near-neutral environment biased toward pH 8.4 will move toward the high-pH environment, eventually moving up the right hand line in Figure 2. In such cases it is possible the pH will tend to 10.4, where another buffering reaction occurs, implying the cracking mechanism changes to the classical high-pH case.

Subsequent shifts in solution pH driven by seasonal or other changes give rise to the possibility of mixed environments that swing reversibly between the two buffered states, or become more acidic or basic, leading to the concept of a spectrum of cracking environments[12-15]. As yet there has been nothing done to discriminate from field conditions the likelihood of NN-pH versus high-pH SCC versus corrosion, nor have aspects related to film formation and stability been addressed, as for example using the concepts in Reference 29. The extent to which cracking develops in these environments depends on factors such as local electrochemical potential and temperature. Lower temperatures will favor acidic conditions, as temperature is inversely proportional to the solubility of $CO_2$. Conversely, where the environment shifts to control by active/passive corrosion and IG SCC, the extent of cracking will be strongly dependent on the local potential and the influence of the loading on the formation of microplastic strains at strain rates that favor crack tip dissolution. Shifts between these cracking mechanisms are very likely the reason that both IG and TG cracking are occasionally found in a given pipeline, or down a given crack.

## Mechanisms and Models

Reviews[5,6] indicate there is some agreement that the NN-pH cracking mechanism involves a hydrogen-related process, with the cracking being predominantly TG and ductile, and generally

free of brittle traits[14]. Consideration of the literature involving hydrogen-related studies shows the effect of hydrogen ranges from embrittling at one extreme, to enhanced plasticity at the other extreme. Early work on hydrogen all pointed to embrittling phenomenon, whereas in the 70s the possibility of enhanced plasticity was introduced[15]. As discussed critically in a recent paper by Lynch[(48)], there are three fundamental mechanistic views of the role of hydrogen in the fracture behavior of metals, including steel. In view of the spectrum of environments just discussed, these mechanisms must be merged with the concepts discussed for high-pH SCC, and a basis to assess which is relevant determined if the industry is to develop a rationale to manage the sometimes conflicting drivers between these SCC processes.

The three accepted high-level mechanistic views of the role of hydrogen in the deformation and cracking response of metals include hydrogen-enhanced decohesion (HEDE)[(e.g.49)], adsorption-induced dislocation-emission (AIDE)[(e.g.50)], and hydrogen-enhanced localized-plasticity (HELP)[(e.g.51)]. HEDE involves weakening of interatomic bonds in regions of high hydrogen concentration, such as crack-tips, high triaxial-stress regions ahead of crack tips, and interfaces, which leads to atomically brittle fracture. AIDE involves the weakening of interatomic bonds at crack tips due to "adsorbed" hydrogen, and so promotes fracture at relatively lower stress due to locally reduced ductility. Finally, HELP involves easier dislocation motion when dislocations, and obstacles to them, are surrounded by hydrogen atmospheres that facilitate enhanced plastic flow – an effect that is quite opposite to both HEDE and AIDE. Combinations of these three mechanisms, with the dominant mechanism depending the material, microstructure, strength, environment, stress-intensity factor, and other variables, have been proposed by Lynch[(52)]. He states "there appears to be some consensus emerging that cleavage-like fractures are mainly promoted by AIDE, brittle intergranular fractures probably occur mainly by HEDE, while slip-band fractures probably involve HELP," with consensus apparently coming in reference to the work of Hänninen[(53)].

While there is still significant disagreement regarding mechanisms of embrittlement, and some of the critical issues remain as discussed recently by Lynch[(52)], the TG cracking in the NN-pH environment does show evidence of macroscopic ductility. Such macroscopic ductility is evident in the crack cross-section shown in Figure 9b. This diminishes interest in such mechanisms for possible adaptation to pipeline SCC analyses. Moreover, the phenomenological work in earlier sections show that indicators available via impedance spectroscopy correlate with spects of the mechanical response, such as cyclic softening. This again points to a ductile hydrogen-related mechanism such as HELP. On this basis, HELP is the most probable candidate to build on for use in subsequent models of NN-pH SCC in analogy to the prior adaptation of concepts like film-rupture, slip-dissolution and similar schemes [(e.g., 51,52)] that embed the basic concept of anodic dissolution[(e.g.,11,12)], which underlies high-pH SCC.

Historically, environmentally assisted cracking under general cyclic loading has been considered to involve SCC in addition to other cracking processes, particularly as the environment becomes more aggressive or as the loading involves larger-amplitude higher-frequency cycling. Terms such as corrosion-fatigue have been introduced when the cyclic amplitude becomes large or the

---

[14] This follows from the comment that NN-pH cracking is often very difficult to distinguish from corrosion-fatigue cracks which tend to show ductile TG characteristics.

[15] While lesser known, work done in Russia by Rebinder[(47)] and his colleagues since the 50s also showed trends where environments likely involving hydrogen were associated with enhanced plasticity.

frequency of cycling increases to limit the role of environment. The term corrosion-fatigue might be most relevant where corrosion leads to pitting, which act as preferential nucleation sites for fatigue initiation, thereby producing a 10-fold or greater synergistic acceleration of the process[e.g. 54]. In contrast, where the effects of environment and fatigue combine during crack growth, the acceleration can be much less significant leading to an increase in cracking rate by a factor of two, or even less. While scientifically such effects are interesting, real-world uncertainty in the properties of the line-pipe steel or of the environment along the RoW can lead to much larger factors – relegating such concerns to the list of second-order issues.

In the limit, as the environment becomes less severe, fatigue ensues. At the other extreme, as the environment becomes increasingly aggressive, sites for crack nucleation and existing crack tips corrode, as do the flanks of these regions, thereby blunting potential cracks. The concept of superposition was introduced in the late 60s to bridge the gap between these extremes and to address the synergistic interaction of environmental effects and fatigue, for both thermal and chemical environments. For fatigue cycling in a chemical environment, such models embed the contribution of fatigue and SCC, with the interaction term considered to address the synergy of these effects including corrosion fatigue[35].

While many have postulated that the hydrogen develops as a result of the cathodic hydrogen reduction reaction that accompanies the corrosion of iron, little has been published to establish that this mechanism can generates sufficient hydrogen to be a factor in NN-pH SCC. On the other hand, reactions leading to hydrogen generation postulated in the form of Reaction 3 provide a robust source of hydrogen that easily drives crack nucleation in NN-pH environments. As indicated earlier, given adequate concentration of the species involved this hydrogen-generation process is self-sustaining. This means that unless action is taken that by design upsets the environment promoting hydrogen generation, significant hydrogen will be available to drive any active hydrogen-related mechanism. Clearly nature can upset this process through seasonal and other swings that impact the RoW. However, thus far serendipity under nature's control has admitted several failures, which means the pipeline community must take an active role in understanding this process and how to interrupt it. The alternative under nature's control is hydrogen will continue to form and be adsorbed driving TG cracking at potentially very high rates. This remains a very significant practical concern. A structure has been presented and model modules formulated that begin to develop this understanding – which must be continued through completion of these modules and their integration into the construct already demonstrated for high-pH SCC.

## Summary and Conclusions

This project has developed and presented results that reflect a much different understanding for high-pH SCC as compared to NN-pH SCC. For the high-pH scenario the level of model development facilitates pipeline simulation, representing as needed the variability of conditions along a pipeline's RoW. The benefit is understanding developed and modeled for high-pH SCC facilitates simulation of trends observed in the field, which in turn can be used in day to day integrity-management decisions. In contrast, the modeling for NN-pH situations is at the level of understanding the mechanisms that underlie the evolution of hydrogen that tends to drive this form of SCC, and the spectrum of environments plausible on pipelines such that once can infer from above ground the nature of the cracking processes affecting the serviceability of a pipeline. Such understanding must be transformed into practical algorithms before this understanding can

have a direct impact via maintenance management. In contrast, simple criteria have been developed to support such maintenance and integrity decisions for the high-pH scenario and illustrated by an example that evaluated some aspects of the effects of a service conversion, indicating such technology also can support rational business decisions.

It remains to move the developing understanding based on the hydrogen generation mechanism, the spectrum of environments, and the related laboratory results forward sufficiently to develop viable phenomenological models in parallel to those for high-pH SCC. Thereafter, these models must be transformed into modules compatible with the structure developed for high-pH SCC, which after validation as modules can be integrated into a more general formulation for pipeline SCC. This approach leverages the value of the past investment while it develops a rational resolution for NN-pH SCC, and the more general problem of pipeline SCC. Several near-term targets have been identified in meeting this longer-term objective – which should be achievable within about a five-year time horizon. Addressing these issues brings with it the fundamental understanding of hydrogen effects on typical pipelines, which has added potential value if the US moves toward a hydrogen economy. The next section identifies and briefly elaborates these aspects. However, space precludes the details to efficiently scope solutions and establish effective project plans based on subtleties well beyond consideration herein.

Key conclusions developing from this project included:

- Optimum conditions for NN-pH SCC kinetics were established via beaker studies, with bicarbonate ion identified as the essential constituent,
- A mechanism for NN-pH SCC that leads to significant hydrogen generation derived from the bicarbonate ion was developed and modeled in a fundamental framework,
- It was found that this mechanism produced hydrogen in sufficient quantity to support crack nucleation and continued cracking under typical pipeline service conditions,
- It was indicated that a spectrum of reversible environments exist that sandwich NN-pH SCC between corrosion that controls at lower pH levels and high-pH SCC bounding the high end, with each of corrosion, high-pH SCC, and NN-pH SCC possible either individually or mutually nearby or even in association with the same crack,
- Reversibility of the environments was found to be driven by seasonal factors that affect temperature (hydrogen solubility) and the availability of other constituents that modify the kinetics of dissolution, anodic dissolution, and hydrogenation and its ingress and interaction with the microstructure,
- The viability of NN-pH SCC mechanism was demonstrated by nucleation in the laboratory, which confirmed NN-pH SCC is possible throughout the United States, as the bounding temperatures reflect that range of climatic conditions,
- The extent of hydrogen generated by this mechanism was quantified as was its effect on microplastic response,
- It was found that bicarbonate ion can be generated in copious quantities thus providing a more that adequate source of hydrogen to drive environmentally assisted cracking,
- While the role of hydrogen was demonstrated, the specific form of environmentally assisted cracking has not yet been quantified – each of the three recognized and competing forms of hydrogen interaction with the microstructure remain plausible – with

some traits observed being consistent with hydrogen enhanced localized plasticity (HELP) and others being more typical of hydrogen embrittlement (HE),

- Electrochemical impedance spectroscopy (EIS) was found to be an effective tool in evaluating the interaction of hydrogen and cycle dependent changes in the steel's surface, and the behavior of the interface that forms between the steel and the cracking environment,
- Functional relationships characterizing NN-pH SCC kinetics were identified and controls for hydrogen effects discussed,
- The environment supporting the NN-pH SCC mechanism was found to be consistent with the constituents typically found with this cracking in the field, particularly in the vicinity of severe cracking that led to in-service ruptures,
- Field criteria to assess high pH SCC severity were assessed and their validation considered in the context of computer simulation of this process and parametric analysis done to simulate control of such SCC via operational changes,
- The effect of in-service factors on NN-pH SCC susceptibility was discussed, with factors that drive the hydrogen generation mechanism being of greatest concern,
- Until the effects of cycle dependent changes in the steel's surface are isolated from the inherent influence of microstructure and its impact on cyclic softening and this is quantified, there is no reasonable expectation that macroscopic empirical testing to probe and empirically trend this behavior will prove effective.

# Recommendations

While rather limited in scope, this work points clearly to the utility of EIS as the means to uncouple the interacting roles of cycle-dependent mechanical effects (like cyclic softening), microstructure, environment, and loading. Until the effects of cycle dependent changes in the steel's surface is isolated from the inherent influence of microstructure and its impact on cyclic softening and quantified, there is no reasonable expectation that macroscopic empirical probes into this behavior at the scale of cracking will prove effective. This assertion is proven by the lack of insight from such testing after more than 70 years of such work coupling the effort first for high-pH and then NN-pH SCC. It follows that the central recommendation from this project is to initiate a combined analytical and experimental assessment targeting isolation of the roles of cycle-dependent microplasticity, mechanical loading history, electrochemical environment, and microstructure, via focused experiments incorporating EIS coupled with related modeling of the phenomenology and analysis of trends and their implications. Only then can we anticipate incremental insight, and thereafter control of SCC.

# References


1. Fessler, R. R., Berry, W. E., Elsea, A. R., Wenk, R. L., Reinhoel, J. E., Investigation of Stress-Corrosion Cracking in Buried Pipelines, AGA NG-18 Project Report No. 24, December, 1970.
2. Parkins, R. N., The Controlling Parameters in Stress-Corrosion Cracking, Proceedings of the 5th Line Pipe Symposium, Paper U, 1974.
3. Parkins, R. and Fessler, R. R., "Line Pipe Stress Corrosion Cracking - Mechanisms and Remedies", Corrosion 86, Paper Number 320, NACE, 1986.
4. Parkins, R. N., and Greenwell, B. S., "The Interface Between Corrosion Fatigue and Stress-Corrosion Cracking", *Metal Science*, 11, pp 405, 1977.
5. Leis, B. N., Rungta, R., and Jentgen, R. L., "Stress-Corrosion Cracking and Fatigue -- A Mechanics-Based Step to an Interactive Model", Embrittlement by the Localized Crack Environment, Edited by R. P. Gangloff, pp. 211-227, 1984.
6. Leis, B. N., "Mechanics Based Analysis of Environmentally Assisted Crack Nucleation in Systems Controlled by Dissolution", Modeling Environmental Effects on Crack Growth Processes, AIME, pp 301-319, 1986.
7. Leis, B. N., "Recurrent SCC in Gas Transmission Pipelines: Service History and Material Property Considerations", AGA NG-18 Report No. 210, February, 1994.
8. Anon, Stress-Corrosion Cracking on Canadian Oil and Gas Pipelines, National Energy Board (of Canada), Report of Inquiry, MH-2-95, November 1996.
9. Parkins, R. N., "Environment Sensitive Cracking (Low pH Stress-Corrosion Cracking) of High-Pressure Pipelines", PRCI Catalog No. 51623, 1990.
10. Parkins, R. N., "A Review of Stress Corrosion Cracking of High Pressure Gas Pipelines", Paper 00363, CORROSION/2000, NACE, 2000: see also Parkins, R. N., "An Overview of Stress-Corrosion Cracking Research Activities for High-Pressure Pipelines", AGA NG-18 Report No. 215, 1994.
11. Fessler, R. R., "Stress-Corrosion-Cracking Gap Analysis", Report on GRI 8293, PRCI Catalog No. L52040, September, 2002.
12. Colwell, J. A., Leis, B. N., and Singh, P., "Crack Initiation in Near-Neutral pH Environments," Environmentally Induced Cracking in Pipeline Systems, Banff, Canada, NACE, pp, 2004.
13. Colwell, J. A., Leis, B. N., and Singh, P. M., "Recent Developments in Characterizing the Mechanism of Near-Neutral pH SCC," NACE SCC Symposium: 05-STG-35(1), Paper No. 05161, 2005.
14. Asher, S. L., Colwell, J. A., Leis, B. N., and Singh, P., "Crack Initiation on Line Pipe Steels in Near-Neutral pH Environments," 16th International Corrosion Conference, 2005.
15. Asher, S. L., Singh, P., Colwell, J. A., and Leis, B. N., "Stress Corrosion Cracking of Pipeline Steel in Near-Neutral pH Environments," NACE 06 – Paper 06175, 2006.
16. Stress Corrosion Cracking (SCC) Threat to Gas and Hazardous Liquid Pipelines, DOT Advisory Bulletin ADB-03-05.
17. Fessler – early model line pipe symp (full cititation to follow)

18. Leis, B. N., and Walsh, W. J., "Mechanics-Based Analysis of Stress-Corrosion Cracking of Line-Pipe Steel in a Carbonate-Bicarbonate Environment", ASTM STP 1049, B. W. Lisagor, T. W. Crooker, B. N. Leis, Eds., pp. 243-265, 1990.
19. Leis, B. N., "Analysis Methods For Stress-Corrosion Cracking", Pipeline Technology Conference, Part B, Oostende, pp. 18.1-11, 1990: see also Leis, B. N., and Parkins, R. N., "Modeling Stress-Corrosion Cracking of High-Pressure Gas Pipelines", 8th Symposium on Line Pipe Research, pp 19.1-19.21, PRCI Catalog No. L51680, 1993.
20. Kurth, R. E., and Leis, B. N., "Probabilistic Modeling of Stress-Corrosion Cracking: Part One – Model Development", Probabilistic and Environmental Aspects of Fracture, ASME PVP Volume 386, 1999, pp 3-12.
21. Leis, B. N., and Parkins, R. N., "Mechanics and Material Aspects in Predicting Serviceability Limited By Stress-Corrosion Cracking", Fatigue and Fracture of Engineering Materials and Structures, Vol 21, 1998, pp 583 – 601.
22. Kurth, R. E., and Leis, B. N., "Probabilistic Modeling of Stress-Corrosion Cracking: Part Two –Validation and Implications for Control", Probabilistic and Environmental Aspects of Fracture, ASME PVP Volume 386, 1999, pp 13-23.
23. Leis, B.N. and Kurth, R.E., "Probabilistic Determination of Hydrotest Frequencies for Controlling Stress-Corrosion Cracking Incidents", Final Report on PR-3-9407, PRCI Catalog No. L51665, May 1999.
24. Beavers, J. A., Appendix D, Section 5, of Canadian Energy Pipeline Association submission to National Energy Board (of Canada) Public Inquiry on Pipeline Stress-Corrosion Cracking, Proceeding MH-2-95, April 1996.
25. Sutherby, R. L., Lambert, S. B., and Plumtree, A., "Modeling of Environmental Crack Growth in Pipeline Steel", Paper 00364, CORROSION/2000, NACE, 2000.
26. Ming, G., PII's SCC Model Formulation, Private communication, Rio, October 2003
27. Beavers, J. A. and Jaske, C., "Effects of Pressure Fluctuations on SCC Propagation", PRCI final Report PR-186-9706, Catalog No. L51872, 2002.
28. Leis, B. N., and Colwell, J. A., "Initiation of Stress-Corrosion Cracking on Gas Transmission Piping", ASTM STP 1298, pp. 34 – 57, 1998.
29. Fessler, R. R., and Barlo, T. J., "Threshold-Stress Determination Using Tapered Specimens and Cyclic Stresses", ASTM STP 821, pp 368-382, 1984.
30. Beavers, J. A., Parkins, R. N., Koch, G. H., and Berry, W. E., "Test Method for Defining Susceptibility of Pipeline Steels to Stress-Corrosion Cracking", PRCI Cat. No. 51484, 1985.
31. Leis, B. N., "Characterization of Axial Flaws in Pipelines, with a Focus on Stress Corrosion Cracking," PRCI Catalog No. L51807, 1997.
32. Beavers NS4 & Cracking (full cititation to follow)
33. Gu, B., Yu, W. Z., Luo, J. L., and Mao, X., Corrosion, 55, 312, 1999.
34. King, F., Jack, T., Chen, W., Wilmott, M., Fessler, R. R., and Krist, K., "Mechanistic Studies of Initiation and Early Stage Crack Growth for Near-Neutral pH SCC on Pipelines," Corrosion/2000, Paper No. 00370, NACE International, 2000.
35. Pourbaix, M., "Lectures on Electrochemical Corrosion", p. 42, NACE International, 1995.
36. Birnbaum, H. K., et al, Mater. Sci. Eng. A, Vol. A176, 1994, p.191-202.
37. Toriano, A. R., Trans. ASM, Vol. 52, pp. 54, 1960.

38. Ugiansky, G. M., and Payer, J. H., editors, "Stress-Corrosion Cracking -- The Slow Strain-Rate Technique", ASTM STP 665, 1979.
39. Parkins, R. N., Leis, B. N., and Christman, T., "Spatial Densities of Stress-Corrosion Cracks in Line-Pipe Steels", PRCI Catalog No. L51654, 1992.
40. Leis, B. N., "Hydrostatic Testing Of Transmission Pipelines: When It Is Beneficial and Alternatives When It Is Not", PRCI Catalog No. L51844, January, 2001.
41. J. Newman, K. Thomas, Electrochemical Systems, 3rd Edition, 2004.
42. Devanathan, M. A. and Stauchurski, Z., Proc. Roy. Soc, Vol. 90, 1962, p. A270.
43. Pyun, Su-Il and Oriani, R. A., Corrosion Science, Vol. 29, May 1989, p. 485.
44. Al-Faquer, F. M., Weil, K.G., and Pickering, H. W., J. of Electrochem. Soc., Vol. 150, May 2003, pp. B211-B216.
45. Castaneda, H. and Leis, B.N., Hydrogen Entry Mechanism For API X-65 Steel Exposed In Near Neutral Solutions Under Adsorption-Activation Conditions, Corrosion 2007, paper No. 07499, Nashville, TN, NACE, 2007.
46. Chaudhari, B. S. and Radhakrishnan, T. P., Corrosion Science, Vol. 30, -1234, December 1990, p. 1219.
47. Wang, X., Hsing, I. and Hu, J., Journal of Electroanalytical Chemistry, Vol. 562, 2004, p. 73.
48. Sanicharane, S., Bo, A., Sompalli, B., Gurau, B. and Smotking, E., Journal of the Electrochemical Society, Vol. 149, May 2002, p. A554.
49. Peter, L., Szucs, E., Filak, L., Vero, B. and Schneider, H., Journal of Applied Electrochemistry, Vol. 33, 2003, pp. 613-617.
50. Leis, B. N. and Parkins, R. N., "Modeling Stress-Corrosion Cracking of High-Pressure Gas Pipelines," 8th Symposium on Line Pipe Research, PRCI Cat. No. L51680, pp 19.1-19.24, Houston TX, 1993.
51. Charles, E. A. and Parkins, R. N., Corrosion, Vol. 51, pp. 518-527.
52. Parkins, R. N. and Singh, P., Corrosion, Vol. 46, 1990, pp. 485-498.
53. Ford, F. P., Taylor, D. F., Andresen, P. L., and Ballinger, R. G., "Corrosion –Assisted Cracking of Stainless Steel and Low-Alloy Steels in LWR Environments," EPRI Report NP5064S, Palo Alto, CA, EPRI, 1987.
54. Ford, F. P., "Mechanisms of Environmental Cracking Peculiar to the Power Generation Industry," EPRI Report NP2589, Palo Alto, CA, EPRI, 1982.
55. Leis, B. N., Colwell, J. A., and Singh, P. M., *Crack Initiation of Line Pipe Steels in Near-Neutral pH Environments*, *NACE 2004*, New Orleans, LA: NACE International.
56. Singh, P., Asher, S., Colwell, J., and Leis, B., Crack Initiation of Line Pipe Steels in Near-Neutral pH Environments, 16th International Corrosion Congress, 2005, Beijing, China
57. Osseo- Assare, K., Trans. IIM, Vol. 90, 1981.
58. Jones, D. A., Corrosion, Vol. 52, No. 5, pp. 356-362, 1996.
59. Yokobori, T., Nemoto, T., Satoh, K., and Yamada, T., Engineering Fracture Mechanics, Vol. 55, No. 1, pp. 47-60, 1996.
60. Mishra, B., Al-Hassan, S., Olson, D. L., and Salama, M. M., Corrosion, Vol. 53, November 1997, p. 852.
61. Nesic, S., Postlethwaite, and Olsen, S., Corrosion, Vol. 52, No.4, 1996.

62. Norsdveen, M., Nesic, S., Nyborg, R., and Stangeland, A., Corrosion, Vol. 59, No. 5, pp. 443-456, 2003.
63. Ford, F.P. Corrosion, Vol. No. 52, 5, p. 379, 1992.
64. Lynch, S.P., "Concerning the Relative Importance of Decohesion versus Slip and Adsorbed versus Solute Hydrogen on Fracture Behavior," 11th International Conference on Fracture, Turin, Paper 3885, 2005.
65. Thompson, A. W. and Bernstein, I. M., "The Role of Metallurgical Variables in Hydrogen Assisted Environmental Fracture," Advances in Corrosion Science and Technology, edited by M. G. Fontanna and R.W. Staehle, Plenum, vol.7, 1980, pp 53–173.
66. Lynch, S.P. "A Comparative Study of SCC, HAC, and LME in Al, Ni, Ti, and Fe Based Alloys," in Hydrogen Effects in Metals, AIME, 1981, pp. 863-871.
67. Tabata, T., and Birnbaum, H.K., "Direct Observations of the Effect of Hydrogen on the Behavior of Dislocations in Iron", Scripta Met., Vol. 17, 1983, pp. 947 – 950: see also Birnbaum, H. K., et al, Mater. Sci. Eng. A, Vol. A176, 1994, p.191-202.
68. Lynch, S.P. "Mechanisms of Hydrogen-Assisted Cracking – A Review," Hydrogen Effects on Material Behavior and Corrosion Deformation Interactions, N. R. Moody et al. (Eds.), pp. 449-466, 2003.
69. Hänninen, H.E. "Stress Corrosion Cracking," Comprehensive Structural Integrity, vol.6, Milne, I. et al. (Eds.), pp. 1-29, 2003.
70. Leis, B. N., Colwell, J. A., and Singh, P. M., "Crack Initiation Mechanisms for Line Pipe Steels in Near-Neutral pH Environments", Battelle Report PR-03-0320, PRCI Catalog L52041, 2005.Parkins, R. N., Corrosion, Vol. 43, 1987, p.130.
71. Morrow, Jo Dean, Cyclic Plastic Strain Energy and Fatigue of Metals, ASTM STP 378, pp 45 - 87, 1958.
72. C. E. Feltner and C. Laird , C., "Cyclic Stress-Strain Response of F.C.C. Metals and Allows--II, Dislocation Structures and Mechanisms," Acta Metallurgica Vol. 15, pp. 1633-1653, 1967
73. Klesnil, M. and Lukas, P., "Fatigue of Metallic Materials", Elsevier, 1980.
74. Chaudhari, B. S. and Radhakrishnan, T. P., Corrosion Science, Vol. 30, -1234, December 1990, p. 1219.
75. Wang, X., Hsing, I. and Hu, J., Journal of Electroanalytical Chemistry, Vol. 562, 2004, p. 73.
76. Iyer, R., Pickering, H. W., and Zamanzadeh, M., J. of Electrochem. Soc., Vol. 136, September 1989.
77. Petit, M.C., Cid, M., Puiggali, M., Amor, Z., Corros. Sci. 31,1990.
78. Oltra, R. and Keddam, M., Corrosion Science Volume 28, Issue 1 , 1988, p. 1-5.
79. Bosch, R. W., Corrosion Science 47, 2005, 125–143.
80. Bosch, R. W., Moons, F., Zheng, J. H., and Bogaerts, W. F., Corrosion–Vol. 57, No. 6.
81. De Levie, R., Electrochimica Acta, 9, 1231, 1964.
82. Castaneda, H., PhD Thesis, Penn State University, 2001.
83. Stonesifer, R. B., Brust, F. W., and Leis, B. N., Eng. Fracture Mech., Vol. 45, No. 3, pp. 357-380, 1993.
84. Sutherby, R. L., Private Communication on lab-scale testing results for SCC in pipe segments, 1998.

85. Leis, B. N. and Brust, F. W., Proc. Pipeline Tech. Conf., Part B, Oostende, pp. 13.11-19, 1990.
86. Eiber, R. J. and Leis, B. N., PRCI Catalog No. L51846, 2002.
87. Fessler, R. R., Proc Int. Pipeline Conf., Conference CD, ASME, Calgary, 2006.